

5-2013

# Holocene Glacial History of Renland, East Greenland Reconstructed From Lake Sediments

Aaron Medford

Follow this and additional works at: <http://digitalcommons.library.umaine.edu/etd>



Part of the [Climate Commons](#)

---

## Recommended Citation

Medford, Aaron, "Holocene Glacial History of Renland, East Greenland Reconstructed From Lake Sediments" (2013). *Electronic Theses and Dissertations*. 1934.

<http://digitalcommons.library.umaine.edu/etd/1934>

This Open-Access Thesis is brought to you for free and open access by DigitalCommons@UMaine. It has been accepted for inclusion in Electronic Theses and Dissertations by an authorized administrator of DigitalCommons@UMaine.

**HOLOCENE GLACIAL HISTORY OF RENLAND, EAST GREENLAND  
RECONSTRUCTED FROM LAKE SEDIMENTS**

By

Aaron Medford

B.S. Lafayette College, 2011

A THESIS

Submitted in Partial Fulfillment of the

Requirements for the Degree of

Master of Science

(in Earth and Climate Sciences)

The Graduate School

The University of Maine

August 2013

Advisory Committee:

Brenda L. Hall, Professor, School of Earth and Climate Sciences and Climate Change Institute, Advisor

George H. Denton, Professor, School of Earth and Climate Sciences and Climate Change Institute

Daniel F. Belknap, Professor, School of Earth and Climate Sciences, Cooperating Professor, Climate Change Institute

Ann C. Dieffenbacher-Krall, Assistant Research Professor, Climate Change Institute

## **THESIS ACCEPTANCE STATEMENT**

On behalf of the Graduate Committee for Aaron Medford I affirm that this manuscript is the final and accepted thesis. Signatures of all committee members are on file with the Graduate School at the University of Maine, 42 Stodder Hall, Orono, Maine.

---

Dr. Brenda Hall, Professor of Sciences and Quaternary and Climate Studies    6/25/2013

## **LIBRARY RIGHTS STATEMENT**

In presenting this thesis in partial fulfillment of the requirements for an advanced degree at the University of Maine, I agree that the Library shall make it freely available for inspection. I further agree that permission for “fair use” copying of this thesis for scholarly purposes may be granted by the Librarian. It is understood that any copying or publication of this thesis for financial gain shall not be allowed without my written permission.

Signature:

Date:

**HOLOCENE GLACIAL HISTORY OF RENLAND, EAST GREENLAND**  
**RECONSTRUCTED FROM LAKE SEDIMENTS**

By Aaron Medford

Thesis Advisor: Dr. Brenda L. Hall

An Abstract of the Thesis Presented  
in Partial Fulfillment of the Requirements for the  
Degree of Master of Science  
(in Earth and Climate Sciences)  
August 2013

The Arctic is responding to the modern increase in temperature, resulting in ice loss and consequent sea-level rise. In order to understand present-day changes, we need to understand how the Arctic has reacted in the past to natural variations in climate forcing. To begin to identify the mechanisms behind climate change, I produced a Holocene glacial and climate record for the Renland Ice Cap, Scoresby Sund, East Greenland, from sediments in glacially fed lakes. I cored Rapids and Bunny Lakes, which are fed by meltwater from the Renland Ice Cap, as well as Raven Lake, which does not receive glacial influx at present. The presence or absence of glacial sediments in Rapids and Bunny Lakes gives information on the size of the Renland Ice Cap.

I studied multiple sediment characteristics in the cores, including magnetic susceptibility (MS), grain size, organic and carbonate content, and color intensity. In general, I identified glacial sediment as grey, inorganic, and with high MS. Non-glacial

material was black or brown with high organic content and low MS. Chronology for the cores came from radiocarbon dating of macrofossils and sieved organic fragments.

My results suggest that the region may have deglaciated as early as ~12.5 ka. The high organic content in all three lakes suggests that the early- to mid-Holocene was warm with periods of limited ice extent, consistent with the Holocene thermal maximum, which has been documented elsewhere. After this warmth, the area cooled during the Neoglaciation that culminated in the largest glacial event of the Holocene during the Little Ice Age. Superimposed on the long-term climate change were multiple centennial- to-millennial-scale glacial advances at ~ 9.4, 8.6-8.8, 8.1-8.3, 7.6-7.8, 7.0-7.5, 5.8-6.0, 4.7-5.0, 3.7-4.0, 3.0-3.6, and ~1.0 (AD 600 and 900) cal. kyBP.

My reconstruction of variations in the Renland Ice Cap matches well with other glacial records from Scoresby Sund and from the wider Northern Hemisphere. In addition, comparison with other glacial records from the Scoresby Sund region suggests that elevation exerts a strong control on the timing, size, and number of glacial advances exhibited at each site. This highlights the need for caution when comparing glacial records from large geographic areas.

The Renland record, along with other Northern Hemisphere data, indicates pervasive millennial-scale climate change throughout the Holocene, with the largest magnitude glacial advance occurring during the Little Ice Age. This pattern favors a cyclical forcing mechanism, such as solar variability or a 'wobbly ocean conveyor,' rather than unique events, such as volcanic eruptions or outburst floods, as a cause of millennial-scale climate change.

## ACKNOWLEDGMENTS

I would like to begin by thanking my advisor, Dr. Brenda Hall, for this great opportunity, as well as for the guidance and knowledge she has passed on. I also want to thank my committee Dr. George Denton, Dr. Daniel Belknap, and Dr. Ann Dieffenbacher-Krall for their expertise and help in improving my thesis.

I owe the National Science Foundation, the University of Maine Graduate School Government, and School of Earth and Climate Science for funding my master's work. Thank you to the School of Earth and Climate Science, the Climate Change Institute, Dartmouth College, and the University of Minnesota Limnological Research Center for the use of lab space and material. In addition, the work in Scoresby Sund, would not have happened without the support of the late Gary Comer.

I was fortunate to join an ongoing project, and I am excited to add my record to the already stellar work done by this group. I want to especially thank my field team Dr. Brenda Hall, Dr. Meredith Kelly, Dr. Tom Lowell, Dr. Yarrow Axford, Paul Wilcox, and Laura Levy for help in collecting and analysis of the data. In addition, I would like to thank Krista Slemmons and Karen Marysdaughter for help in processing the cores.

I am grateful to my family for their support throughout the last two years, giving me unconditional support. I would like to thank the faculty and staff in the Climate Change Institute and School of Earth and Climate Sciences; it has been a great and rewarding experience being able to work with you. I would like to thank my fellow graduate students, especially the game night group, for support and encouragement. Finally, I would like to acknowledge the geology department at Lafayette College, who laid the foundation that allowed me to accomplish what I did.

## TABLE OF CONTENTS

ACKNOWLEDGMENTS.....	iii
LIST OF TABLES.....	vii
LIST OF FIGURES.....	viii
CHAPTER	
1. INTRODUCTION.....	1
1.1 Overview.....	1
1.2 Background.....	4
2. METHODS.....	7
2.1 Field Work.....	7
2.2 Lab Work.....	10
3. RESULTS.....	16
3.1 Lake Setting.....	16
3.1.1 Glacial Lakes.....	16
3.1.2 Conceptual Model.....	23
3.1.3 Non-Glacial Lake.....	26
3.2 Sediment Core Descriptions.....	31
3.2.1 Rapids Lake.....	31
3.2.1.1 RPD11-1B-1.....	31



3.2.2 Bunny Lake.....	37
3.2.2.1 Southern Basin: BNL11-1A-1.....	37
3.2.2.2 Southern Basin: BNL11-1B-1.....	42
3.2.2.3 Northern Basin: BNL11-2A-1.....	43
3.2.2.4 Northern Basin: BNL11-2A-2.....	48
3.2.3 Raven Lake.....	50
3.2.3.1 RAV11-1A-1.....	50
3.2.3.2 RAV11-1A-2.....	54
3.2.3.3 RAV11-2A-1.....	55
3.2.3.4 RAV11-3A-1.....	58
4. DISCUSSION .....	61
4.1 Age Model.....	61
4.1.1 Radiocarbon Date Quality.....	61
4.1.2 Rapids Lake.....	62
4.1.3 BNL11-1.....	62
4.1.4 BNL11-2.....	63
4.1.5 Raven Lake.....	65
4.2 Lake History.....	67
4.2.1 Raven Lake.....	67
4.2.2 Rapids Lake.....	69
4.2.3 Bunny Lake.....	73
4.3 Glacial History of Raven, Rapids, Bunny Lake.....	78

4.4 Comparison of Climate Records.....	81
4.4.1 Comparisons between the Renland Glacial Record and the Renland Ice Core .....	81
4.4.2 Holocene Glacier and Climate Fluctuations in Greenland.....	85
4.4.3 Comparisons between the Glacial Record and the GISP2 Ice Core.....	91
4.4.4 European Holocene Glacial and Climate Records.....	92
4.4.5 North American Holocene Glacial and Climate Record.....	93
4.5 Holocene Climate Forcing.....	94
5. CONCLUSIONS .....	99
REFERENCES.....	101
APPENDIX A: DETAILED GRAIN SIZE MEASUREMENT METHOD.....	110
APPENDIX B: CORE LOGS.....	112
BIOGRAPHY OF AUTHOR.....	126

## LIST OF TABLES

Table 1 Basic information for each of the cored lakes.....	9
Table 2 Radiocarbon samples.....	13
Table 3 Basic information on each of the cores.....	18
Table 4 Age model for master cores.....	65
Table 5 Timing of glacial advances of the Renland Ice Cap.....	75

## LIST OF FIGURES

Figure 1 ASTER image showing Scoresby Sund.....	5
Figure 2 A detailed image of the study area.....	8
Figure 3 Delta at southwest outlet of Large Lake (view to the southwest).....	17
Figure 4 Image of Rapids and Bunny Lakes (view to the northeast).....	17
Figure 5 Bathymetric map of Rapids Lake.....	20
Figure 6 Aerial image of area surrounding Rapids and Bunny Lakes.....	21
Figure 7 Bathymetric map of Bunny Lake.....	22
Figure 8 Conceptual model of glacial input into Rapids and Bunny Lakes.....	24
Figure 9 Image of Raven Lake (view to the south).....	27
Figure 10 Bathymetric map of Raven Lake.....	29
Figure 11 Aerial Image of the area surrounding Raven Lake.....	30
Figure 12 Rapids Lake cores plotted by depth below water surface.....	32
Figure 13 Radiocarbon dates for RPD11-1.....	33
Figure 14 Data for RPD11-1, the master core for Rapids Lake.....	34
Figure 15 Bunny Lake cores plotted by depth below water surface.....	38
Figure 16 Radiocarbon dates for BNL11-1.....	39
Figure 17 Data for BNL11-1, the master core for the south basin in Bunny Lake.....	40
Figure 18 Radiocarbon dates for BNL11-2.....	45
Figure 19 Data for BNL11-2, the master core for the north basin in Bunny Lake.....	46

Figure 20 Relationship between color intensity and percent organic material.....	47
Figure 21 Raven Lake cores plotted by depth below water surface.....	51
Figure 22 Radiocarbon dates for RAV11-1.....	52
Figure 23 Data for RAV11-1, the master core for Raven Lake.....	53
Figure 24 Radiocarbon dates for RAV11-2A-1.....	56
Figure 25 Data for RAV11-2A-1.....	57
Figure 26 Radiocarbon dates for RAV11-3A-1.....	59
Figure 27 Data for RAV11-3A-1.....	60
Figure 28 RPD11-1 age model.....	64
Figure 29 BNL11-1 age model.....	64
Figure 30 BNL11-2 age model.....	66
Figure 31 RAV11-1 age model.....	66
Figure 32 Comparison with Greenland ice cores.....	82
Figure 33 Comparison of Holocene glacial margin records from the Northern Hemisphere .....	87
Figure 34 Initial description of core BNL11-1A-1.....	112
Figure 35 Initial description of core BNL11-1B-1.....	113
Figure 36 Initial description of core BNL11-2A-1.....	114
Figure 37 Initial description of core BNL11-2A-2.....	115
Figure 38 Initial description of core BNL11-3A-1.....	116
Figure 39 Initial description of core RAV11-1A-1.....	117
Figure 40 Initial description of core RAV11-1A-2.....	118
Figure 41 Initial description of core RAV11-2A-1.....	119

Figure 42 Initial description of core RAV11-3A-1.....	120
Figure 43 Initial description of core RAV11-4A-1.....	121
Figure 44 Initial description of core RPD11-1A-1.....	122
Figure 45 Initial description of core RPD11-1B-1.....	123
Figure 46 Initial description of core RPD11-1C-1.....	124
Figure 47 Initial description of core RPD11-2A-1.....	125

# CHAPTER 1

## INTRODUCTION

### 1.1 Overview

Natural changes in forcing have produced significant variations in Earth's climate (Zachos et al., 2005). Arctic amplification, a process by which multiple feedbacks strengthen the climate response to climate change, may allow northern polar regions to react more quickly and to a larger degree to climate forcing than other parts of the globe (e.g., Miller et al., 2010; Serreze and Barry, 2011; ACIA, 2005). The National Aeronautics and Space Administration (NASA) surface temperature reconstruction (Hansen et al., 2010) indicates that the Arctic has warmed among the most of any region globally during the last 100 years, and the Arctic environment has begun to change in response to these warmer temperatures. For example, sea-ice spatial extent and thickness are decreasing (e.g., ACIA, 2005; Rothrock et al., 1999; Kwok et al., 2009; Chapman and Walsh, 1993) at a rate faster than models have predicted (Stroeve et al., 2007). The Greenland Ice Sheet (GIS) is thinning due to increased velocity and discharge of outlet glaciers (e.g., Krabill et al., 2004; Howat et al., 2007; Stearns and Hamilton, 2007; Rignot and Kanagaratnam, 2006). Moreover, additional processes linking seasonal surface melt and ice-flow speed in the GIS suggest that the ice sheet will contribute more melt and increase sea-level rise faster than previously predicted (Parizek and Alley, 2004; and references within).

In order to help predict accurately how the Arctic and Greenland, specifically, will respond to future change, both natural and anthropogenic, we need a complete understanding of past climate variability. The Holocene (the past ~11,500 calendar years)

is a period of relatively stable interglacial climate (e.g., Bond et al., 1997; Fronval and Jansen, 1997) upon which centennial- and millennial-scale climate anomalies are superimposed. Hypotheses to account for these climate fluctuations include solar variability (e.g., Bond et al., 2001; Denton and Karlén, 1973), ocean circulation (Denton and Broecker, 2008), and increased volcanic activity (Miller et al., 2012). The climate in the Holocene is important because modern human societies developed during this time. In addition, it is the climate in which our society exists today. Therefore, climate shifts during the Holocene, even small fluctuations, may have had a profound impact on the growth and development of human societies. By creating a detailed climate record for the Holocene, we can understand better the relationship between humans and climate.

One way to understand the causes of past climate change and to assess whether current variations are unique, is to develop high-resolution temporal records over a variety of scales and environments spanning the globe. By determining the spatial extent, timing, and interhemispheric relationship of Holocene events, we can understand better the initial forcing and feedbacks producing the observed climate shifts. Moreover, because the Holocene is the most recent time period, most deposits from this time have not been eroded, altered, or destroyed. Therefore, detailed and high-resolution climate records from multiple proxies spanning the globe can be constructed. This detail will allow for accurate identification of the response of the climate system and identification of the forcing. East Greenland is a prime location to produce a detailed climate record, because abundant glacial deposits there allow for a high-resolution record to be constructed. The Renland Ice Cap has been drilled to bedrock, and the resulting local climate record will allow for comparison with the climate record derived from changes in



the glacial margin. In addition, the region is optimally located to record variations in circulation in the North Atlantic Ocean.

Previous work in the Scoresby Sund region of East Greenland (Fig. 1) indicates that the largest spatial extent of glaciers in the Holocene was during the Little Ice Age (LIA) (AD ~1150-1850) (e.g., Hall et al., 2008; Kelly et al., 2008; Lusas, 2011). Because the LIA glacial advance surpassed the limits of older Holocene glaciations and thus eroded or buried deposits from those time periods, the Holocene moraine record commonly is limited and skewed heavily towards the youngest event. In order to develop a record for the entire Holocene, I analyzed past glacier fluctuations from nearby lake sediments, which are a complementary, continuous, high-resolution proxy. Lake sediments have been used previously to reconstruct the Holocene glacial and climatic record in Greenland (e.g., Larsen et al., 2011; Lusas, 2011; Wagner and Melles, 2002; Kaplan et al., 2002; Cremer et al., 2001; Briner et al., 2010), and Scandinavia (e.g., Bakke et al., 2005; Dahl et al., 2003; Levy et al., submitted). One approach is to use a threshold lake that receives glacial sediments only when the ice is large enough to surpass a bedrock barrier and to contribute melt water into the watershed. In such situations, the presence or absence of glacial sediment affords information on glacier size and proximity to the lake. In addition, some researchers (e.g., Dahl et al., 2003; Nesje et al., 2001) also have reconstructed ice fluctuations from lakes that always receive glacial meltwater. Here, the principle is that the amount and grain size of glacial material increases as the glacier nears the lake. In general, glacial sediments are inorganic, grey (for most rock types), and clay-rich, as opposed to non-glacial sediments, which tend to be high in organic material, brown or black in color, and silt rich.

Specifically, in this study my goals are to:

- Constrain fluctuations of Renland Ice Cap throughout the Holocene to produce a glacial and climate history;
- Compare my high-resolution record to existing reconstructions of Holocene climate change both in Greenland and worldwide;
- Use multiple climate records to address questions concerning the forcing and amplifications responsible for Holocene climate variability.

My specific objectives to address the goals posed above include:

- Coring lakes that receive meltwater and sediment from the Renland Ice Cap, as well as a non-glacially fed control lake in the same region;
- Analyzing the cores using multiple proxies, including stratigraphy, loss-on-ignition, magnetic susceptibility, and grain size;
- Interpreting the data in terms of glacial size and presence/absence;
- Studying aerial photography, satellite images, and ground observations to identify geomorphic features to help constrain glacial history of region.

## **1.2 Background**

Scoresby Sund (~69-72°N, 21-30°W) trends west-east and is the largest fjord system on the east coast of Greenland (Fig. 1). It drains the Greenland Ice Sheet (GIS) into the North Atlantic. Isolated, independent ice caps and mountain glaciers cover the

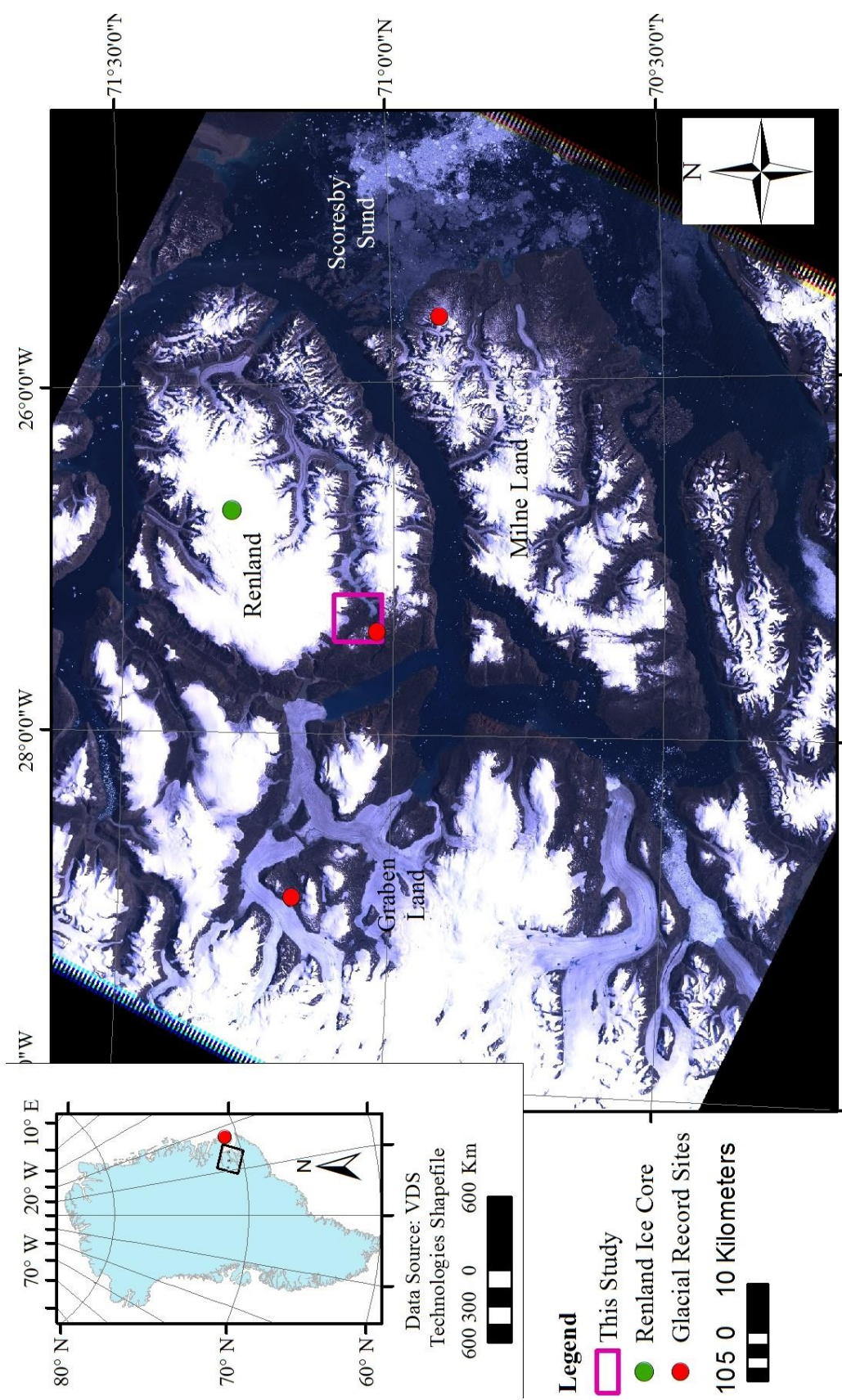


Figure 1: ASTER image showing Scoresby Sund. This study is part of a larger project to obtain glacial records from Scoresby Sund, including Milne Land (Levy et al., in review), Graben Land (Wilcox, 2013), and Liverpool Land (inset) (Lowell et al., 2013; Lusas, 2011). My study area is outlined by the purple box on the southwestern margin of Renland Ice Cap.

plateaus and mountain chains of the region. Renland (~70.5-71.5°N, 24-28°W) (Fig. 1), the focus of this study, is a plateau rising as high as 2340 m elevation, with a gently undulating topography. It is underlain mostly by granite and paragneisses from the Caledonian orogeny (Leslie and Nutman, 2000). At present, a small ice cap (1200 km<sup>2</sup>) a few hundred meters thick (Johnsen et al., 1992) covers most of Renland. Evidence suggests that the ice cap has remained isolated from the GIS, even during the Last Glacial Maximum (LGM) (Johnsen et al., 1992). I chose to study Renland, in part, because the ice cap has been cored to bedrock and has a climate record that extends into the Eemian interglacial (Johnsen et al., 1992). The Holocene is well preserved in this core (Johnsen et al., 1992), which allows a detailed comparison with the lake records developed herein.

Previous studies suggest that glacier size is related largely to summer temperature, whereas temperature proxies from the Greenland ice cores represent conditions over a full year (Koerner, 2005; Denton et al., 2005). Thus, the proximity of the Renland ice core to my field area allows for comparison of average yearly conditions from the ice core and summer temperatures from glacier fluctuations as derived from lake sediments. Denton et al. (2005) used this type of comparison to help determine climate seasonality in the region during the Younger Dryas.

## CHAPTER 2

### METHODS

#### 2.1 Field Work

I identified potential lakes through detailed study of aerial photographs and satellite images. An ideal field area should have multiple glacially fed lakes, at least one non-glacially fed lake (as a control), and only a single glacier contributing melt water to the watershed. Furthermore, the lake preferably should have high organic productivity, so that when the glacial signal is absent there is a large contrast between the two types of depositional environments (Dahl et al., 2003). In August 2011, I retrieved sediment cores from lakes in Renland that met most of these characteristics. The studied lakes most likely receive glacial material from more than one glacier during the Holocene, which I discuss in more detail in the conceptual model section. First, our field team constructed a bathymetric map for each lake to identify the optimal coring location. We measured depths by crossing the lake multiple times on a zodiac with a Humminbird device. We used Dr. Depth (<http://www.drdepth.se/>), a sea-bottom mapping software, to analyze the data. Paul Wilcox of the University of Cincinnati produced the final bathymetric maps. We chose coring locations on the basis of depth, as well as on the surrounding topography, and preferentially selected deep, flat basins.

The field team cored three lakes in Renland, two of which were glacially fed (Rapids Lake and Bunny Lake) (Fig. 2), and one of which was non-glacial (Raven Lake) (Table 1). Although Raven Lake does not receive glacial sediment at present, there are abandoned channels feeding into the lake that head near a faint drift limit just distal to a prominent LIA drift edge. Bunny and Rapids Lakes are a part of a chain of lakes. The

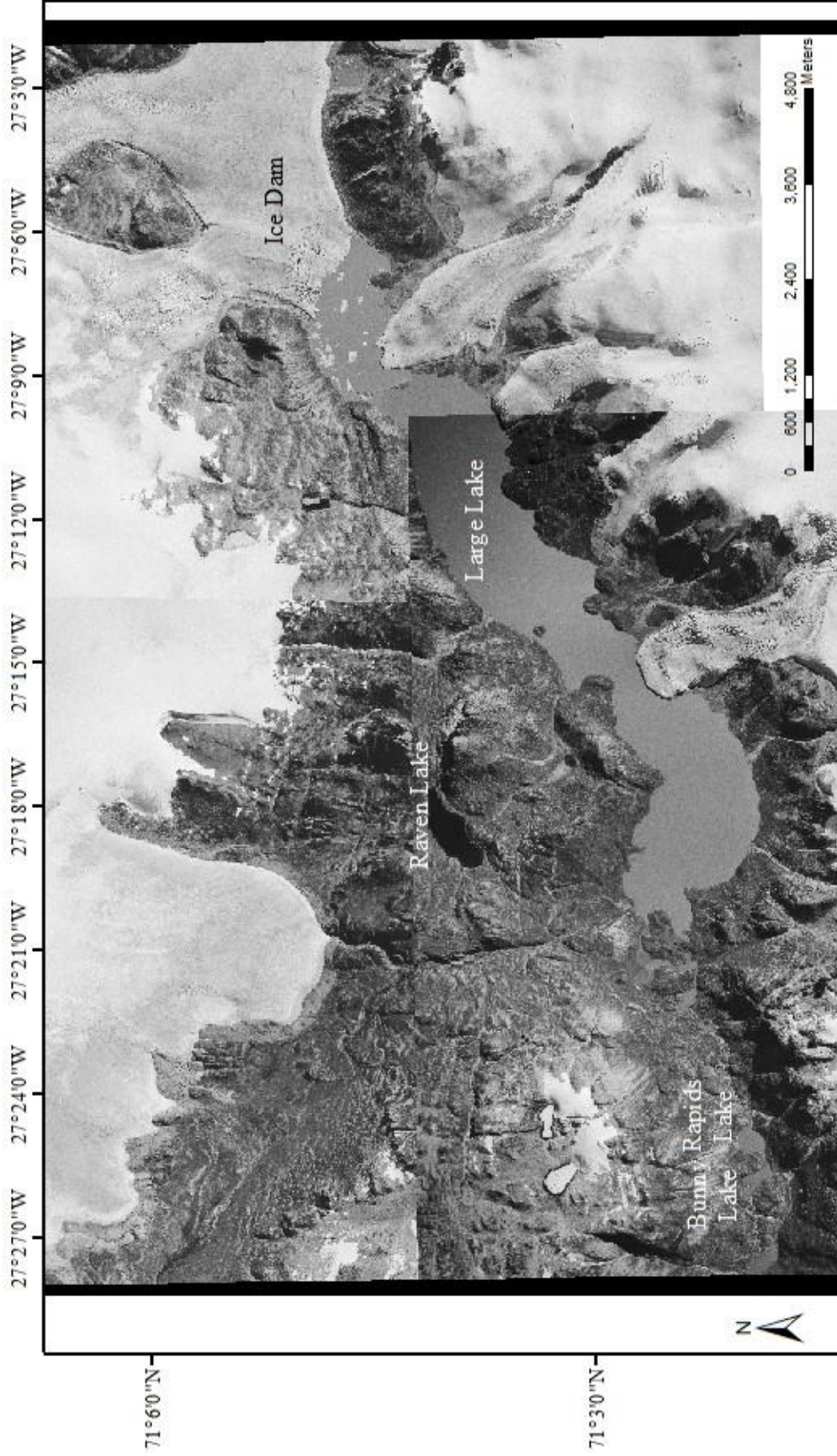


Figure 2: A detailed image of the study area. At present, Large Lake is dammed to the northeast by outlet glaciers of Renland Ice Cap and a small ice cap to the south and flows through a bedrock outlet to the southwest into a series of bedrock-floored streams and lakes. We cored two of those lakes, Rapids and Bunny, as well as a third lake, Raven, which does not receive glacial sediment at present. A large delta is being built onto the outlet of Large Lake from a meltwater stream flowing from Renland Ice Cap.

Table 1: Basic information for each of the cored lakes.

Lake	Core Prefix	Latitude	Longitude	Elevation (m)	Max. Depth (m)	Type
Rapids Lake	RPD11	71.032483	27.41535	824	30	Glacially Fed
Bunny Lake	BNL11	71.031183	27.42675	819	14	Glacially Fed
Raven Lake	RAV11	71.06601	27.31106	1054	20	Control

glacial signal in these lakes is controlled by the size and outflow of Large Lake (informal name) at the head of this chain. The size of this first lake is a function of the amount of glacial melt water and the position of ice-cap outlet glaciers that, at times, terminate in the lake.

The coring platform was formed from two zodiac boats joined by a metal “A” frame. We used a modified Bolivian coring system (Myrbro and Wright, 2008) to retrieve the sediment cores. We lowered the polycarbonate tube (1.5 m in length, 7.6 cm diameter) by a wire from our platform. The wire could be replaced with screw-on metal rods in water depths <15 m. When we reached the depth to start coring, we tied off the piston and began to hammer the tubing down by raising and then dropping a weight. The whole corer was pulled up by the wire (or rods), and before the bottom of the tube was removed from the water, it was capped and then sealed with electrical tape. Any excess tubing was cut off, and Zorbitrol preserved the sediment-water interface. The top was then capped and sealed. We shipped cores to the Limnological Research Center (LRC) at the University of Minnesota.

Cores were named using the following convention:

PFX11-MX-N

- PFX=Prefix of cored lake
- “11” indicates that cores were collected in 2011.
- M= Site number. Sites are typically delineated by changing anchor locations
- X =Hole letter. A different letter represents the boat was moved a few meters without changing the anchor location.
- N=Thrust number.

## **2.2 Lab Work**

At the LRC, I used a Geotek Multisensor Core Logger to analyze whole cores, measuring sediment density, acoustic wave velocity, electrical resistivity, and magnetic susceptibility (MS) at approximately five-centimeter resolution. I then split and cleaned each core and archived half at the LRC. With a Geotek XYZ Core Scanner, I measured a higher-resolution MS record (0.5 cm) for each core. DMT CoreScan Colour captured high-resolution digital images (10 pixels/mm). In addition, I performed a first-order stratigraphic analysis, along with preliminary correlations of cores taken from the same lake.

Following preliminary analysis at the LRC, I shipped the cores overnight to the University of Maine and placed them in cool storage. I established a master core for each lake to focus the analysis. The ideal master core included the longest sediment record, contained the most sediment, had easy-to-identify tie points between core segments, and



was composed of the minimum number of segments necessary to cover the entire stratigraphic record.

After each master core was constructed, I analyzed them in detail. I sampled for radiocarbon dating with the focus on bracketing distinct changes in sediment type. I also spaced samples along the length of the core. I collected two types of samples. Initially, I took samples of macro-scale organic material, such as algae or leaves. I preferred macrofossils to all other sample types. These samples were washed with deionized (DI) water to remove sediment. If no macrofossils were present, I looked for organic-rich layers. I sieved sediment from such layers through a 63  $\mu\text{m}$  mesh using DI water. This process concentrated any organic material. If macrofossils could be seen, I removed them using tweezers. If none were present, I dated the concentrated organic material. After the radiocarbon samples were taken, I placed them in a  $\sim 50^\circ\text{C}$  oven until dry and then sent them to The National Ocean Sciences Accelerator Mass Spectrometry (NOSAMS) facility for analysis.

I calibrated the radiocarbon dates using CALIB v.6.1.0 (Stuiver and Reimer, 1993) and the INTCAL09 data set (Reimer et al., 2009). I assumed that any reservoir effect is negligible because of the presumed low residency time of water in these lakes and the absence of carbonate bedrock in the watershed. Lusas (2011) obtained a modern age from aquatic algae at the sediment-water interface of Emerald Lake, which has characteristics similar to lakes used in this study and which is also in the Scoresby Sund region. Ages are presented as the mean value of the  $2\sigma$  age range and are reported as calibrated years before present (cal. yBP) with an associated  $2\sigma$  error (Table 2). If there were multiple possible calibrated ranges, that with the highest probability was used in the

text and to construct age models. I present all possible age ranges above ten percent confidence in Table 2, and the majority of samples used in the age models have a confidence over eighty-five percent.

Following methods outlined in Bengtsson and Enell (1986), I performed loss-on-ignition (percent organic content) and percent carbonate analysis on the cores. The percent carbonate value potentially also could reflect clays losing water in the mineral structure. However, for simplicity I will refer to this value as percent carbonate throughout the rest of the paper. I also performed grain-size analysis based on procedures developed at Northern Arizona University's Sedimentary Records of Environmental Change Lab for preparing samples for a Coulter counter. I present a detailed description in Appendix A. I took samples for both types of analyses at two-centimeter intervals.

Table 2: Radiocarbon samples. Dates were calibrated with CALIB 6.1.

ID	Core	Depth: Below Start of Sed. (cm)	Sample Type	Radiocarbon Age ( $^{14}\text{C}$ yBP)	Error ( $1\sigma$ )	$\delta^{13}\text{C}$ (per mil)	Confidence (percent)	cal. yBP	Error ( $2\sigma$ )	Cal Age (AD/BC)
OS-95595	BNL-11-1A-1	13	Sieved	425	40	-26.6	15	350	26	1600 AD
							85	481	53	1470 AD
OS-96874	BNL11-1A-1	27.4	Macro	1150	30	-30.8	96	1062	85	889 AD
OS-96906	BNL11-1A-1	51	Sieved	2910	25	-31.7	77	3023	61	1074 BC
							23	3273	185	1174 BC
OS-95587	BNL-11-1A-1	97	Sieved	6380	30	-25.0	70	7298	40	5349 BC
							30	7384	34	5435 BC
OS-95586	BNL-11-1B-1	56	Sieved	6290	40	-29.7	100	7237	80	5288 BC
OS-95640	BNL-11-1B-1	77	Macro	7170	50	-24.6	89	7994	67	6045 BC
OS-100375	BNL11-2A-1	4	Macro	280	20	-24.2	50	307	19	1644 AD
							49	402	27	1548 AD
OS-100376	BNL11-2A-1	27.8	Sieved	1440	25	-32.8	100	1337	38	613 AD
OS-100377	BNL11-2A-1	19	Sieved	1460	20	-31.7	100	1346	39	605 AD
OS-100378	BNL11-2A-1	50.5	Sieved	3400	40	-31.0	93	3642	86	1693 BC
OS-100379	BNL11-2A-1	60	Sieved	3280	30	-32.6	99	3511	68	1562 BC
OS-100380	BNL11-2A-1	64	Sieved	3670	30	-33.5	100	3997	91	2048 BC
OS-100381	BNL11-2A-1	65	Sieved	3480	30	-32.7	97	3762	76	1813 BC
OS-100382	BNL11-2A-1	76.5	Sieved	3430	30	-32.9	81	3670	60	1721 BC
							12	3808	18	1859 BC

Table 2: Continued

ID	Core	Depth: Below Start of Sed. (cm)	Sample Type	Radiocarbon Age ( $^{14}\text{C}$ yBP)	Error ( $1\sigma$ )	$\delta^{13}\text{C}$ (per mil)	Confidence (percent)	cal. yBP	Error ( $2\sigma$ )	Cal Age (AD/BC)
OS-100516	BNL11-2A-1	77	Sieved	4410	30	-34.4	95	4960	94	3011 BC
OS-100517	BNL11-2A-1	96	Sieved	5250	30	-34.2	66	5978	53	4029 BC
							18	6098	22	4149 BC
OS-100777	BNL11-2A-1	104	Sieved	6520	35	-28.7	8	7344	16	5395 BC
							86	7459	46	5510 BC
OS-100518	BNL11-2A-2	3	Sieved	6450	30	-29.0	100	7370	58	5421 BC
OS-100519	BNL11-2A-2	9.5	Sieved	6710	30	-28.6	20	7532	23	5578 BC
							78	7589	33	5640 BC
OS-100520	BNL11-2A-2	15	Sieved	7300	35	-29.9	100	8101	76	6152 BC
OS-100521	BNL11-2A-2	22.5	Sieved	7470	35	-30.2	43	8234	36	6285 BC
							57	8323	48	6374 BC
OS-100778	BNL11-2A-2	26	Sieved	7960	40	-31.8	94	8841	150	6892 BC
OS-100522	BNL11-2A-2	29.5	Sieved	7870	35	-29.8	97	8678	100	6729 BC
OS-100779	BNL11-2A-2	33	Sieved	8500	50	-30.1	100	9494	51	7545 BC
OS-96048	RPD11-1B-1	5	Macro	960	20	-23.1	66	835	39	1116 AD
							34	912	17	1038 AD

Table 2: Continued

ID	Core	Depth: Below Start of Sed. (cm)	Sample Type	Radiocarbon Age ( <sup>14</sup> C yBP)	Error (1σ)	δ <sup>13</sup> C (per mil)	Confidence (percent)	cal. yBP	Error (2 σ)	Cal Age (AD/BC)
OS-96047	RPD11-1B-1	17.5	Macro	200	20	-25.2	18	7	7	1944 AD
							47	168	22	1783 AD
							26	282	14	1668 AD
OS-96058	RPD11-1B-1	21	Macro	250	25	-26.5	20	161	10	1789 AD
							70	299	19	1651 AD
OS-96045	RPD11-1B-1	39	Sieved	1990	25	-24.5	100	1940	53	10 AD
OS-95933	RPD11-1B-1	99	Macro	7330	55	-24.1	90	8115	103	6166 BC
OS-95567	RAV11-1A-1	9	Sieved	1080	35	-25.0	100	994	62	956 AD
OS-96907	RAV11-1A-1	24	Sieved	1890	25	-32.1	94	1831	60	119 AD
OS-95590	RAV11-1A-1	56	Macro	3660	30	-29.5	100	3992	92	2043 BC
OS-96908	RAV11-1A-1	108	Sieved	5300	35	-30.7	98	6088	99	4139 BC
OS-96909	RAV11-1A-1	125.8	Sieved	5740	40	-31.2	100	6541	102	4592 BC
OS-95588	RAV11-1A-2	4	Sieved	5880	30	-30.4	97	6697	57	4748 BC
OS-95589	RAV11-1A-2	11	Sieved	6960	35	-28.6	96	7778	85	5829 BC
OS-95566	RAV11-2A-1	9	Sieved	5250	45	-30.4	87	6022	102	4073 BC
							13	6162	18	4213 BC
OS-95569	RAV11-2A-1	71	Sieved	8180	50	-27.7	1	9145	132	7196 BC
OS-100776	RAV11-3A-1	17	Sieved	10650	55	-29.9	96	12614	89	10665 BC

## **CHAPTER 3**

### **RESULTS**

Our field team retrieved approximately 12.5 m of sediment, with 447 cm in total length (five cores) from Bunny Lake, 471 cm (five cores) from Raven Lake and 330 cm (four cores) from Rapids Lake (Table 3). An initial core description performed at the LRC is provided in Appendix B for every core.

#### **3.1 Lake Setting**

##### **3.1.1 Glacial Lakes**

Large Lake receives meltwater predominantly from the Renland Ice Cap, as well as a lesser amount from a small ice cap to the south. Large Lake currently drains to the southwest through a series of shallow, turbulent bedrock-floored streams and lakes. It is dammed on the north-east end by a confluence of different outlet glaciers from the Renland Ice Cap, and the ice cap to the south. If the dam were removed, the lake would drain to the northeast and the southwest outlet might be abandoned. An incised channel that heads at the Renland Ice Cap margin enters Large Lake at the west end and is building a large delta that partially blocks the outlet. The delta is positioned so the meltwater is able to flow both into Large Lake, as well as directly into the outlet stream to the south-west (Fig. 3).

We cored two lakes, Rapids and Bunny (Fig. 4), along the stream that exits Large Lake. Meltwater enters Rapids Lake through rapids and a waterfall. The current is confined to the southern edge of the lake and exits to the southwest in a shallow stream which then flows into Bunny Lake.

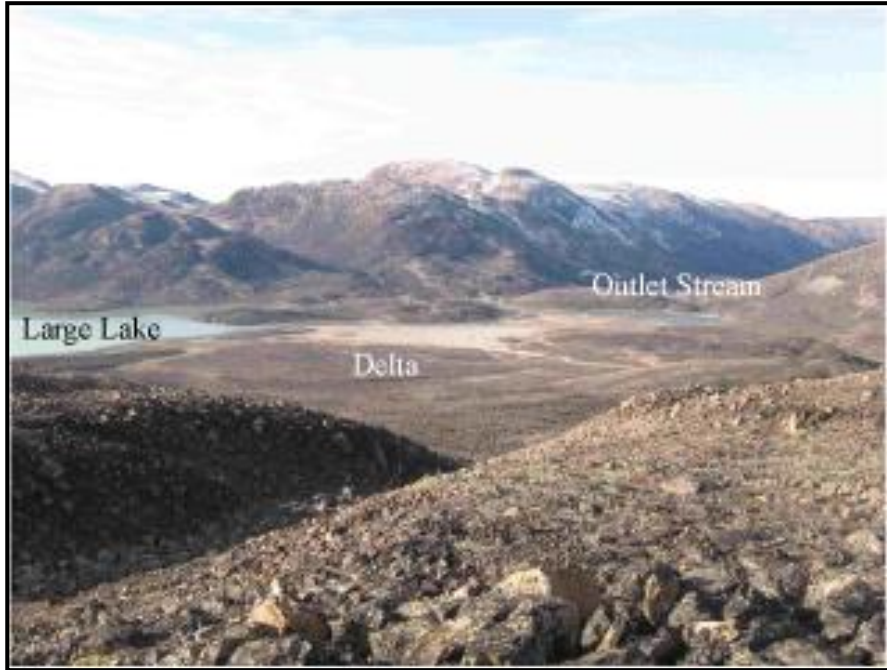


Figure 3: Delta at southwest outlet of Large Lake (view to the southwest). Image showing the delta at the mouth of the stream from Renland Ice Cap, as well as the outlet of Large Lake. View is to the south.



Figure 4: Image of Rapids and Bunny Lakes (view to the northeast). Image showing the area surrounding Rapids and Bunny Lakes. View is to the east. The area surrounding the lakes is covered by lichen-encrusted boulders and bedrock.

Table 3: Basic information on each of the cores.

Lake	Date Collected	Core Name	Water			Longitude	Elevation (m)	Core Length (m)	Depth of Core		Depth of Core Bottom below sediment surface
			Depth (m)	Latitude	Longitude				Top below Sed. Surface	Bottom below sediment surface	
Rapids Lake	8/29/2011	RPD11-1A-1	24.4	71.03248	27.41535	824	1.20	-0.2		1.0	
Rapids Lake	8/29/2011	RPD11-1C-1	24.4	71.03248	27.41535	824	0.70	-0.2		0.5	
Rapids Lake	8/29/2011	RPD11-2A-1	18	71.03307	27.4133	819	1.00	-0.2		0.8	
Rapids Lake	8/29/2011	RPD11-2B-1	18	71.03307	27.4133	819	0.40	-0.1		0.3	
Bunny Lake	8/30/2011	BNL11-1A-1	11.4	71.03118	27.42675	819	1.15	-0.2		1.0	
Bunny Lake	8/30/2011	BNL11-1B-1	11.4	71.03118	27.42675	819	1.44	0.2		1.6	
Bunny Lake	8/30/2011	BNL11-2A-1	10.1	71.03233	27.42822	823	1.30	-0.2		1.1	
Bunny Lake	8/30/2011	BNL11-2A-2	10.1	71.03233	27.42822	823	0.50	1.3		1.8	
Bunny Lake	8/30/2011	BNL11-3A-1	10.1	71.03233	27.42822	823	0.60	0.9		1.5	
Raven Lake	8/26/2011	RAV11-1A-1	15.5	71.06601	27.31106	1054	1.56	-0.1		1.4	
Raven Lake	8/26/2011	RAV11-1A-2	15.5	71.06601	27.31106	1054	0.70	1.6		2.3	
Raven Lake	8/26/2011	RAV11-2A-1	15.5	71.06601	27.31106	1054	0.93	1.3		2.2	
Raven Lake	8/26/2011	RAV11-3A-1	15.6	71.06601	27.31106	1054	0.83	1.9		2.7	
Raven Lake	8/26/2011	RAV11-4A-1	15.6	71.06601	27.31106	1054	0.88	1.2		2.1	



Rapids Lake is composed of a single steep-sided basin that reaches ~30 m depth (Fig. 5). It is surrounded by steep topography that shows evidence of mass movement, including a rockfall scar. The area surrounding the lake is covered by predominantly large, lichen-covered boulders set in a sandy matrix. The lichen-covered boulders suggests a relative stable slope that allows for lichen growth (Fig. 6).

Rapids Lake is separated from Bunny Lake by large ridges of uncertain origin. The overall feature has approximately 10 m of relief with multiple, closely spaced ridges each with 2 m relief composing the crest. Large lichen-covered boulders make up the dominant grain size on the surface. A partial reindeer skeleton was found within the deposit. This landform may represent a moraine complex, till-covered bedrock, or a large mass movement deposit. There is insufficient evidence to eliminate any of these hypotheses.

Bunny Lake (Fig. 7) has two major basins. The stream current flows through the deeper (~14 m) southern basin (Fig. 7) and exits to the northeast. The northern basin is slightly shallower (~10 m) and is removed from the current.

Bunny Lake is surrounded by steep slopes that display highly weathered, lichen-encrusted till and exposed bedrock slopes. There is evidence of past mass movements on these slopes. An abandoned stream channel enters the lake from a plateau to the south. Both this plateau and a similar one to the north are lichen-free in satellite imagery. This suggests that small ice caps or snowbanks were present on both plateaus in the recent past. Thus, this channel is a potential source of sediment into Bunny Lake, although it is likely to be small compared to that delivered from the river.

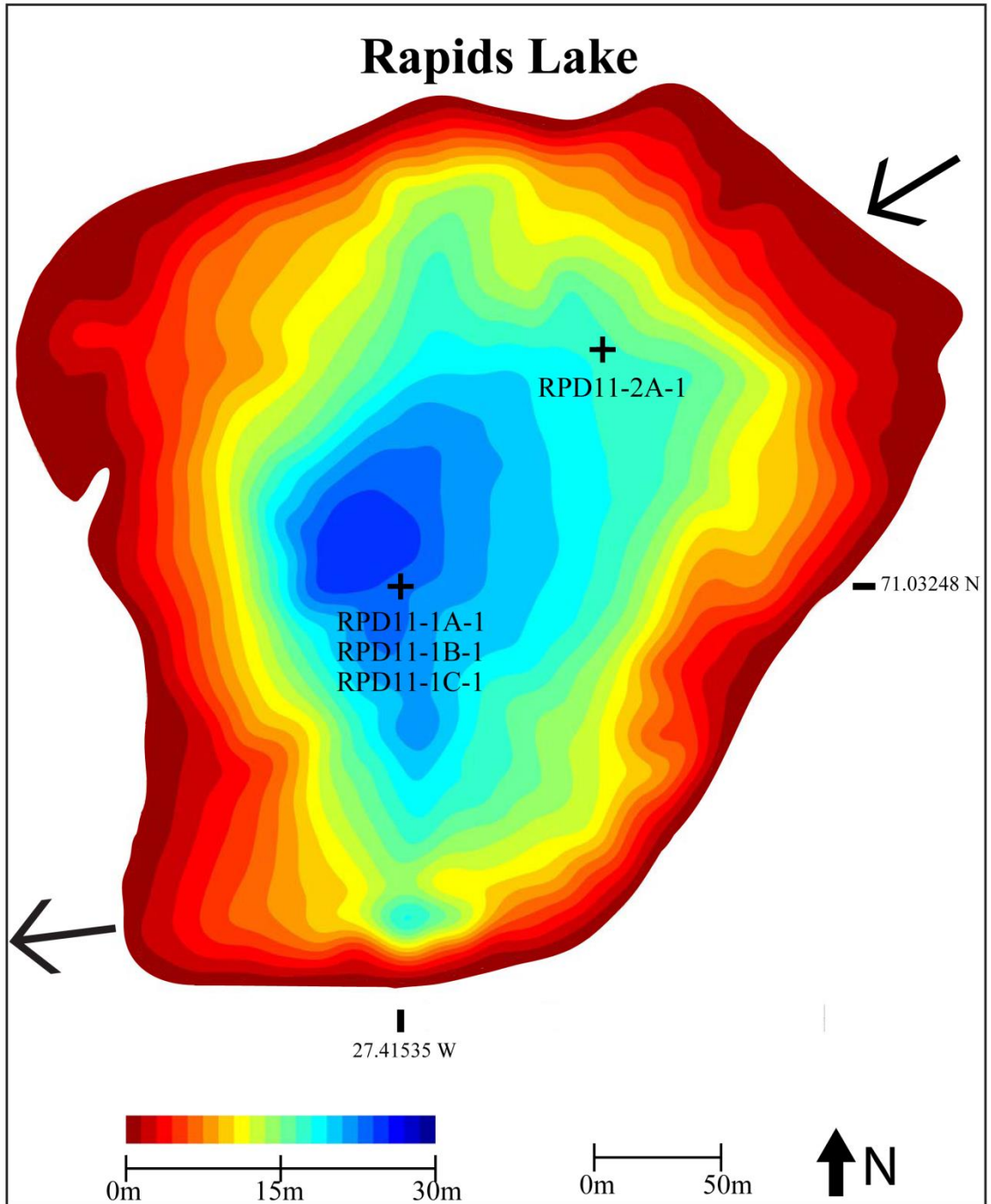


Figure 5: Bathymetric map of Rapids Lake. Image created by Paul Wilcox of the University of Cincinnati. Color scale represents depth in meters below lake surface. Second Scale represents horizontal distance. The black arrows indicate the inlet and outlet for the lake.

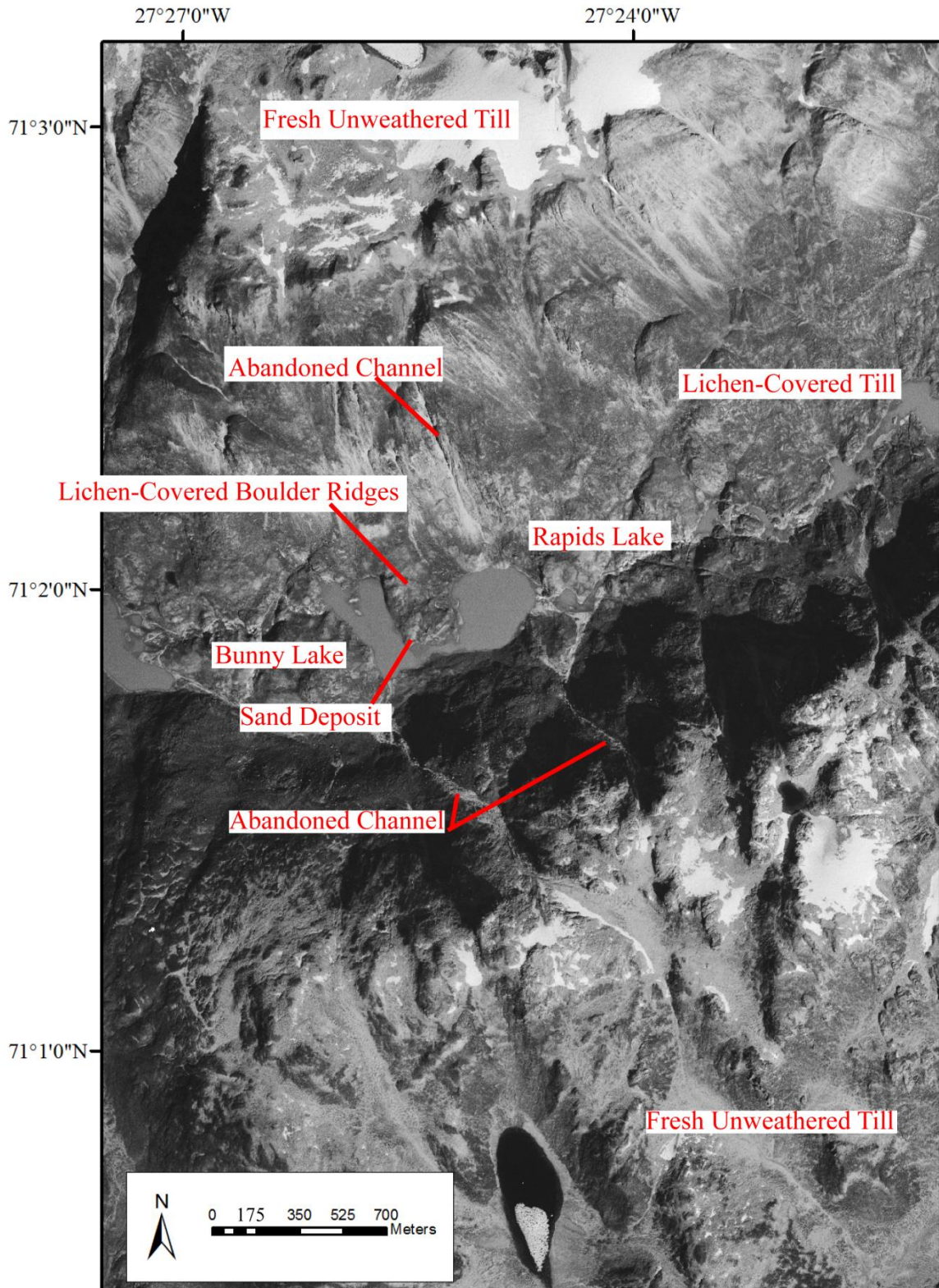


Figure 6: Aerial image of the area surrounding Rapids and Bunny Lakes. Geomorphic features indicated.

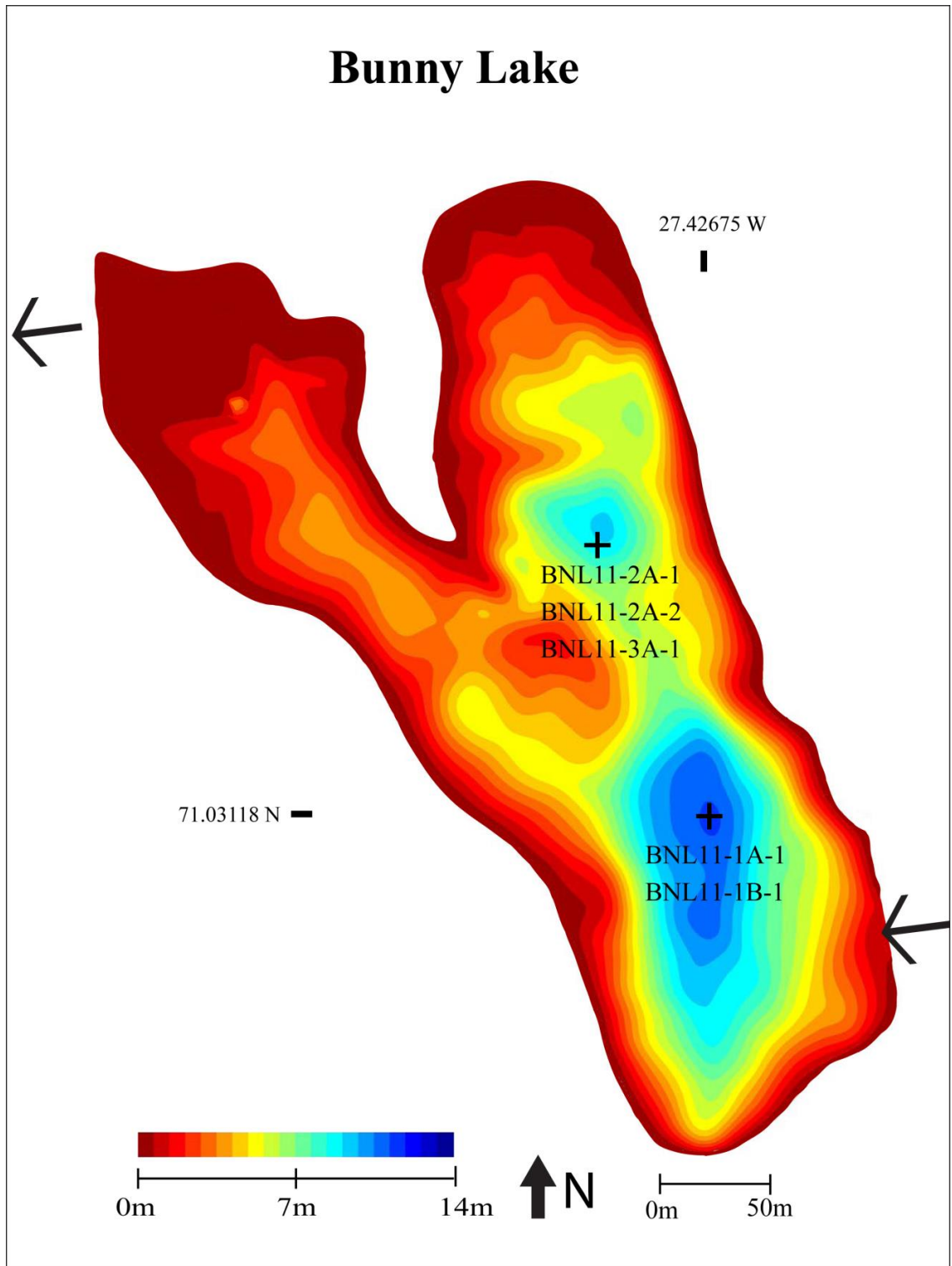


Figure 7: Bathymetric map of Bunny Lake. Image created by Paul Wilcox of the University of Cincinnati. Color scale represents depth in meters below lake surface. Second Scale represents horizontal distance. The black arrows indicate the inlet and outlet for the lake.

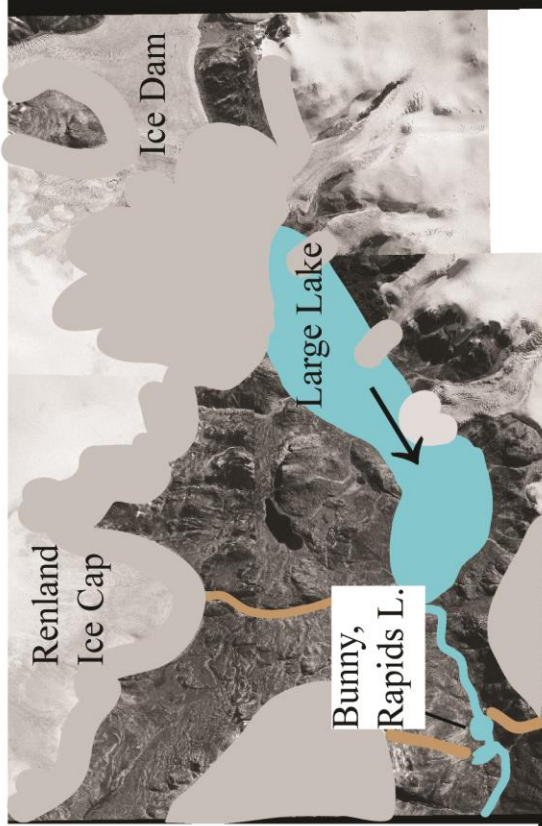
### 3.1.2 Conceptual Model

Glacial silt in Rapids and Bunny Lake is derived from overflow from Large Lake, which is fed by both outlet glaciers that terminate in the lake and by meltwater channels that extend from the surrounding ice caps (Fig. 8). Even if the outlet glaciers were to experience a modest retreat, the meltwater channels, particularly the large channel extending from Renland Ice Cap to the delta at the west end of the lake, still would contribute meltwater to the lake. Therefore, when Bunny and Rapids Lake lack glacial sediments, Large Lake, as well as any meltwater channels, must be cut off from the chain of lakes that include Bunny and Raven Lake.

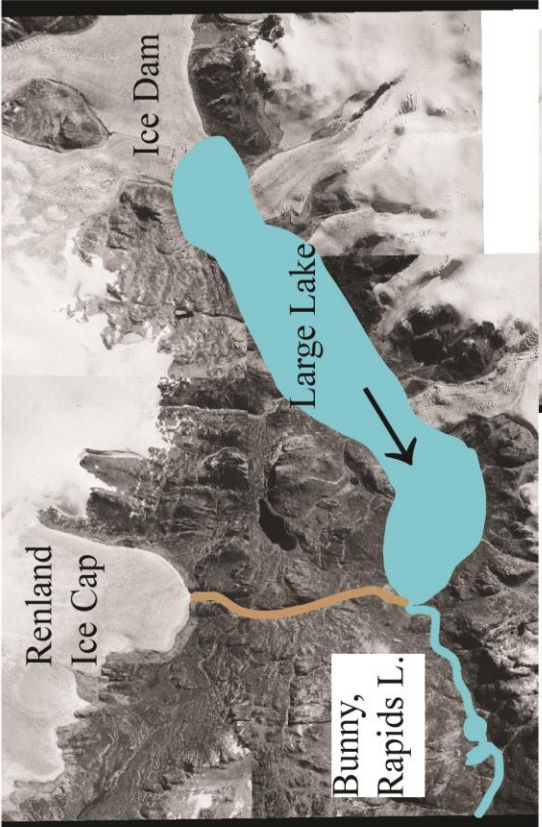
A major control on Large Lake is the behavior of the surrounding glaciers. At present, expanded glaciers dam the lake to the northeast, causing drainage to be through the western outlet into Bunny and Rapids Lakes. If the lake were not dammed by ice, water likely would flow to the northeast due to the slope of the topography. Thus, overflow of silt-laden meltwater to the west and into Bunny and Rapids Lake is a function of the presence or absence of the ice dam, not necessarily the volume of meltwater produced by the Renland Ice Cap.

Ultimately, the record produced in this study records the size of the Renland Ice Cap and the adjacent ice cap to the south. In particular, the presence of glacial sediments in Bunny and Rapids Lakes reflect times when the ice caps were sufficiently large to produce an ice dam on the northeast end of Large Lake. The ice dam controls the size of Large Lake, and therefore, whether or not the lake drains over the western bedrock outlet into Bunny and Rapids Lakes. When Large Lake can drain into Bunny and Rapids Lake, the sedimentation in both lakes is swamped by the glacial influx.

Figure 8: Conceptual model of glacial input into Rapids and Bunny Lakes. A basic model showing three key time periods. During maximum Holocene extent (LLA), outlet glaciers from Renland Ice Cap and the small ice cap to the south dammed Large Lake, which overflowed to the southwest. Expanded and new glaciers are depicted with grey color. In addition, small ice caps or snow banks on the plateaus north and south of Rapids and Bunny Lakes may have contributed glacial sediment to these lakes. These plateaus are not snow-covered at present. Today, glacial sediment reaches Bunny and Rapids Lakes because of overflow from Large Lake, and to a lesser extent because of a meltwater stream from Renland Ice Cap. During the Holocene Thermal Maximum (HTM), ice cap retreat (dotted lines represent smaller glaciers) likely allowed Large Lake to drain to the northeast. The lack of obvious glacial sediment throughout much of this time period in cores from Rapids and Bunny Lakes suggests that the meltwater stream from Renland Ice Cap today that forms the delta at the west end of Large Lake either also drained to the northeast or was inactive.



Little Ice Age



Present

HTM

Because the ice dam may take some time to form, the appearance of glacial sediment in Bunny and Rapids Lakes may be delayed compared to the time when the climate first cools and the glaciers begin to advance. The ice dam may fail multiple times during its initial formation before it becomes stable and large enough to confine Large Lake and allow it to increase to a level where it will overflow to the west. Once built, the ice dam should be stable, because the bedrock outlet should control the size of the lake. This prevents the lake from rising to a high level where it would float the dam. During deglaciation, as climate begins to warm, the dam may weaken to a point where the lake breaks through, causing a catastrophic drainage.

The plateaus on either side of Bunny and Rapids Lakes are a second potential source of glacial sediments. Lichen-free areas indicate recent cover by ice or snow. If these ice masses became sufficiently large, they may have contributed meltwater into Rapids and Bunny Lakes through the now abandoned channels that head on the plateau.

### **3.1.3 Non-Glacial Lake**

Raven Lake (Fig. 9) has an expansive, relatively flat bottom with two minor basins, the deepest of which reaches ~20 m (Fig. 10). The southwestern section of the lake is extremely shallow, less than one meter deep, and we did not create a bathymetric map of that portion.

There was only minor outflow from the lake during our field expedition, and this occurred as seep through a boulder-filled channel to the south (Fig. 11). The only obvious inflow to the lake is through a groundwater-fed channel at the eastern edge of the lake.





Figure 9: Image of Raven Lake (view to the south). Image showing the area surrounding Raven Lake. View is to the south. The area is covered predominantly by lichen-encrusted boulders. Note tents for scale.

This is sufficient to be forming a small delta. However, an increase in lake level of less than a meter would reverse this water-flow direction and create a second outlet to the southeast. A former spillway is cut into bedrock at the western end of the lake at 1064 masl, ~14 m above current lake level.

Glacial meltwater does not flow into the lake at present. However, an abandoned channel enters the northeast end of the lake and heads just distal to the LIA drift limit adjacent to Renland Ice Cap. However, because of the angularity of the boulders and the abundance of precariously perched and weathered talus in the channel, it appears that the channel has been inactive for a long time. A second channel enters the lake from the north and is incised into till. This channel heads in the highlands between the Renland Ice Cap and Raven Lake and does not appear to have been active for a long time. There is no obvious water source. This abandoned channel features two deposits of well-sorted sand,

each with five of meters relief. The upper sediments occur in flat-lying layer, which overlie dipping beds. The sand is in contrast to the large lichen-covered boulders that compose the surrounding drift. I infer that these sand deposits are deltas. These deltas occur at about 14 m above present-day lake level, the same elevation as the former bedrock spillway, and indicate a significantly higher lake level in the past, although their age is not constrained. For these higher lake levels to have occurred, the lower outlets must have been blocked by ice or by sediments. Thus, these features may date to early in the deglacial period.

The terrain surrounding the lake is covered by with lichen-encrusted boulders in a sandy matrix. I interpret this deposit as till. Till with such weathering elsewhere in the Scoresby Sund region has yielded surface exposure ages of ~10-12 ka (Lowell et al., 2013). In the valley east of the lake, the till forms multiple linear ridges, each with a few meters in relief and spaced ~20 m apart; based on geometry, these ridges are likely moraines. A second set of more continuous ridges occurs approximately one kilometer east in the same valley and has a relief of ~10 m. These ridges slope down to the southeast. I infer that they also are moraines. Due to differences in orientation and scale, the two sets may be of different age. There are also ridges near the groundwater inlet at the southeast end of the lake. These are segmented and somewhat chaotic, but the overall orientation is across the valley. A small-scale, roughly circular depression a few meters

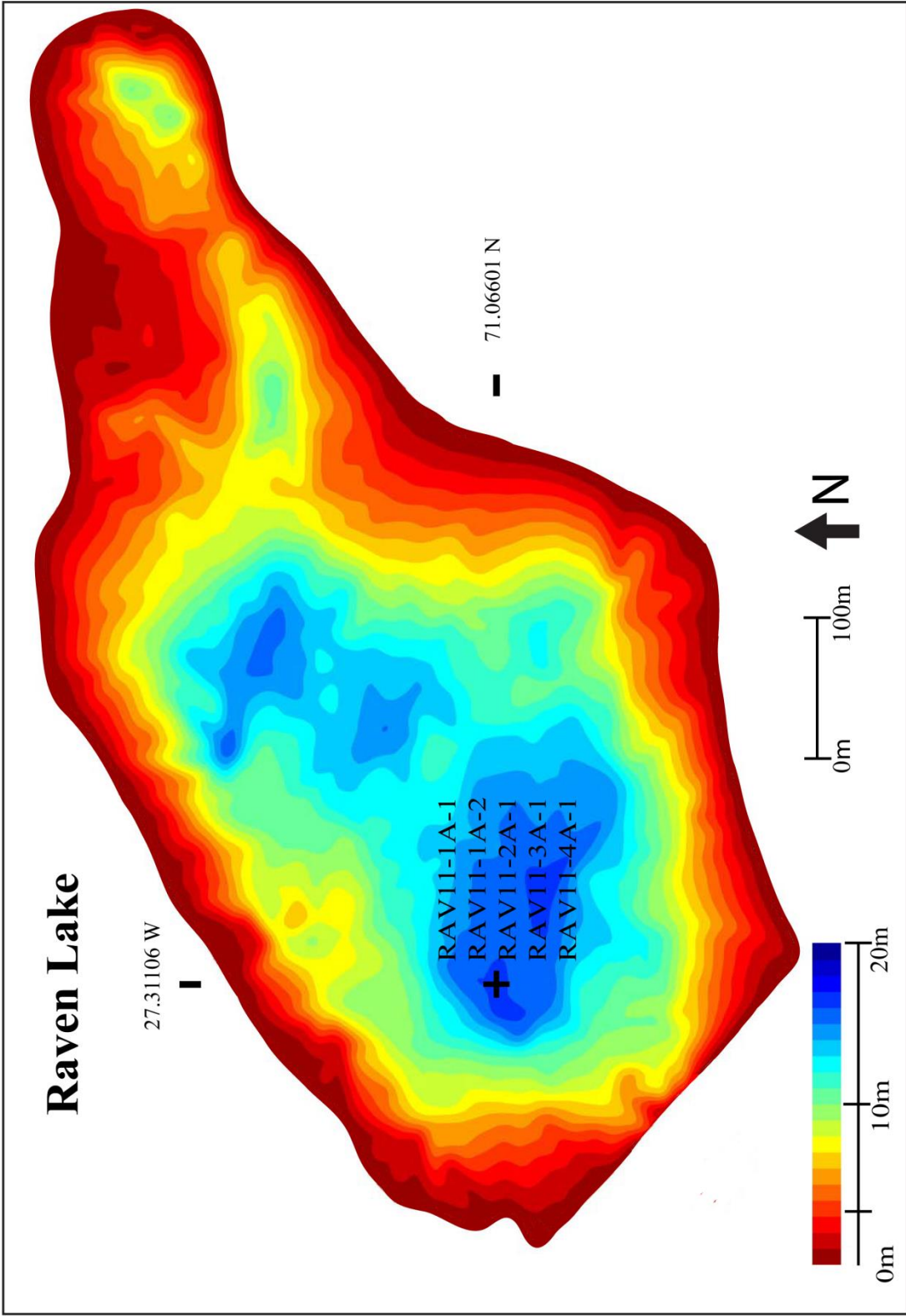


Figure 10: Bathymetric map of Raven Lake. Image created by Paul Wilcox of the University of Cincinnati. Color scale represents depth in meters below lake surface. Second Scale represents horizontal distance.

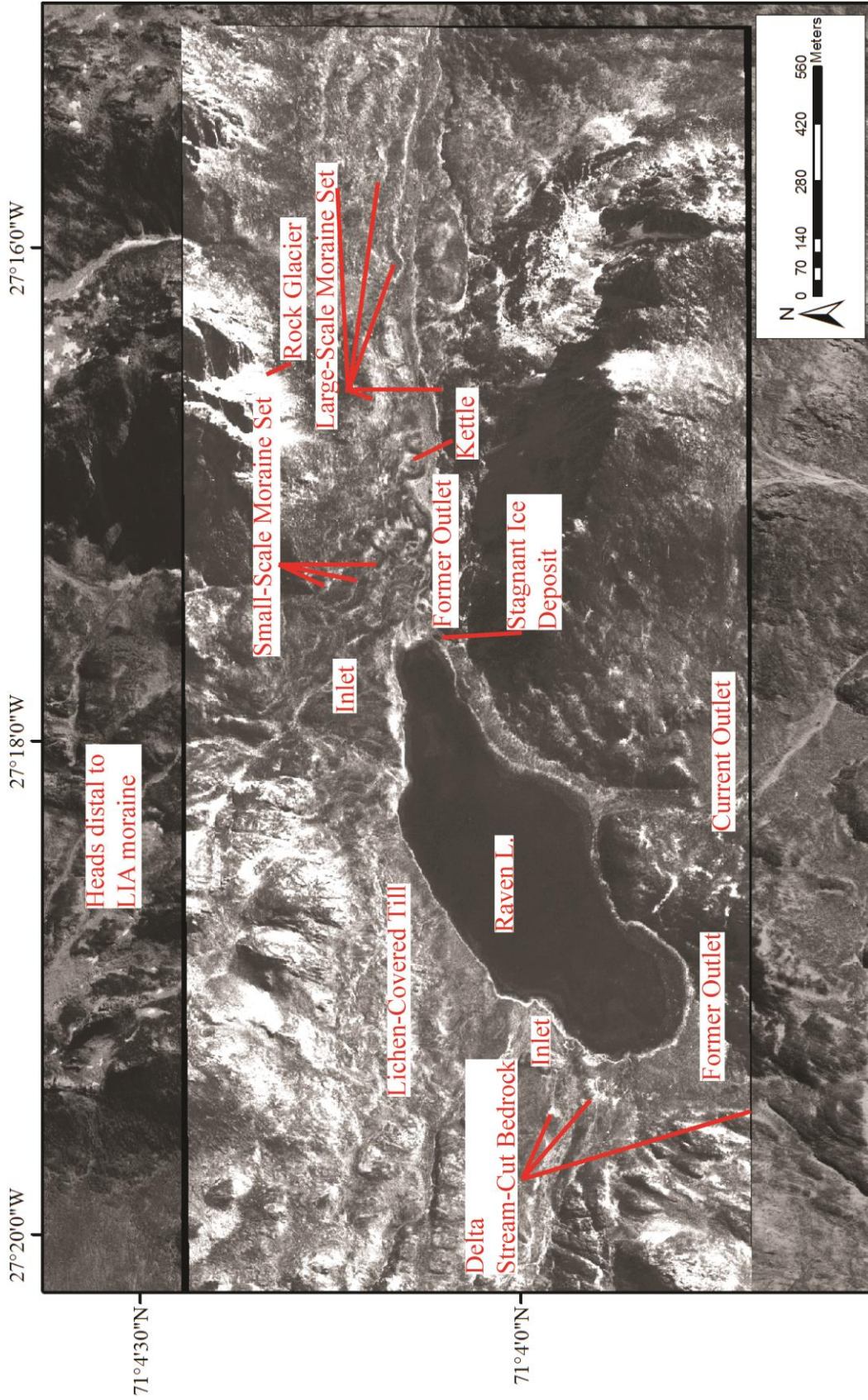


Figure 11: Aerial image of the area surrounding Raven Lake . Geomorphic features indicated.

deep may be a kettle. On the opposite side of the valley, close to lake level, there are multiple hills with a few meters in relief that are composed predominantly of sand and gravel with a few large boulders. All of these features may represent ice-recession or stagnation features.

On the east slope of the same valley, there is a large deposit (~20 m of relief) with a steep front and a broad flat top is composed of large, lichen-covered boulders. Based on its form and composition, this deposit is a relict rock glacier (Martin and Whalley, 1987).

## **3.2 Sediment Core Descriptions**

### **3.2.1 Rapids Lake**

We took four cores from Rapids Lake (Table 3, Fig.12). Because they all show the same stratigraphy, I chose the longest record, RPD11-1B-1, as the master core (Fig. 13, 14).

#### **3.2.1.1 RPD11-1B-1**

From the base of the sediments (112 cm depth) to 83 cm depth, RPD11-1B-1 is composed of a laminated black (10 YR 2/1) clayey-silt (Fig. 13, 14). Coarser reddish-gray (2.5 YR 6/1) layers of clayey-silt punctuate the darker clayey silt at 101-104, 90, 89, and 83 cm depth. Two massive reddish-gray fine sand layers with black flecks also occur at 98-99 and 94-9 cm depth.

The laminated black clayey silt is overlain abruptly by a very finely laminated dark brown clayey-silt at 83 cm depth. This unit is 46 cm thick with laminations (approximately 0.1 cm thick) that vary slightly in color with the predominant color being

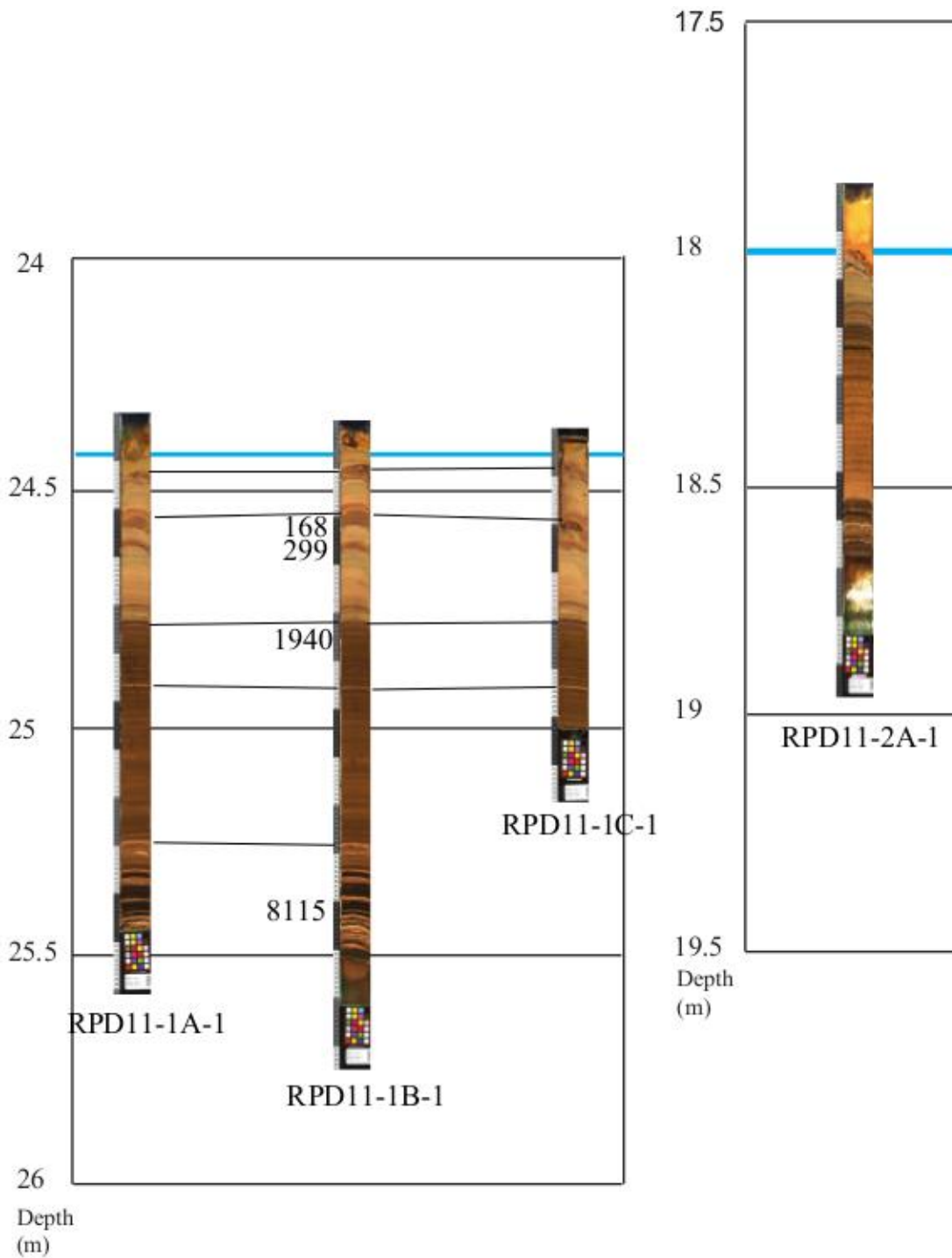


Figure 12: Rapids Lake cores plotted by depth below water surface. Ages of radiocarbon dates are given in cal. yBP. Black lines between cores show tie points, and blue lines show the sediment-water interface. Note change of scale for RPD11-2A-1.

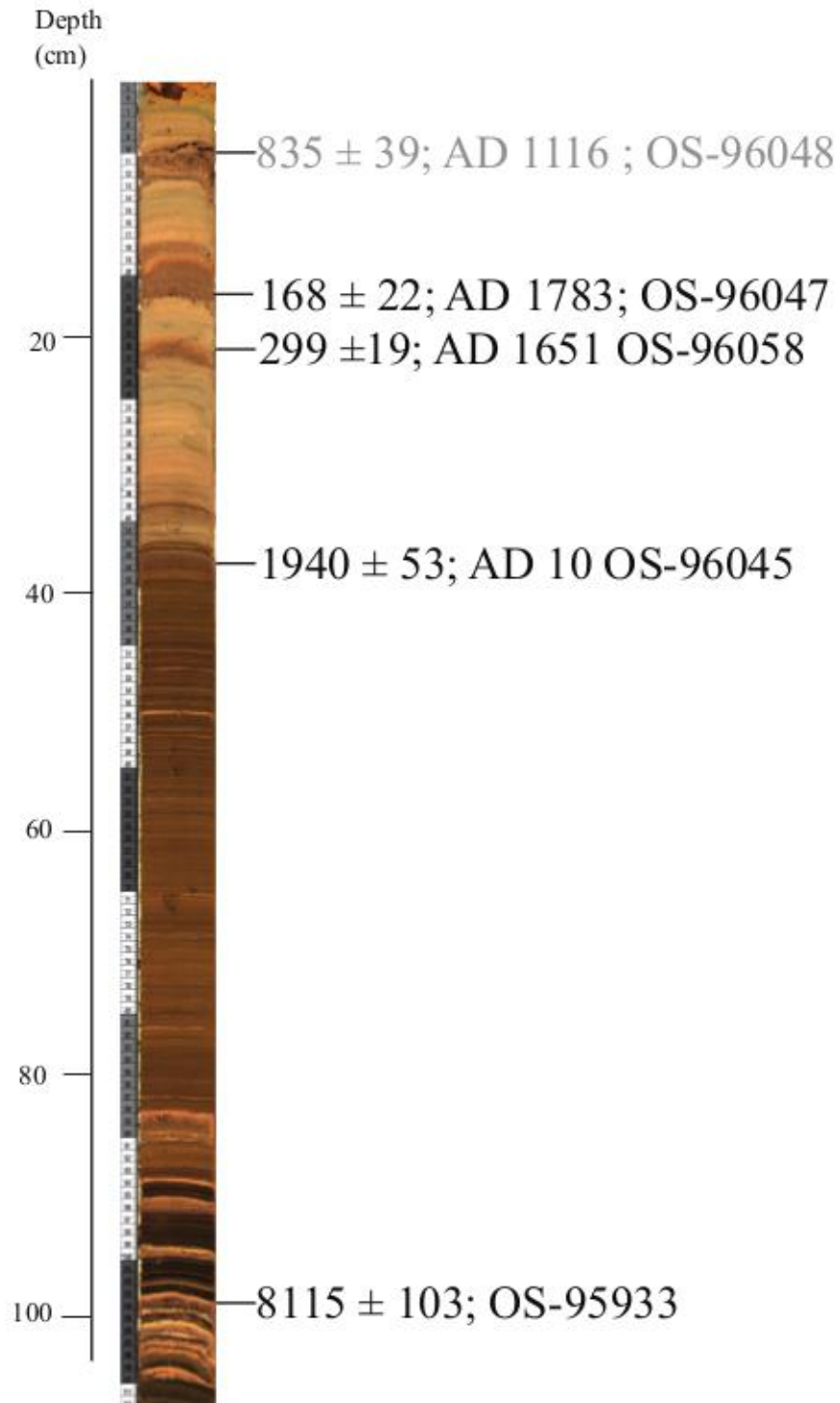


Figure 13: Radiocarbon dates for RPD11-1. The grey number is out of stratigraphic order and is omitted from further discussion.

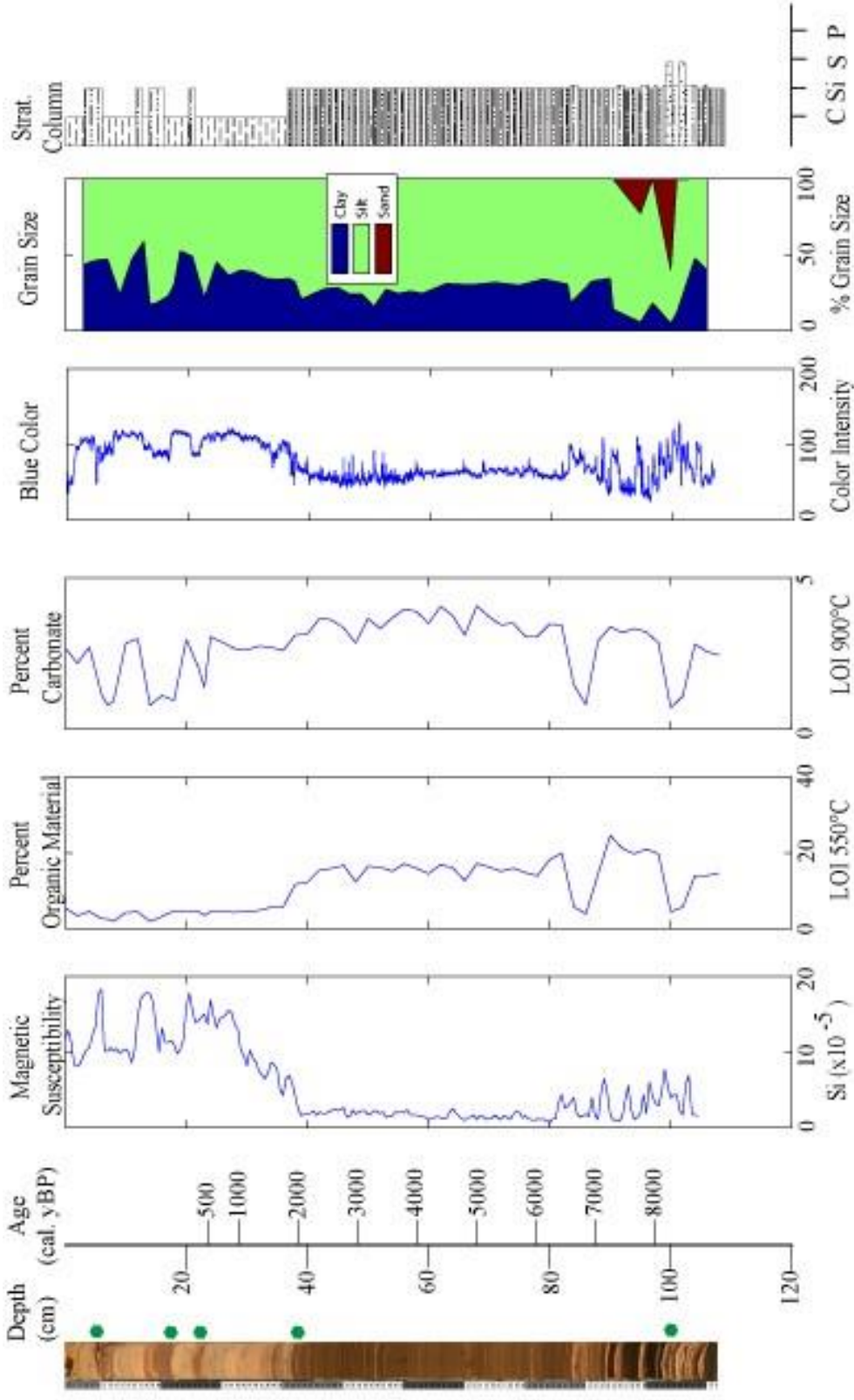


Figure 14: Data for RPD11-1, the master core for Rapids Lake. Ages were calculated with the age model. Y-axis tick marks relate to depth. The first grain size panel shows data measured on a Coulter Counter, whereas that in the stratigraphic column was based on visual observation. The first grain size panel is separated into percent clay (blue), silt (green), and sand (red). The stratigraphic column width is determined by grain size clay (c), silt (Si), sand (S), and pebble (P). Green points indicate location of radiocarbon samples.



dark brown (7.5YR 3/2). Black flecks occur at 75-82 cm depth. A prominent, light-colored band (0.3 cm thick) is present at 51 cm depth. Additional gray bands (0.1 mm thick) occur at 82, 76, 68.5, and 65 cm depth and at every few centimeters between 40-53 cm depth.

There is an intercalated transition at 37-38 cm depth from the lower laminated dark brown sediment to the overlying laminated (centimeter-scale) gray (7.5YR 6/1) silty-clay. The gray clay persists to the top of the core. A massive dark brown (7.5YR 3/2) clayey-silt is interbedded in the gray clay at 21-22, 15-17, 13-14, and 5-8 cm depth. The dark brown clayey-silt is capped with oxidized layers at 21 and 14 cm depth. We started coring RPD11-1B-1 above the sediment-water interface, and therefore the top sediment represents the modern lake bottom.

Magnetic susceptibility (MS) throughout the core is variable. Generally, values are low ( $\sim 1 \times 10^{-5}$  SI) in laminated organic-rich silts and high ( $\sim 5 \times 10^{-5}$  SI) in the gray clays and sands. At ~83-38 cm depth, the values change to a low background level ( $\sim 2 \times 10^{-5}$  SI) corresponding to the very finely laminated dark brown silt. The MS gradually increases throughout this unit. In the upper 40 cm, the MS alternates between  $\sim 10 \times 10^{-5}$  SI for the dominant gray clay, and  $\sim 19 \times 10^{-5}$  SI for the interbedded dark brown silt.

The percent organic material and percent carbonate show variability similar to that of the MS data and stay relatively constant from 116-81 cm depth (at 20% and 3%, respectively) except for two major decreases at 87 and 101 cm depth. That at 101 cm depth corresponds to a sand layer, whereas the drop at 87 cm depth does not have an obvious connection with a sedimentological change. The lack of significant variability in

the organic content despite many sedimentological changes results in part from the two-centimeter sampling interval. From 83-38 cm depth, organic material and percent carbonate remain at ~15% and 4%, respectively, although both gradually decrease upward. The sediment becomes less organic (one percent) at the transition to clay at 38 cm depth) and maintains this low level throughout the upper part of the core. The dark brown silt that interrupts the clay unit is even less organic.

The blue color intensity profile resembles the inverse of the organic content but shows more detail because of higher sampling resolution. Rapid fluctuations occur in the color intensity from 83 cm depth to the bottom of the core and vary with sedimentology. The blue color remains relatively constant (~125) from 83-38 cm depth, although above 60 cm, the profile is more variable. The color intensity lowers to ~100 at the contact with the overlying gray clay. This value is maintained to the top of the core except for within the interbedded dark brown clayey silt in which the blue color increases slightly.

I sent four samples of algae macrofossils and one sample of sieved organic fragments for radiocarbon analysis at NOSAMS (Table 2). Algae from an organic-rich fine sand at 104 cm depth yielded an age of  $8115 \pm 103$  cal. yBP (OS-95933). Algae samples OS-96047 ( $168 \pm 22$  cal. yBP) and OS-96058 ( $299 \pm 19$  cal. yBP) bracket the gray clay layer at 17-21 cm depth. I collected (OS-96045,  $1940 \pm 53$  cal. yBP) from a one-centimeter-thick organic-rich layer from the dark brown laminated silt, at two centimeters below the transition at 38 cm depth. The uppermost algae sample (OS-96048,  $835 \pm 39$  cal. yBP) came from directly below the upper gray clay unit at 5 cm depth.

### **3.2.2 Bunny Lake**

I established two master cores for Bunny Lake (Table 3, Fig. 15) BNL11-1A-1 and BNL11-1B-1 form the master core (Fig. 16, 17) for the southern basin, whereas BNL11-2A-1 and BNL11-2A-2 are used for the northern basin (Fig. 18, 19).

#### **3.2.2.1 Southern Basin: BNL11-1A-1**

Very dark grayish-brown (10YR 3/2) clayey silt (25% clay and 75% silt) composes the sediments from 26-114 cm depth, (Fig. 16, 17). The lowest 15 cm is very finely laminated (millimeter-scale), alternating between the dominant black (5YR 2/2) sediment and less prominent very dark grayish-brown (10YR 3/2) and rare gray (10YR 6/1) laminae. The unit is mostly massive above 26 cm depth, and the color grades from black (5Y 2.5/1) at 97 cm depth to very dark brown (10YR 2/2) at 51 cm depth, a color it maintains to the top of the unit. A band of relatively organic material occurs from 60-61 cm depth, and layers of massive gray (10YR 6/1) clayey-silt occur at 52.5, 86 and 97.5-99 cm depth.

Gray (10YR 6/1) laminated (centimeter-scale) clayey silt to silty clay (~25% clay at bottom of the unit to 65% at the top) overlies these lower sediments with an abrupt contact at 37 cm depth. Two thin oxidized layers (20.5 cm and 21 cm depth) and a reddish-brown silt layer (21.5 cm depth) punctuate this unit. An abrupt transition to a massive, dark reddish gray (2.5YR 3/1), silty fine sand occurs at 14 cm depth. This unit extends to five centimeter depth where there is an intercalated transition with the overlying silty clay. A massive reddish-brown layer (2.5YR 5/2) composed of equal parts

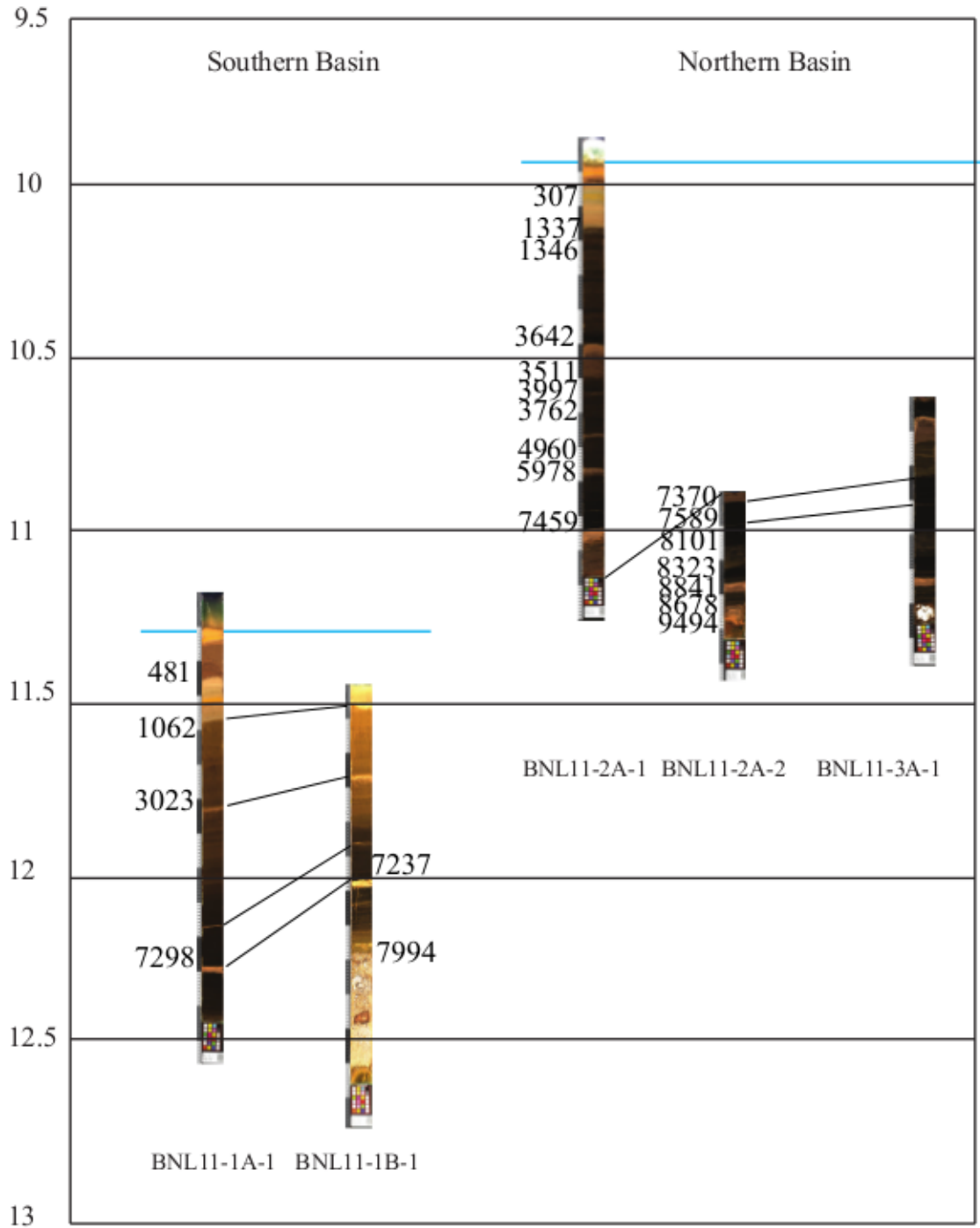


Figure 15: Bunny Lake cores plotted by depth below water surface. Ages of radiocarbon dates are given in cal. yBP. Black lines between cores show tie points, and blue lines

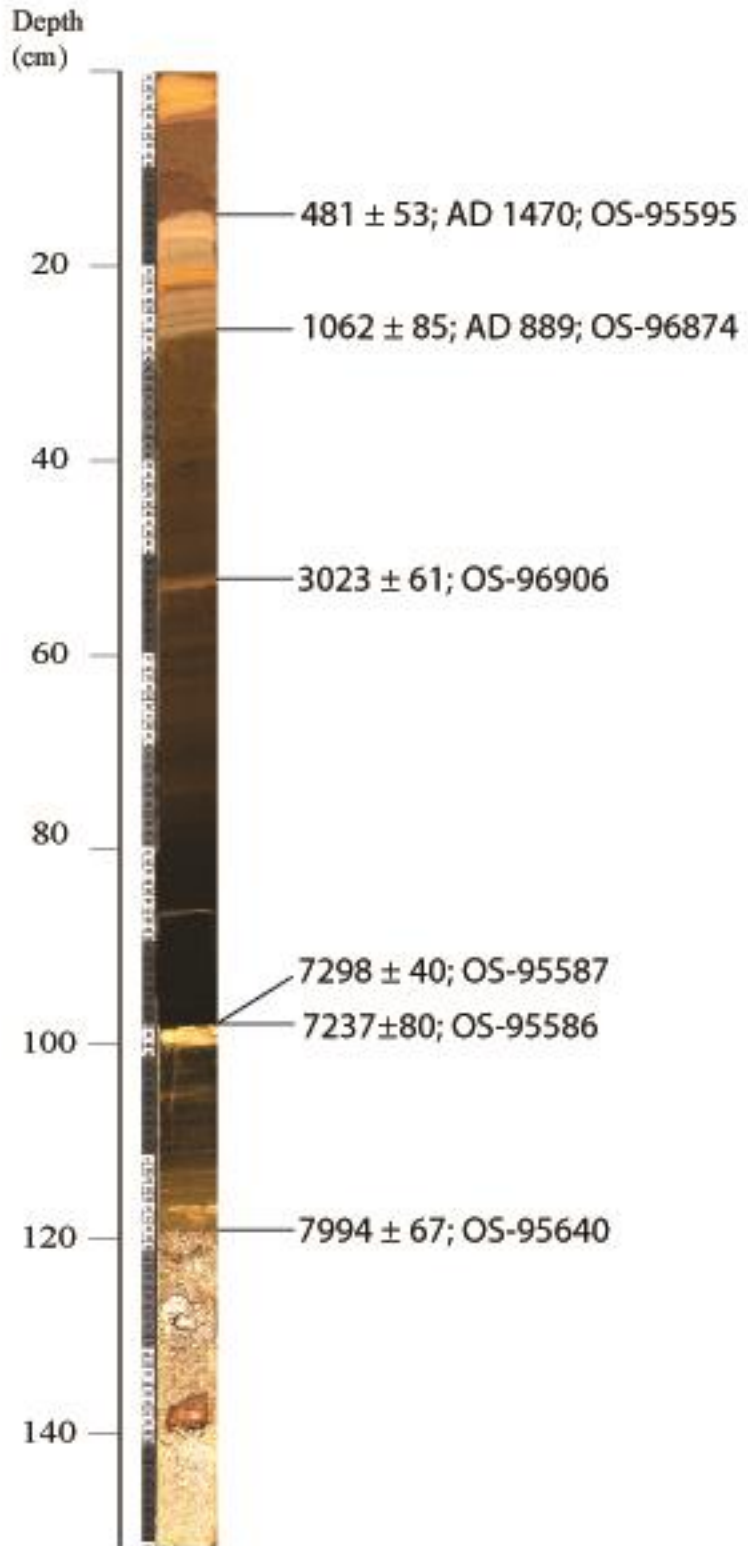


Figure 16: Radiocarbon dates for BNL11-1.

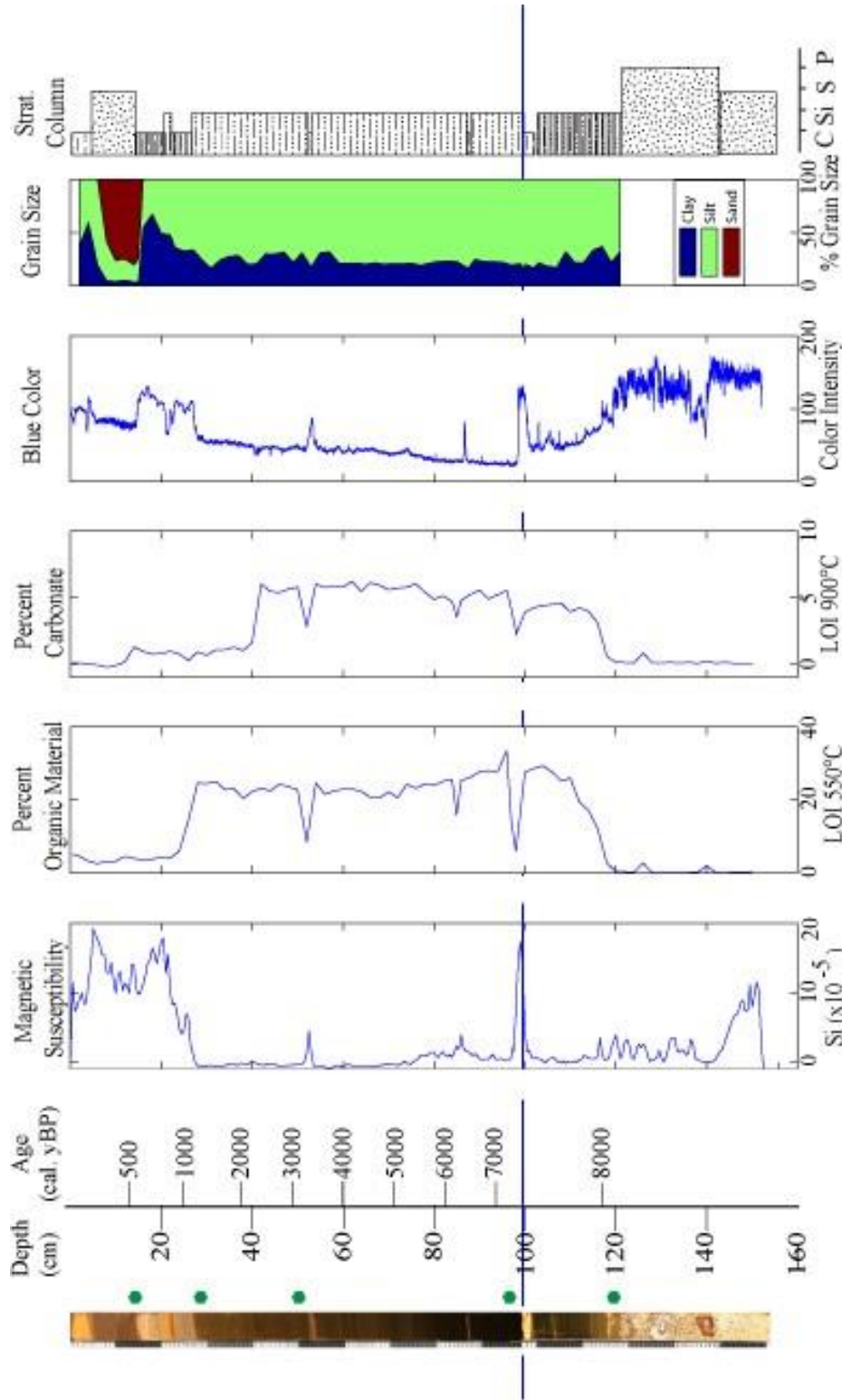


Figure 17: Data for BNL11-1, the master core for the south basin in Bunny Lake. Ages were calculated with the age model. Y-axis tick marks relate to depth. The blue line indicates a core break between BNL11-1A-1 and BNL11-1B-1. The first grain size panel shows data measured on a Coulter Counter, whereas that in the stratigraphic column was based on visual observation. The first grain size panel is separated into percent clay (blue), silt (green), and sand (red). The stratigraphic column width is determined by grain size clay (c), silt (Si), sand (S), and pebble (P). Green points indicate location of radiocarbon samples.

of clay and silt occurs from 0-5 cm depth and is punctuated by a single oxidized layer (0.5 cm thick) at 3 cm depth. We started to collect the core above the sediment-water interface, and therefore the top sediment represents the modern lake bottom

The MS data remain relatively stable throughout the lowest 88 cm of the core ( $\sim 1 \times 10^{-5}$  SI). This background level is punctuated by sharp peaks reaching as much as  $\sim 15 \times 10^{-5}$  SI, which correspond to the light gray silty-clay layers. From 26-21 cm depth, the MS steadily increases and is relatively high ( $\sim 14 \times 10^{-5}$  SI) in the upper part of the core, regardless of grain size. There are two peaks, one at 5 cm depth, and a second at 21 cm depth.

Throughout the core, the percent organic material and percent carbonate generally change together and show similar trends except between 40-50 cm. The values for organic material start at  $\sim 25\%$  at the bottom of the core and gradually decrease to  $\sim 20\%$  at 26 cm depth. Organic content shows significant and distinct decreases corresponding to the light gray clayey-silt layers at 51, 86, and 97-99 cm depth. At the sedimentological transition at 26-21 cm depth, the value decreases from 20% to  $\sim 1\%$  and stays low through the upper 26 cm of the core despite variations in sedimentology. The percent carbonate remains low (1-5%) throughout the core.

The blue color intensity gradually increases from the brown organic silt near the base to the top of the core. Superimposed on this overall trend are prominent spikes at the gray clayey-silt layers at 51, 86, and 97-99 cm depth, and above 26 cm depth, where it shows three peaks. The blue color intensity appears to correlate negatively with the percent organic material (Fig. 20).

I sent four samples to the NOSAMS (Table 2). Sample OS-95587 ( $7298 \pm 40$  cal. yBP) was from directly above the gray inorganic band at 97 cm depth. An additional sample (OS-96874), from directly above the prominent gray inorganic band at 51 cm depth, yielded an age of  $3023 \pm 61$  cal. yBP. OS-95595 ( $481 \pm 53$  cal. yBP) and OS-96874 ( $1062 \pm 85$  cal. yBP) bracket the top and bottom, respectively, of the gray inorganic unit occurring from 13-26 cm depth.

### **3.2.2.2 Southern Basin: BNL11-1B-1**

BNL11-1B-1 (Fig. 16, 17) is composed of poorly sorted sand and gravel from 78-110 cm depth. Clasts are sub-rounded and are of a variety of sizes and lithologies, including crystalline rocks such as granite. The largest clast is approximately five centimeters in diameter. Below 99 cm depth, the larger-sized gravel particles are absent and only sand is present.

At 78 cm depth, there is an abrupt transition to a silt unit that occurs to 5 cm depth. From 59-78 cm depth, the silt is laminated (millimeter-scale), and the sediment grades in color from very dark brown (10YR 2/2) at the base to black (5YR 2.5/1) higher in the unit. Gray (10YR 6/1) bands (0.1 cm thick) punctuate the more organic-rich brown silt every few centimeters. Above 59 cm depth, the silt is massive and grades from black (5Y 2.5/1) to very dark brown (10YR 2/2) at ~35 cm depth to very dark grayish-brown (10YR 3/2) in the upper 10 cm of the unit. This organic-rich silt is punctuated by gray (10YR 6/1) massive silt layers at 57-59 (2 cm thick), 46 (0.5 cm thick), 27 (1 cm thick), and 6 (0.5 cm thick) cm depth. Massive, dark reddish-gray (2.5YR 5/2), silt overlies the



darker organic-rich silts with an abrupt contact at 5 cm. An organic-rich layer occurs at the contact.

From the bottom of the core to 78 cm depth, both organic and carbonate content are negligible. At 78 cm depth, these increase to 30% and 5 %, respectively, corresponding to the change to silt. Between 10-78 cm depth, organic material and carbonate remain relatively except at 27, 46, and 57 cm depth where the values decrease, corresponding to the light-colored layers. MS increases at these same depths. A very slight decrease in organic content occurs higher in the unit, but does not correspond to any increases in MS. The upper five centimeters of the core show high MS values ( $\sim 10 \times 10^{-5}$  SI) and low organic and carbonate content (4% and 1%, respectively).

The blue color intensity follows the same pattern as the other proxies and is consistently high in the lowest ~30 cm of core. At 78 cm depth, the blue color decreases to ~50 and shows a gradual baseline rise throughout the rest of the core. Superimposed on this trend are sharper increases at 27, 46, and 57 cm depth, corresponding to gray clay layers. It also increases in the highest six centimeters of the core.

AMS dates of an algal macrofossil from 78 cm depth at the contact between clayey-silt and the underlying sand and gravel yielded an age of  $7994 \pm 67$  cal. yBP (OS-95640). Sieved organic fragments at 57 cm depth directly above the large prominent gray inorganic layer produced an age of  $6290 \pm 40$  cal. yBP (OS-95584).

### **3.2.2.3 Northern Basin: BNL11-2A-1**

The lowest 10 cm of BNL11-2A-1 are a massive dark reddish gray (2.5YR 3/1) fine sand (Fig. 18, 20). A sharp contact between the sand and a layer of massive gray

(10YR 6/1) clay (3 cm thick) occurs at 108 cm depth. At 105 cm depth, the sediment changes to a massive organic silt which persists with some interruptions to 19 cm depth. The color changes gradually from black (5Y 2.5/1) at the base of this unit to dark grayish-brown (10YR 3/2) at the top. Black bands of silt, occurring approximately 5-10 cm apart, occur throughout the unit. In addition, massive gray (10YR 6/1) clayey-silt bands punctuate the grayish-brown silt at 102.5 (0.1 cm thick), 99 (0.2 cm thick), 87-88.5 (1.5 cm thick), 78 (0.5 cm thick), 65.5 (0.1 cm thick), and 51-60 cm depth. Dark reddish-gray sand compose the lowest portion of the gray layer at 87.5-88.5 cm and 53-60 cm depth.

An intercalated transition occurs at 17-21 cm depth from the very dark grayish-brown silt to layered (centimeter-scale) gray (10 YR 6/1) clay, which persists until 4 cm depth. Between 8 and 9 cm depth, five oxidized layers (0.1 cm thick) punctuate this clay. A massive dark reddish-gray (2.5YR 3/1) fine sand occurs from 3-4 cm depth and is overlain by a reddish-brown (2.5YR 5/2) clay. This latter unit persists to the top of the core, interrupted only by an oxidized layer (0.1 cm thick) at 2 cm depth.

The MS data for the core follows the changes in sediments, with the clayey silt having the higher values. Each gray band has a corresponding peak in the MS values, reaching  $\sim 15 \times 10^{-5}$  SI. The brown silt has lower MS, values, with an average of  $\sim 9 \times 10^{-5}$  SI. Organic material and carbonate content stay at approximately 20% and 4% percent, respectively, in the brown silt, and both decrease significantly at the gray clayey-silt layers. The blue color intensity is low for the organic-rich brown silt ( $\sim 20$ ). The values peak, at the gray bands. The color intensity is highest in the upper gray clay unit (upper 27 cm of core).

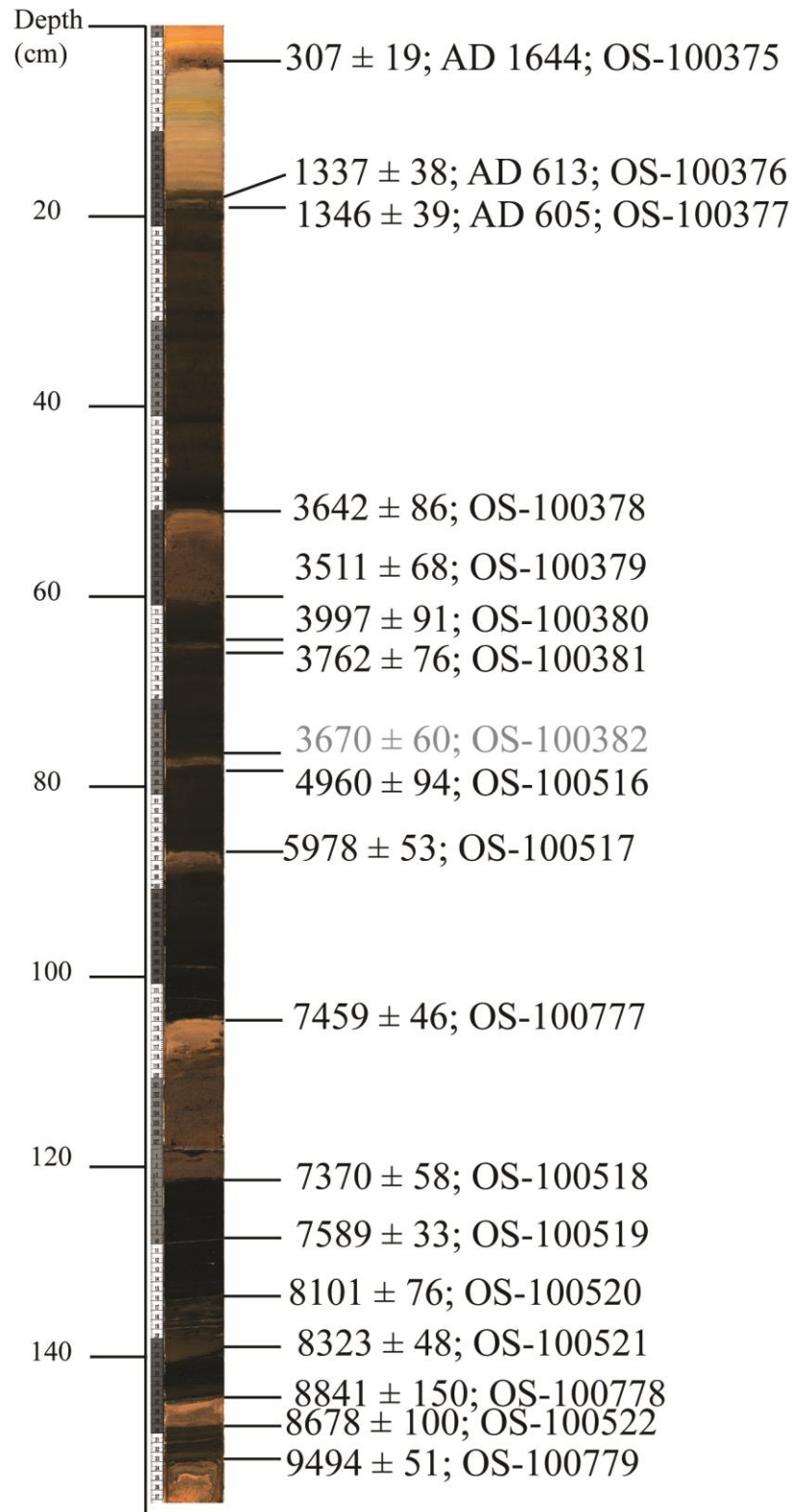


Figure 18: Radiocarbon dates for BNL11-2. The grey number is out of stratigraphic order and is omitted from further discussion.

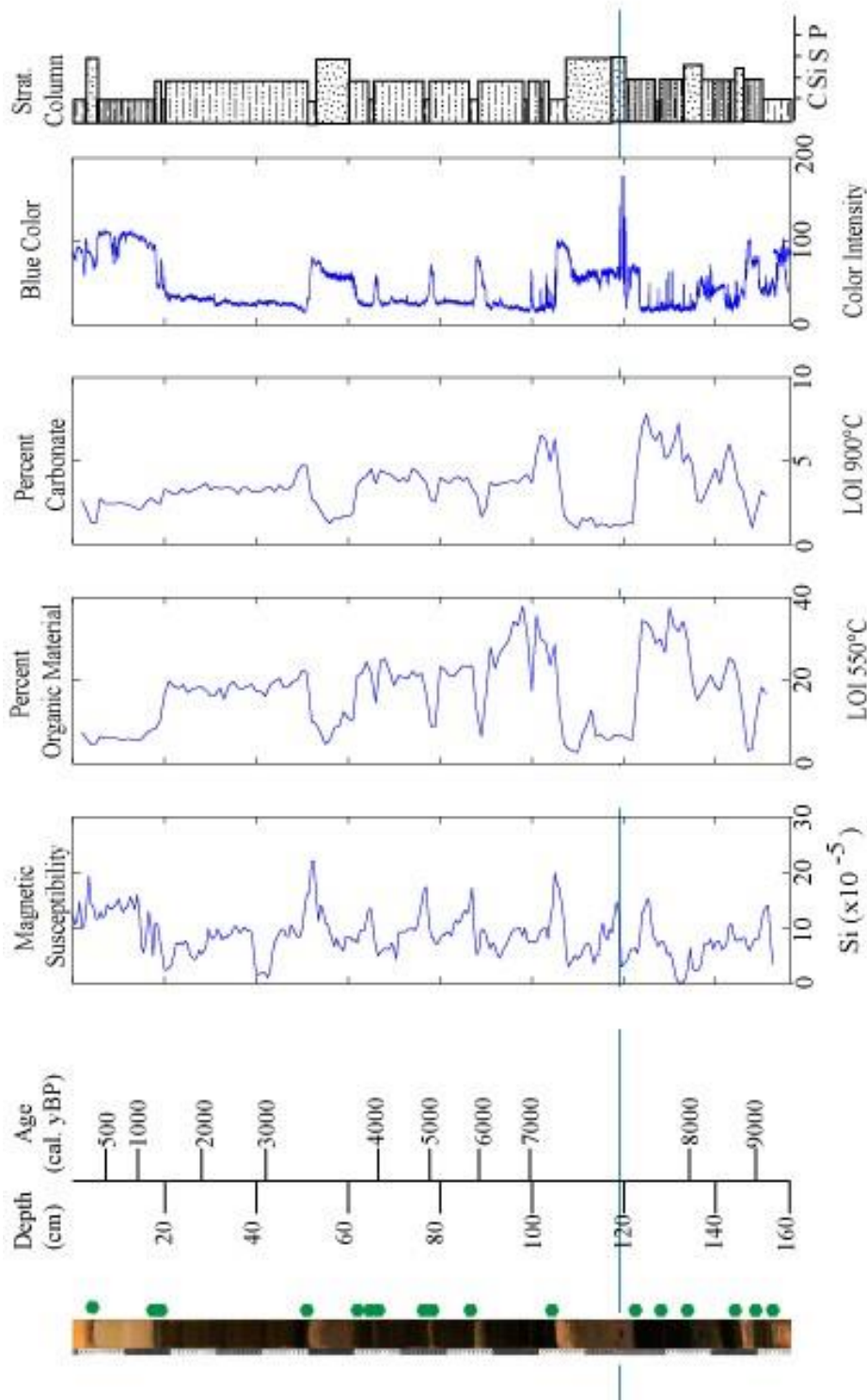


Figure 19: Data for BNL11-2, the master core for the north basin in Bunny Lake. Ages were calculated with the age model. Y-axis tick marks relate to depth. The blue line indicates a core break between BNL11-2A-1 and BNL11-2A-2. The first grain size panel shows data measured on a Coulter Counter, whereas that in the stratigraphic column was based on visual observation. The first grain size panel is separated into percent clay (blue), silt (green), and sand (red). The stratigraphic column width is determined by grain size clay (c), silt (S), sand (S), and pebble (P). Green points indicate location of radiocarbon samples.

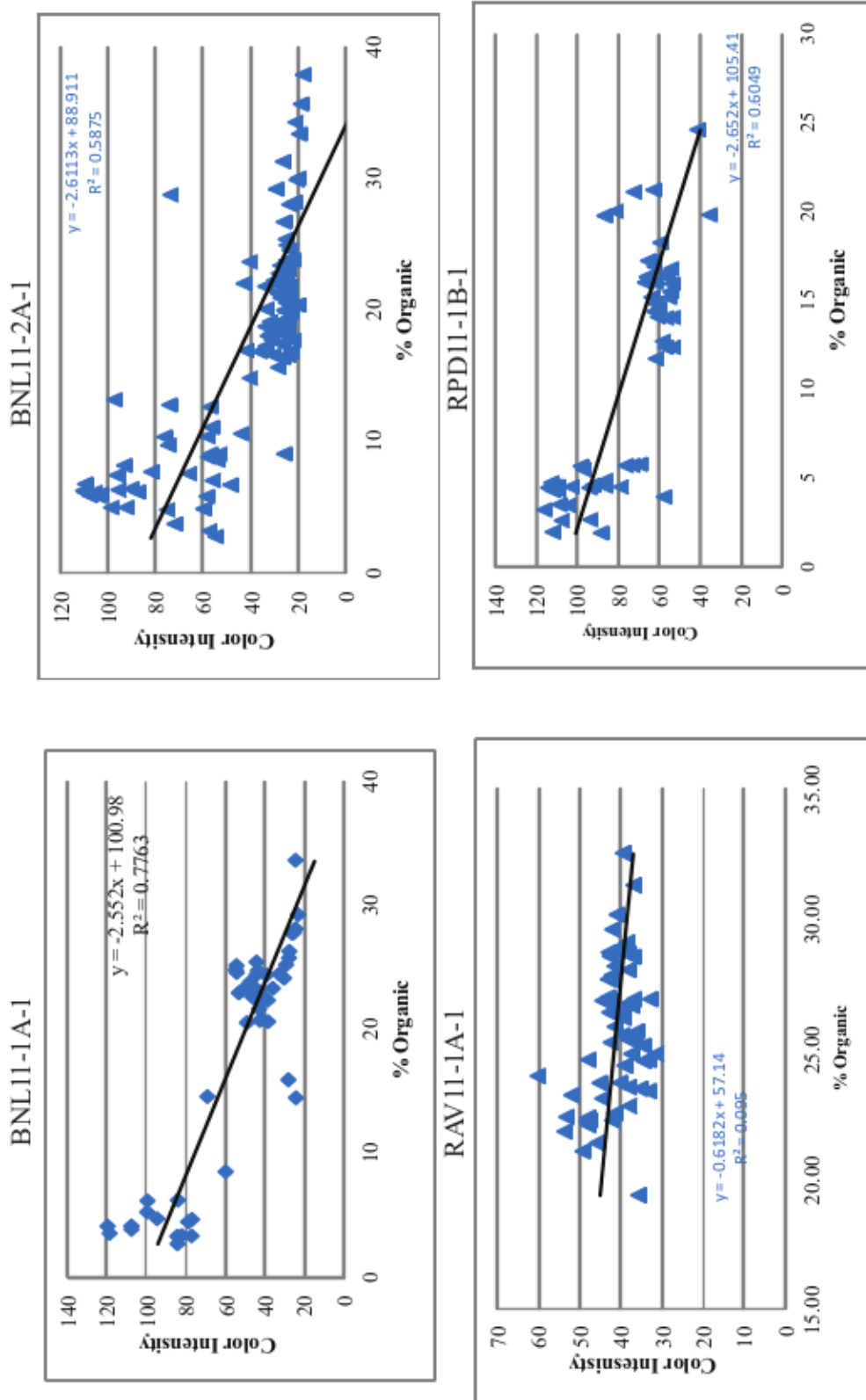


Figure 20: Relationship between color intensity and percent organic material. I constructed the graphs by running running 20-pt means through blue-color values. I then compared the color intensity with organic content of a centimeter around each point. Overall, there is a strong relationship between color intensity and percent organic material.

I sent 11 samples for AMS radiocarbon dating (Table 2). Samples OS-100517 ( $5978 \pm 53$  cal. yBP) and OS-100777 ( $7459 \pm 46$  cal. yBP) were from directly above gray clay layers at 87 cm and 105 cm depth. Radiocarbon samples bracket the other gray clay bands at 77.5-78.5 (top: OS-100382,  $3670 \pm 60$  cal. yBP; bottom: OS-100516,  $4960 \pm 94$  cal. yBP), 65.5-66 (top: OS100380,  $3997 \pm 91$  cal. yBP; bottom: OS-100381,  $3762 \pm 76$  cal. yBP), and 51-60 cm depth (top: OS-100378,  $3642 \pm 86$  cal. yBP; bottom: OS-100379,  $3511 \pm 68$  cal. yBP). In addition, samples OS-100376 ( $1337 \pm 38$  cal. yBP) and OS-100377 ( $1346 \pm 39$  cal. yBP) bracket the top and bottom, respectively, of the transition from 15-19 cm depth between the brown silt and clay. An algae macrofossil (OS-100375) was collected at two centimeters depth, the transition from the reddish-gray sand and clay. It yielded an age of  $307 \pm 19$  cal yBP.

#### **3.2.2.4 Northern Basin: BNL11-2A-2**

BNL11-2A-2 is a continuation of BNL11-2A-1 (Fig. 18, 19). The lowest sediment, at 32-38 cm depth, is composed of tan silt with organic flecks. This sediment became liquefied during coring, and sedimentary structures are not preserved. At 32 cm depth, a dark greenish gray (GLEY 1 3/104) laminated (millimeter-scale) silt abruptly overlies the tan silt and extends to 29 cm depth. An abrupt contact, at 29 cm depth, separates this laminated silt from tan (10YR 6/1) sediment that grades upward from fine sand to silt at 27 cm depth. This is overlain sharply by laminated (millimeter-scale) dark greenish-gray (GLEY 1 3/104) and black silt, which composes the sediment from 20-27 cm depth. This unit grades into massive tan (10 YR 6/1) and black fine sand which persists until 15 cm depth. The contact with the overlying unit, a very finely laminated

(millimeter-thick) dark greenish gray and black silt, is abrupt. This silt occurs from 3-15 cm depth. A millimeter-thick tan band interrupts the silt at 10 cm depth. Massive, very dark brown (10 YR 2/2) fine sand overlies the silt with an abrupt contact and continues to the top of the core.

In general, the MS values are high in the gray clays ( $\sim 10 \times 10^{-5}$  Si) and decrease when the sediment is laminated, organic-rich silt ( $\sim 5 \times 10^{-5}$  Si). The gray sands reach MS values of  $\sim 15 \times 10^{-5}$  Si. The percentage of organic and carbonate material change together. Organic and carbonate content are at  $\sim 15$  and 3 %, respectively, in the lowest laminated silt. Both decrease to background levels in the overlying tan fine sand but then increase to  $\sim 20$ -25% for organic material and 4-6% for carbonate in the laminated brown silt at 15-25 cm depth. Above 15 cm depth, both organic content and carbonate rise to their highest levels in the core. Both decrease to 2% in the fine sand at 0-4 cm depth.

I obtained seven radiocarbon samples (Table 2) all of which were from sieved organic fragments. Sample OS-100779 yielded an age of  $9494 \pm 51$  cal. yBP and came from directly above the liquefied part of the core at 32 cm depth. OS-100778 ( $8441 \pm 150$  cal. yBP) and OS-100522 ( $8678 \pm 100$  cal yBP) were taken from directly above and below the sand band at 25-27 cm depth. Samples OS-100520 ( $8101 \pm 76$  cal. yBP) and OS-100521 ( $8323 \pm 48$  cal.yBP) bracketed the massive tan and black fine sand layer at 15 and 22.5 cm depth. Sample OS-100519, taken from directly above the tan band at 9.5 cm depth, yielded an age of  $7589 \pm 33$  cal. yBP. The sample from three centimeters depth, at the boundary between the fine sand and laminated silt, dated to an age of  $7370 \pm 58$  cal. yBP (OS-100518).

### **3.2.3 Raven Lake**

We collected five cores from Raven Lake (Fig. 21, Table 3). The master core (Fig. 22, 23) is composed of RAV11-1A-1 and RAV11-1A-2. In addition, I analyzed RAV11-2A-1 (Fig. 24, 25) to determine if any gap exists between the two segments. I also analyzed RAV11-3A-1 (Fig. 26, 27), the core that penetrated deepest into the sediments.

#### **3.2.3.1 RAV11-1A-1**

RAV11-1A-1 (Fig. 22, 23) is composed of finely laminated silt throughout the entire core (0-141 cm depth). The laminae are bundled into larger color bands (centimeter-scale), which alternate between among dark grayish-brown (2.5Y 3/2), olive brown (2.5Y 4/4), and black, clayey-silt. The basal portion of the core, 134-140 cm depth, appears to have been slightly liquefied during coring. Grain size varies throughout the core despite the lack of visible sedimentological changes. Sediments range from 60% clay and 40% silt to 90% silt and 10% clay. A sustained decrease in grain size occurs from 134 to 109 cm depth. From 87-134 cm depth, the dark brown and black silt bands become thinner (0.5 cm thick). Finely laminated silt occurs between 87 and 45 cm depth. Between 29 and 45 cm depth, there is a massive light-brown silt with organic-rich bands at 37, 38, and 38.5 cm depth. The upper section of the core consists of very finely laminated silt.



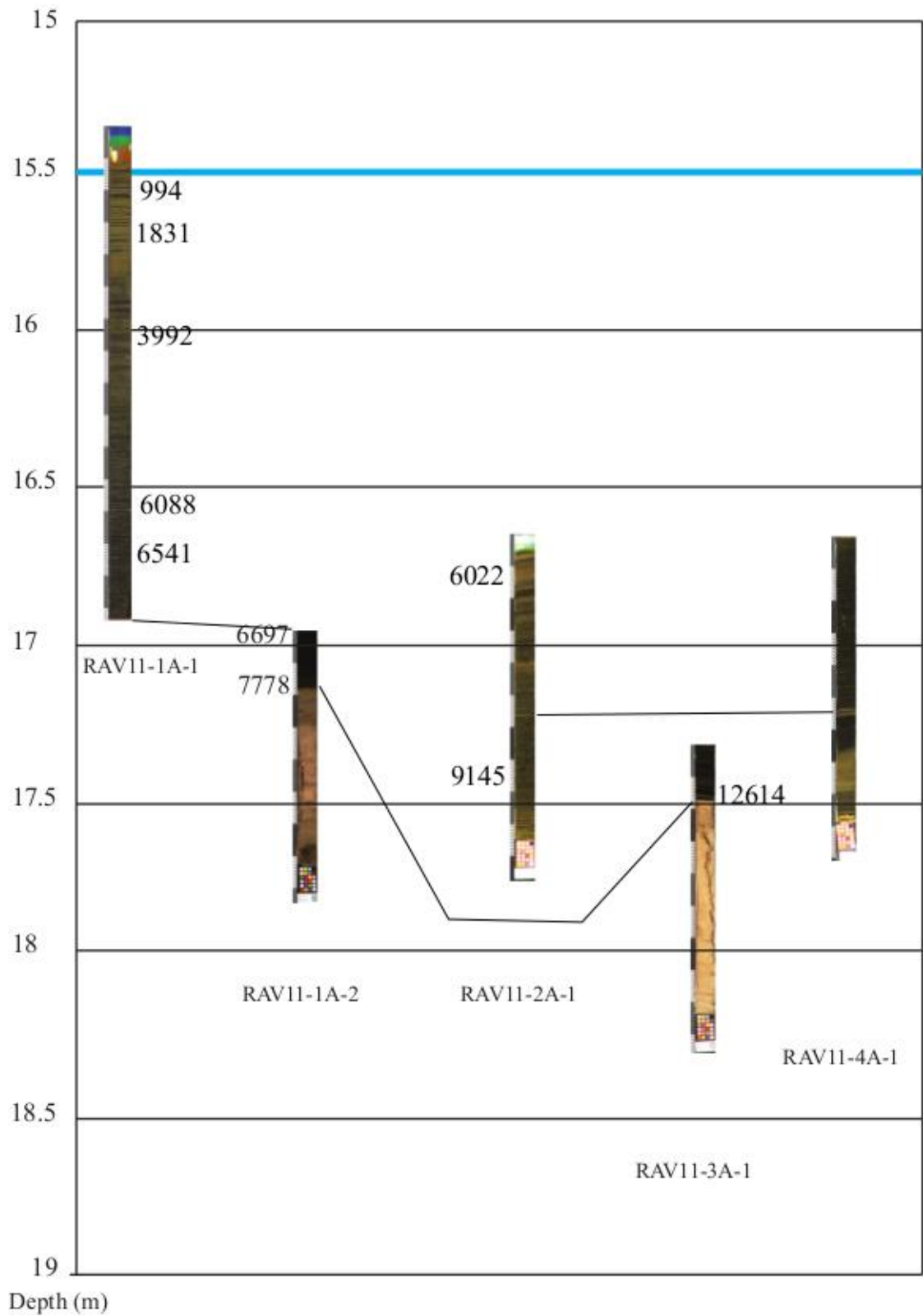


Figure 21: Raven Lake cores plotted by depth below water surface. Ages of radiocarbon dates are given in cal. yBP. Black lines between cores show tie points, and blue lines show the sediment-water interface.

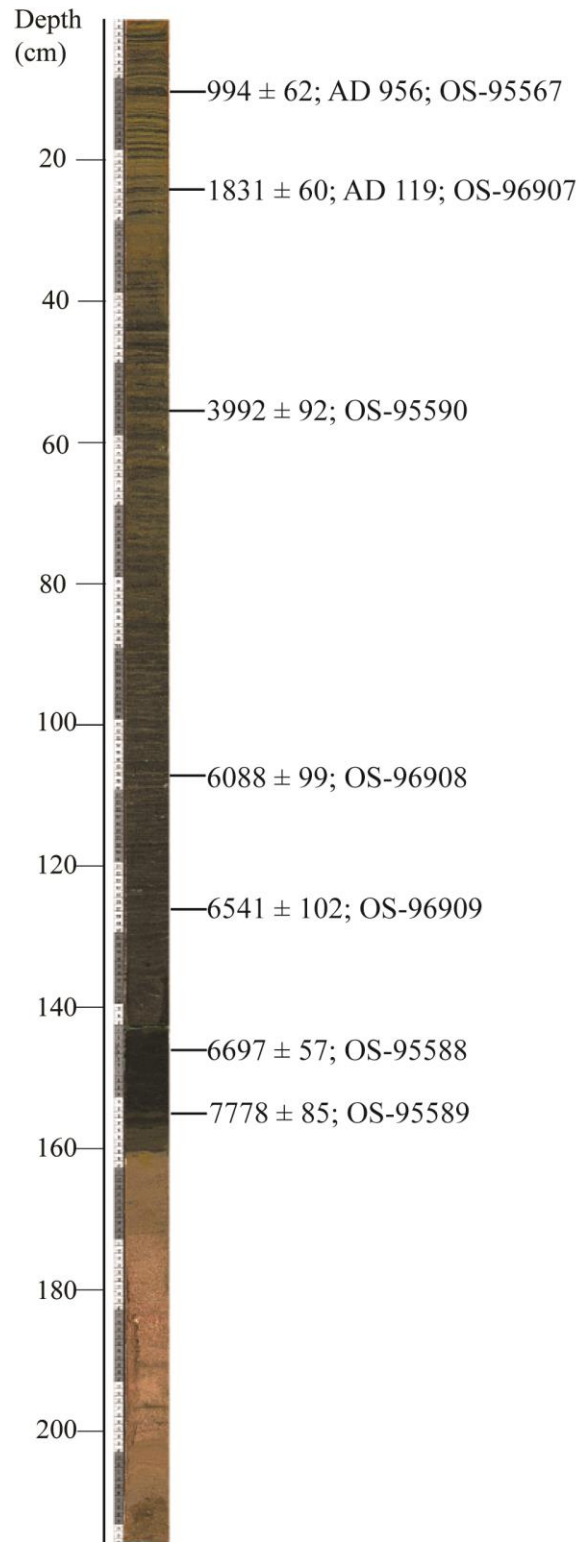


Figure 22: Radiocarbon dates for RAV11-1.

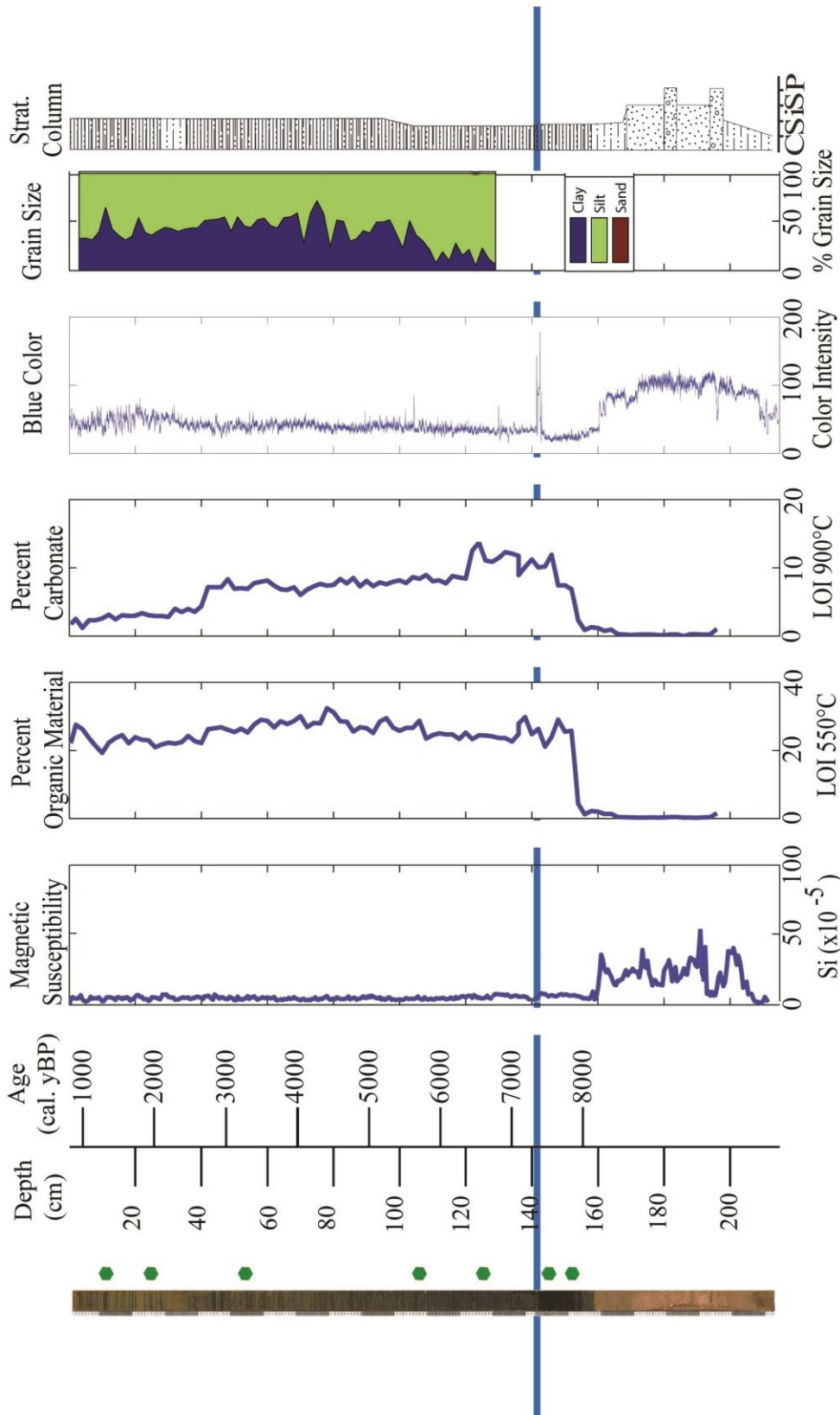


Figure 23: Data for RAV11-1, the master core for Raven Lake. Ages were calculated with the age model. Y-axis tick marks relate to depth. The blue line indicates a core break between RAV11-1A-1 and RAV11-1A-2. The first grain size panel shows data measured on a Coulter Counter, whereas that in the stratigraphic column was based on visual observation. The first grain size panel is separated into percent clay (blue), silt (green), and sand (red). The stratigraphic column width is determined by grain size clay (c), silt (Si), sand (S), and pebble (P). Green points indicate location of radiocarbon samples.

Sediments show only minor fluctuations in MS around a mean of  $4 \times 10^{-5}$  SI. The highest values ( $\sim 9 \times 10^{-5}$  SI) occur between 38 and 35 cm depth, corresponding to a massive band of silt. The percent organic material also shows only minor variations around a mean of  $\sim 27\%$ . A slight peak occurs around 90 cm depth. In contrast, percent carbonate decreases up core in two steps at 40 and 120 cm depth. The blue scale, similar to the MS and organic content, fluctuates only slightly.

Despite the abundance of organic material in the sediments, I did not find any macrofossils. Therefore, I selected radiocarbon samples to be spaced evenly throughout the core (Table 2). Five AMS samples dated were from 125.5 cm (OS-96909,  $6541 \pm 102$  cal. yBP), 111 cm (OS-96908,  $6088 \pm 99$  cal. yBP), 56 cm (OS-95590,  $3992 \pm 92$  cal. yBP), 24 cm (OS-96907,  $1831 \pm 60$  cal. yBP), and 9 cm depth (OS-95567,  $994 \pm 62$  cal. yBP).

### **3.2.3.2 RAV11-1A-2**

RAV11-1A-2 (Fig. 22, 23) is the second thrust in the same hole, and therefore the core should be a continuation of RAV11-1A-1.

Basal clay coarsens upward into silt and sand from 73-58 cm depth. Pebbles are present below 66 cm depth. This unit grades into a pink and gray (5YR 5/1) sand that extends to 29 cm depth. This sand has distinct medium-grained sand and pebble bands intermixed with fine sand layers. The sand unit grades into a massive pink and gray (5YR 5/1) silt, which occurs from 18-29 cm depth. Finely laminated (millimeter-scale) silt overlies this silt with a sharp contact at 18 cm depth. Laminae combine to form alternating centimeter-thick bands of dark grayish-brown (2.5Y 4/2), olive brown (2.5Y

4/4), and black sediment. From 15-18 cm depth, the silt is a massive dark grayish-brown (2.5Y 4/2).

MS data are variable and range as high  $55 \times 10^{-5}$  SI. The organic and carbonate content are negligible. At the contact with the organic silt at 18 cm depth, the organic material increases to ~25%, which it maintains through the upper part of the core. Carbonate increases ~11%. Color intensity follows the same pattern as other proxies.

I found only limited macrofossils in the laminated organic silt and therefore had to sieve samples to concentrate the organic remains present. I sent two samples for analysis (Table 2). Sample OS-95588 (4 cm depth) yielded an age of  $6697 \pm 57$  cal. yBP, and sample OS-95589 (11 cm depth) provided an age of  $7778 \pm 85$  cal. yBP

### **3.2.3.3 RAV11-2A-1**

RAV11-2A-1 (Fig. 24, 25) is composed of a finely laminated (millimeter-scale) silt. The fine laminations group together to form larger color bands (centimeter scale), alternating between olive brown (2.5Y 4/4) and black. A change in color occurs at 82 cm depth, and the core alternates between very dark brown (2.5 Y 3/1) and black. This sediment type persists throughout the core except for prominent light tan layers (0.1-0.5 cm thick) at 29 and 56 cm depth.

The MS and color intensity vary around a mean of  $\sim 2 \times 10^{-5}$  SI and 70, respectively, throughout the core. The MS has a large, sharp, short peak of  $\sim 42 \times 10^{-5}$  SI at 67 cm depth. A smaller corresponding peak also occurs in the color profile. I did not identify any change in sediment type at this depth.

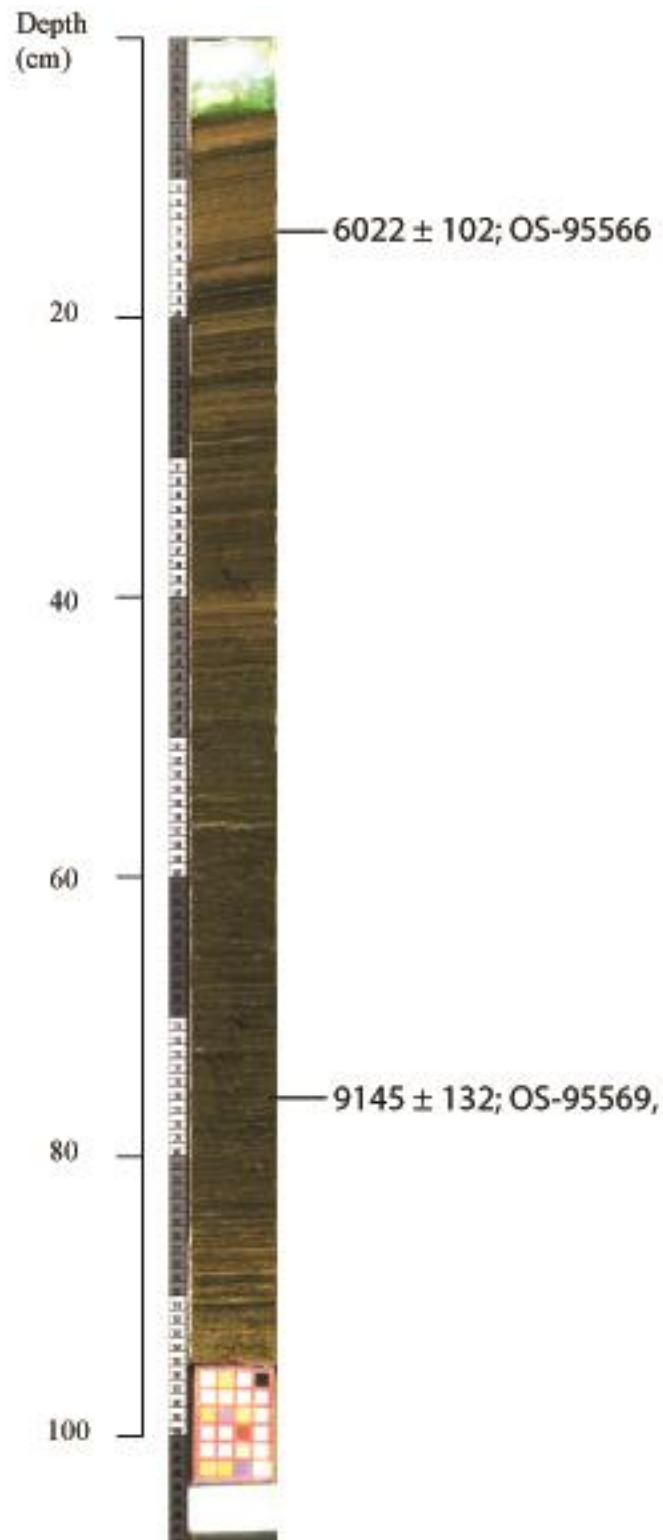


Figure 24: Radiocarbon dates for RAV11-2A-1.

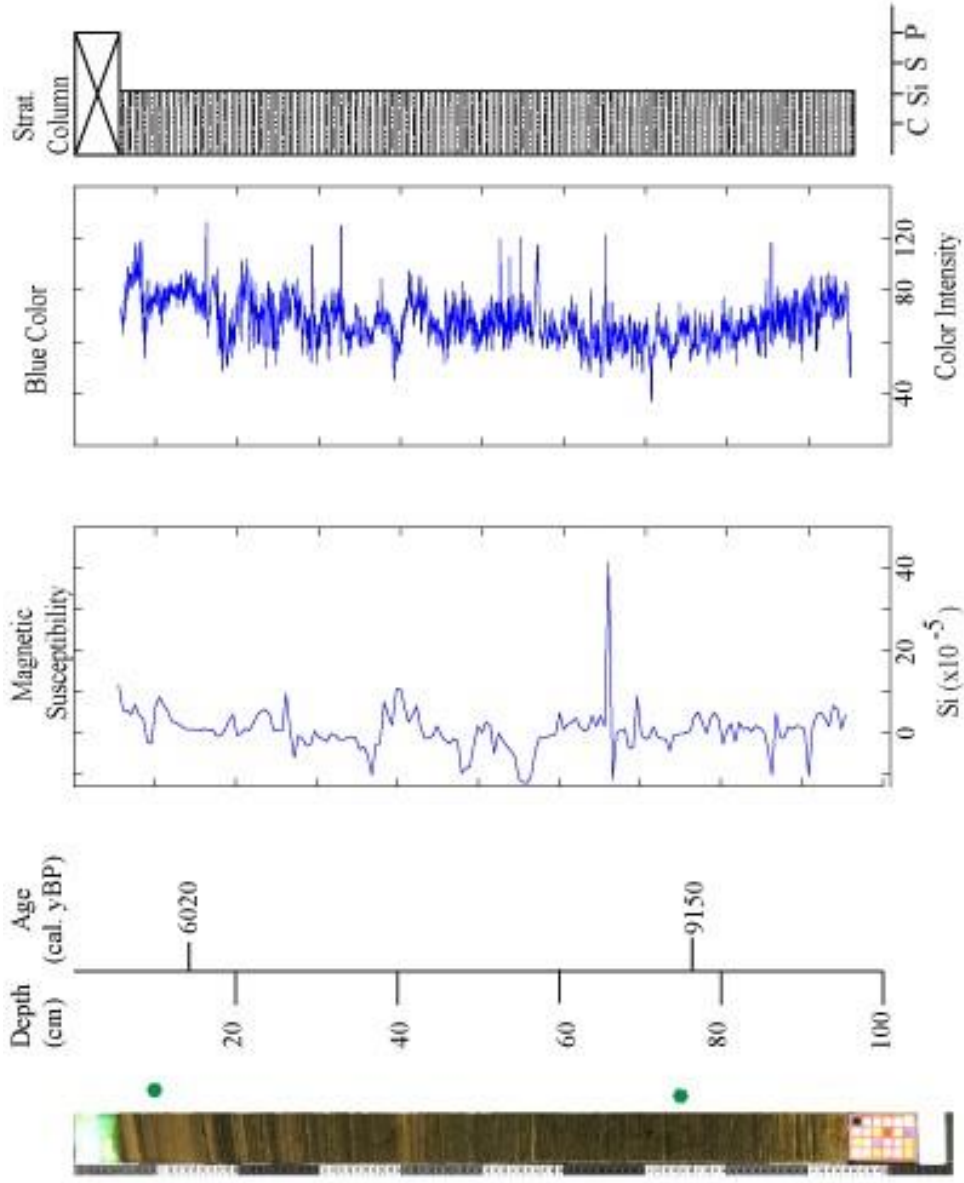


Figure 25: Data for RAV11-2A-1. Y-axis tick marks relate to depth. The first grain size panel shows data measured on a Coulter Counter, whereas that in the stratigraphic column was based on visual observation. The first grain size panel is separated into percent clay (blue), silt (green), and sand (red). The stratigraphic column width is determined by grain size clay (c), silt (Si), sand (S), and pebble (P). Green points indicate location of radiocarbon samples.

I sent two samples for AMS radiocarbon dating (Table 2). Sample OS-95566 (14 cm depth) yielded an age of  $6022 \pm 102$  cal. yBP. The second sample (OS-95569, 76 cm depth) dated to  $9145 \pm 132$  cal. yBP.

#### **3.2.3.4 RAV11-3A-1**

The lowest 58 cm of RAV11-3A-1 is composed of poorly-sorted, pink-gray (5YR 5/1) medium-grained sand (Fig. 26, 27). From 17-25 cm depth, the sand becomes finer and alternates with multiple bands of clay at 17-19 cm depth. At 17 cm depth, the sediment changes abruptly to a finely laminated (millimeter-scale) silt that persists to the top of the core. The laminae are grouped together to form larger, dark olive gray (5Y 3/2) and black bands (centimeter-scale).

MS values vary significantly in the sand, ranging from  $\sim 0.38 \times 10^{-5}$  SI and drop abruptly at 17 cm depth to  $\sim 6 \times 10^{-5}$  in the silt. Color intensity shows a similar pattern being highest in the sand ( $\sim 125$ ) and decreasing abruptly at the contact with the overlying silt.

A radiocarbon sample (OS-100776, table 2) directly at contact between the sand and laminated silt (17 cm depth) dated to  $12,525 \pm 96$  cal. yBP.



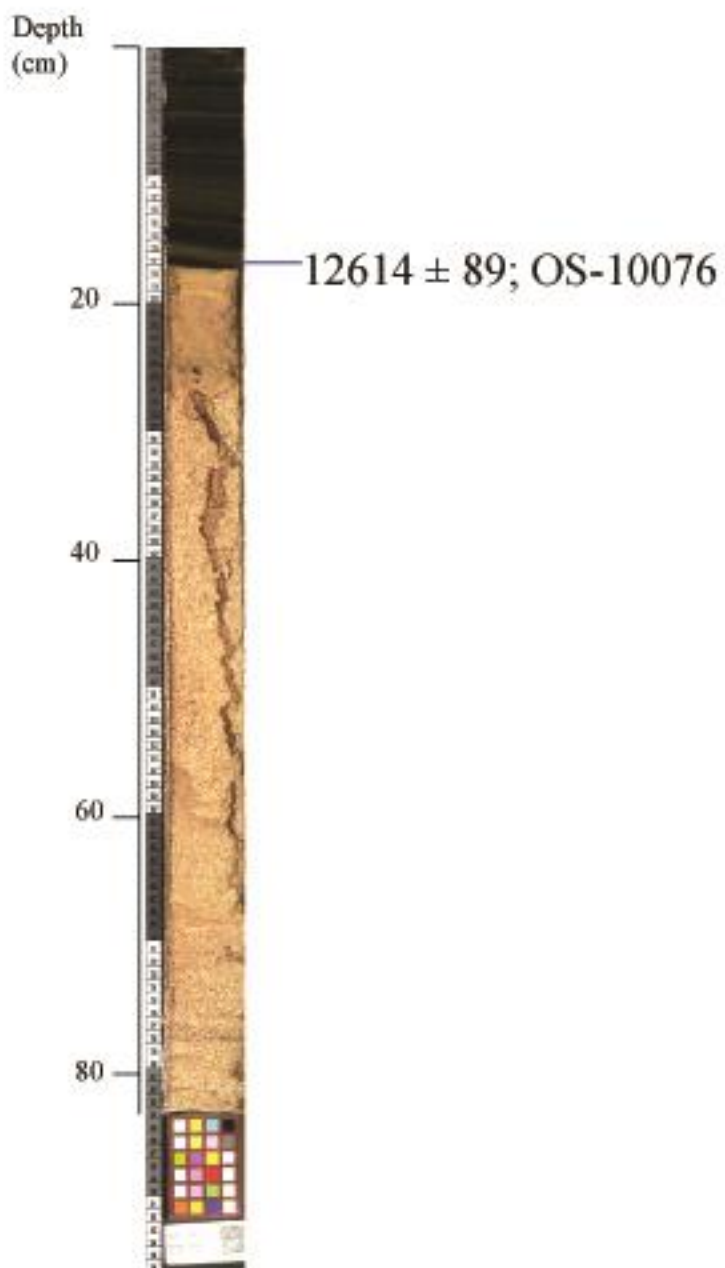
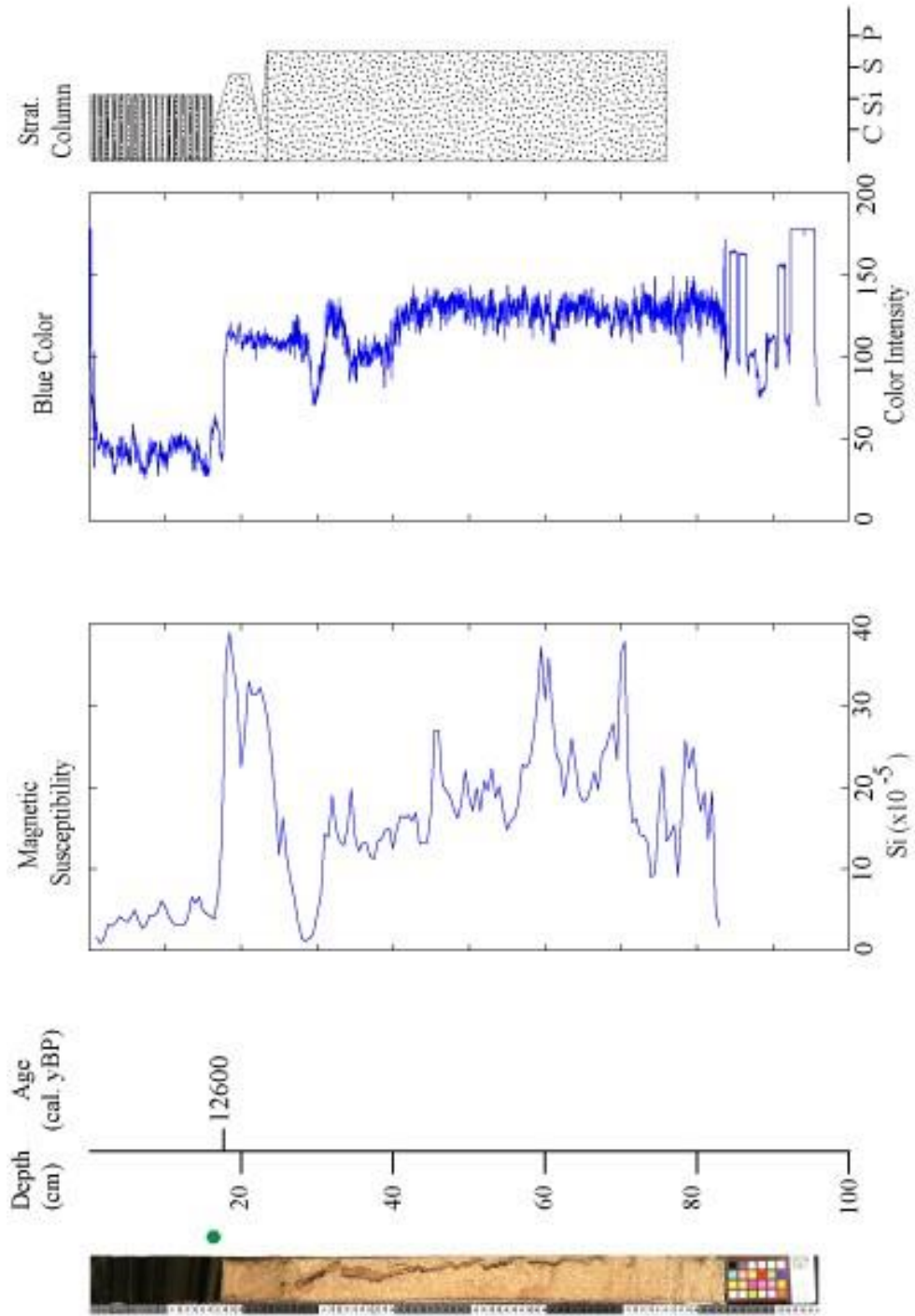


Figure 26: Radiocarbon dates for RAV11-3A-1.



FFigure 27: Data for RAV11-3A-1. Y-axis tick marks relate to depth. The first grain size panel shows data measured on a Coulter Counter, whereas that in the stratigraphic column was based on visual observation. The first grain size panel is separated into percent clay (blue), silt (green), and sand (red). The stratigraphic column width is determined by grain size clay (c), silt (Si), sand (S), and pebble (P). Green points indicate location of radiocarbon samples.

## CHAPTER 4

### DISCUSSION

#### 4.1 Age Model

##### 4.1.1 Radiocarbon Date Quality

Thirty-nine samples were dated for this study, and only two (OS-96948, OS-100382) yielded ages inconsistent with their stratigraphic position. The measured  $\delta^{13}\text{C}$  for the radiocarbon samples are similar to accepted values for lake algae (Meyers and Lallier-Vergès, 1999).

There is no evidence for a significant reservoir effect in the studied lakes. Bedrock surrounding the lakes lacks carbonate material. Moreover, water entering Bunny and Rapids Lakes flowed over bedrock for a large distance and with a great deal of turbulence, causing aeration of the water. Rapid and Bunny Lakes, in particular, should be well-mixed, because of the through-flowing current. All lakes recorded summer temperatures above 4°C. As the surface water cools to 4°C during the winter freeze up it will sink to the bottom of the lake, mixing the water and preventing long residence times. Finally, Lusas (2011) obtained a modern age for lacustrine algae at the sediment-water interface in a very similar lake farther east in the Scoresby Sund region. For all of these reasons, I do not anticipate any significant reservoir effect either from input of old carbon or long water residence times.

### **4.1.2 Rapids Lake**

The age model for the Rapids Lake master core is based on five radiocarbon dates (Table 4, Fig. 28). Sample OS-96048, at 10 cm depth, produced an age significantly older than the next two lower dates and thus may contain reworked organic material washed in from the land. Because it is out of stratigraphic order, and because it appears anomalous old for such a shallow depth, I consider it to be in error. Therefore, for the rest of the discussion I ignore OS-96048.

Ideally, the age model would take into account different deposition rates documented by significant changes in sediment type. However, due to the lack of radiocarbon dates below 38 cm depth, the age model for the lower 70 cm of the master core was based on the best fit between samples OS-96045 and OS-95933 and is thus only a first-order approximation of age. I also set the top of the sediments at -60 cal. yBP (using the convention that year 0 is AD 1950), since it appeared that we collected the sediment-water interface.

### **4.1.3 BNL11-1**

The master core for southern Bunny Lake, BNL11-1, was constructed from BN11-1A-1 and BNL11-1B-1 (Table 4, Fig. 29). Based on stratigraphic correlation, I matched the three gray bands that punctuate the organic-rich silt in both cores tying 107 cm depth in BNL11-1A-1 with 87 cm depth in BNL11-1B-1. Radiocarbon dates (OS-95587, OS-95586) confirm the overlap at this depth within error of the ages.

Six radiocarbon dates provide the basis for the age model in the upper 120 cm of the master core. Below 120 cm depth, I did not find any organic material, so the age of

this section is unconstrained. Several thin (0.1 cm thick) gray bands punctuate the organic-rich silt from 98-120 cm depth, a characteristic not observed in the organic-rich silt higher in the core. Therefore, I fit two separate lines between the radiocarbon ages in both units to provide a sedimentation rate.

#### **4.1.4 BNL11-2**

BNL11-2, the master core for the northern basin of Bunny Lake, is constructed from BNL11-2A-1 and BNL11-2A-2, the second thrust in the same hole (Table 4, Fig. 30). I used eighteen dates to produce the age model. OS-100382 ( $3430 \pm 30$  cal. yBP) is anomalously young for its depth compared to the surrounding radiocarbon dates. Even with the two sigma range of the calibrated radiocarbon date, OS-100382 differs from both the age model and the surrounding radiocarbon dates. Therefore the radiocarbon date is significantly young and out of stratigraphic position. For the remainder of the paper I ignore this sample. Other dates, such as OS-100378 and OS-100379, are not in proper sequence, but are within error of each other so the difference is not significant.

I divided the core into three segments composed predominantly of non-glacial organic-rich silt to account for variations in the sedimentation rate that may have occurred during the Holocene. Breaks between segments occurred at large, grey, inorganic layers. Within each segment, I fit a line through the radiocarbon dates to produce the age model.

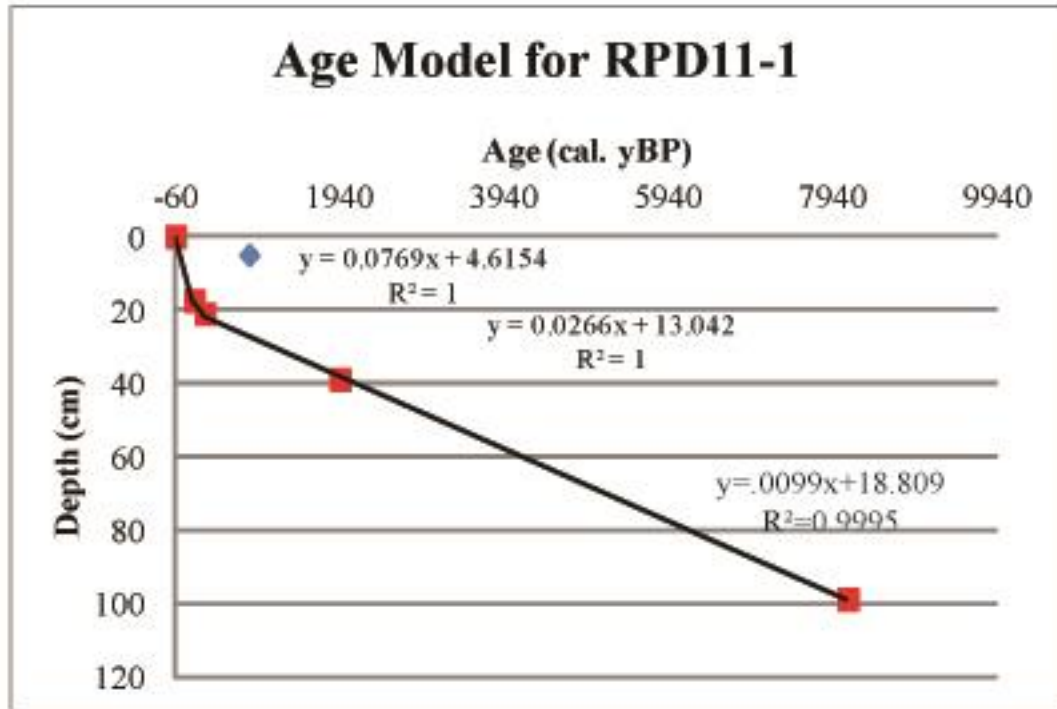


Figure 28: RPD11-1 age model. Red squares show radiocarbon dates. Light blue diamonds are out of stratigraphic order and are omitted.

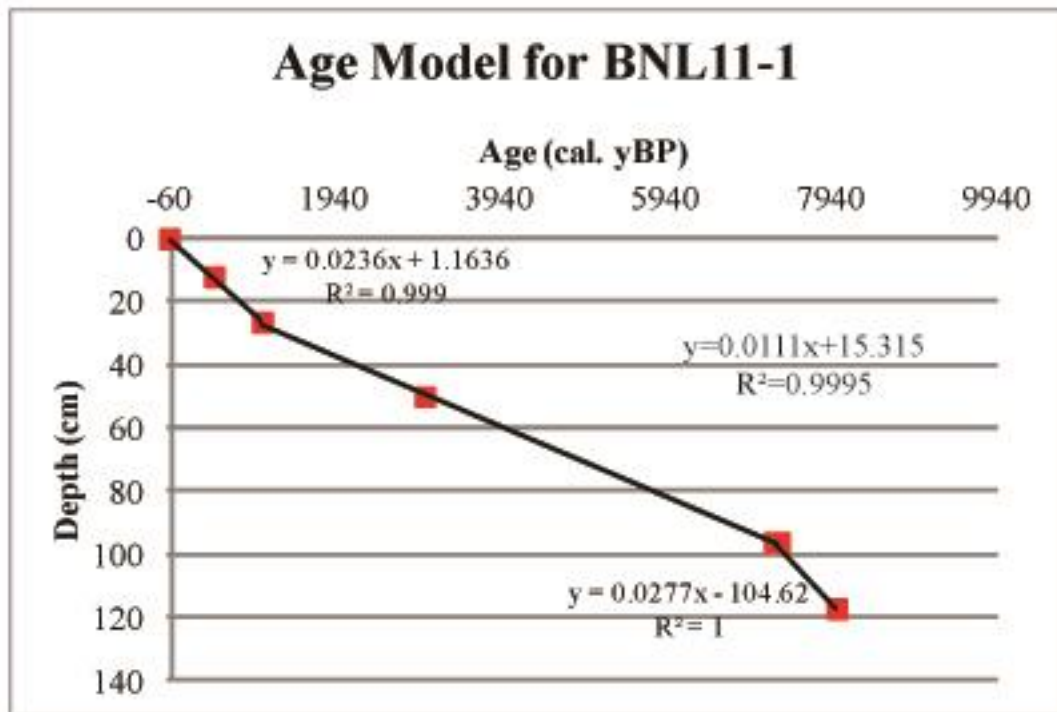


Figure 29: BNL11-1 age model. Red squares show radiocarbon dates.

Table 4: Age model for master cores.

Core	Depth (cm)	R <sup>2</sup>	Age Model
BNL11-1	0-26.4	0.999	$Age = \frac{(depth - 1.1636)}{0.0236}$
	26.4-96	0.9995	$Age = \frac{(depth - 15.315)}{0.0111}$
	96-120	1	$Age = \frac{(depth + 104.62)}{0.0277}$
	120-153		Nothing dated
BNL11-2	0-51	0.9995	$Age = \frac{(depth - 0.2087)}{0.0139}$
	51-60.5		
	60.5-104.5	0.9935	$Age = \frac{(depth - 22.576)}{0.0109}$
	104.5-122		
	122-155	0.9243	$Age = \frac{(depth - 19.106)}{0.0143}$
RPD11	0-17.5	1	$Age = \frac{(depth - 4.6053)}{0.0769}$
	17.5-21	1	$Age = \frac{(depth - 13.0248)}{0.02672}$
	39-107	0.9995	$Age = \frac{(depth - 18.809)}{0.0099}$
RAV11	0-160	0.9742	$Age = \frac{(depth + 18.369)}{0.0221}$
	160-214		Nothing dated

#### 4.1.5 Raven Lake

I constructed the master core, RAV11-1, from RAV11-1A-1 and RAV11-1A-2 (Table 4, Fig. 31). There was no organic matter below 160 cm depth, so the age of the deepest sediments is unknown. Above 160 cm depth, the core is very finely laminated gyttja, and the sedimentation rate appears to be relatively constant. I fit a line through all seven radiocarbon dates to provide control for the age model.

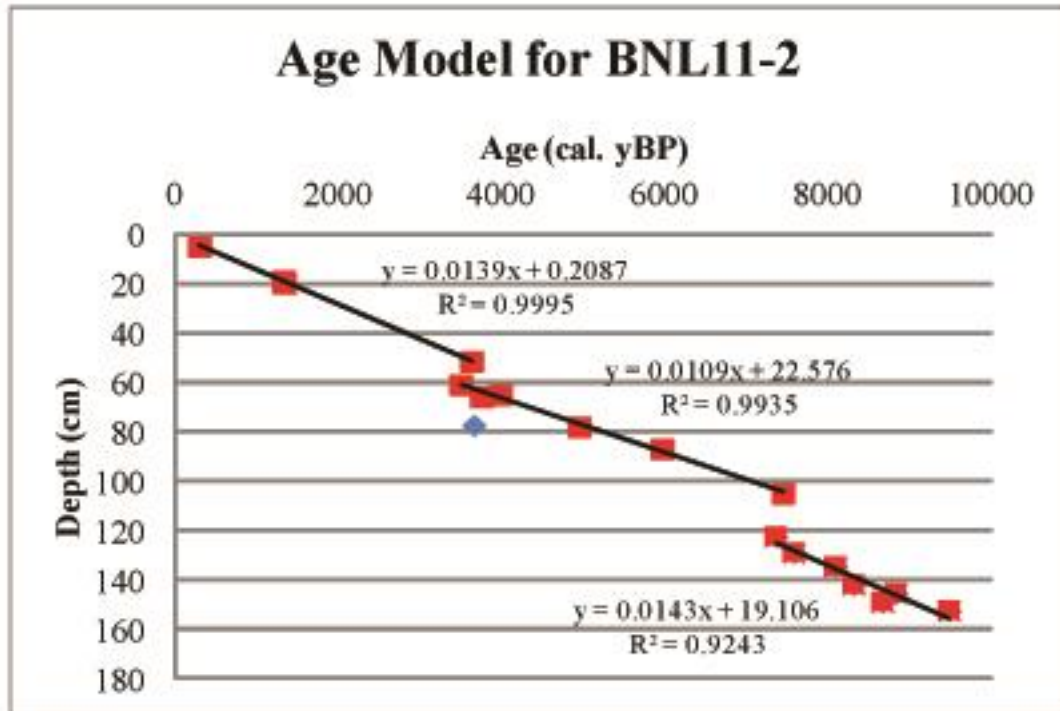


Figure 30: BNL11-2 age model. Red squares show radiocarbon dates. Light blue diamonds are out of stratigraphic order and are omitted.

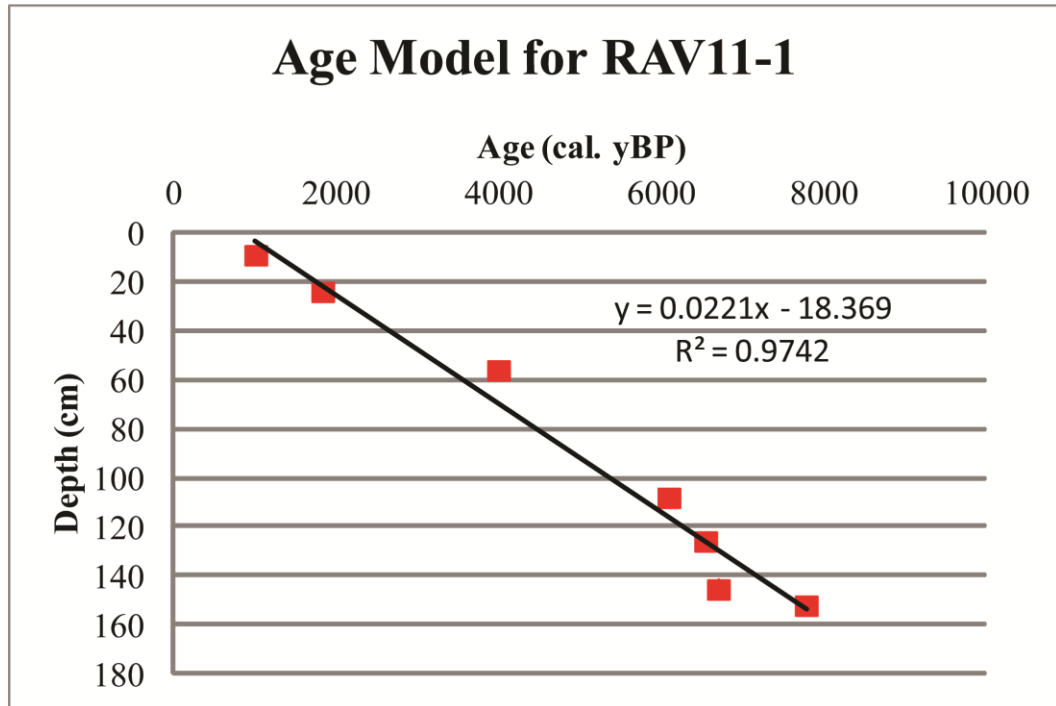


Figure 31: RAV11-1 age model. Red squares show radiocarbon dates.



## 4.2. Lake History

### 4.2.1 Raven Lake

The lowest sediments in the Raven Lake cores, coarse sand and gravel commonly set in a clay matrix, likely represent ice-proximal conditions during deglaciation of the area. From 160-210 cm depth, RAV11-1 is characterized by interbedded sand and gravel which show oscillations between finer and coarser sediment. These changes in grain size may represent variations in the glacier, with the larger sediment representing times when the margin was closer to the lake. They also could represent differences in the type of sediment deposited from an adjacent ice margin. Due to the lack of dating constraints, I am unable to identify the time scale of these fluctuations.

Laminated gyttja overlies the sand and gravel. A radiocarbon date from RAV11-3A-1 at the contact with the sand, provides a minimum-limiting age for onset of organic sedimentation and for deglaciation of the lake of  $12,614 \pm 89$  cal. yBP (OS-100776). A second radiocarbon date from RAV11-1A-2, taken eight centimeters above the same transition dates to  $7778 \pm 85$  cal. yBP (OS-95589). A sample from RAV11-2A-1 at a lower depth than the contact from sand to gyttja in RAV11-1 yielded an age of  $9145 \pm 132$  cal. yBP (OS-95569). RAV11-2 does not contain the deglacial-gyttja contact, so I am unsure how closely this age constrains the transition, However, this date is at least broadly consistent with the old age for deglaciation obtained from RAV11-3A-1.

The depth of the sand/gyttja contact differs among cores and indicates that the sand surface has topography. In RAV11-1A-2, the transition from sand to silt occurs at ~1720 cm below lake surface level, but in RAV11-3A-1 it occurs at 1770 cm depth. The silt continues to depths greater than 1770 cm in RAV11-2A-1, so the contact must be

even lower. During deposition, the coarse sediments either were not laid down as a flat surface, or subsequent erosion created an irregular topography. When the gyttja was deposited in the lake, it ponded in the deeper sections first. However, additional radiocarbon samples need to be dated from the contact to help support this claim.

Very finely laminated silts occur throughout the rest of the core. Although one cannot be certain, it is possible that these laminae are varves. The lowest 50 cm of the laminated organic silt is coarser than the top 110 cm. A gradual transition to the smaller grain size is centered at ~110 cm depth at ~5800 cal. yBP. and may represent a mid-late Holocene change in climate. Before grain size was measured, I removed organic material and biogenic silica which make up a large fraction of Raven Lake sediments. Therefore, the measured grain size represents inorganic material washed or blown into the lake. The increase in grain size could represent a mid-Holocene increase in local runoff from precipitation or snowpack melt, or an increase in wind.

Conditions were relatively stable from ~5800 cal. yBP to present at Raven Lake. Although the MS does not show any significant changes, the percent of organic material decreases above ~80 cm depth and carbonate throughout the core from 12% at the base to near 1%. This carbonate may be associated with algae blooms (Stabel, 1986). If so, the decrease in carbonate and organic material may represent a change in the lake ecosystem over time.

The lack of any obvious glacial input in this lake constrains the size of the Renland Ice Cap over the Holocene to within ~200 m of the present-day margin. The abandoned channel that enters the northeast end of the lake heads just distal to the LIA drift edge about 200 m from the current glacial margin. The glacier could not have

advanced past the stream head or silt-laden meltwater would have entered Raven Lake. Such sediment is absent from the lake after initial deglaciation in late-glacial time. Thus, I infer meltwater produced by the glacier during the LIA and during other expansions of similar or smaller size would have by-passed Raven Lake and drained through the prominent meltwater channel that extends from the present-day glacial margin to Large Lake.

The purpose of a control lake, such as Raven Lake, is to highlight evidence of non-glacial events, such as storms or landscape erosion, that can be interpreted mistakenly as being of glacial origin. In Raven Lake, there is no evidence, such as bands of inorganic silt or sand, of any event disrupting normal sedimentation. Therefore, it is likely that the significant changes in sedimentation observed in the nearby glacially fed lakes are the result of glacial activity and not other factors.

#### **4.2.2 Rapids Lake**

The lowest radiocarbon date in Rapids Lake cores affords a minimum age for deglaciation of  $8115 \pm 103$  cal. yBP (OS-95933) and comes from interbedded silt and fine sand that overlies coarser sand lost during retrieval. I interpret the variation between laminated black silt, coarser reddish gray silt, and reddish gray fine sand from 84-108 cm depth as representing glacial meltwater variations across a threshold. Glacial material (reddish-gray silt and sand) entered the lake from 8100-8800 (99-106 cm depth), 7700-7800 (95-96 cm depth), 7300 (91-92 cm depth), 7100 (89.5 cm depth), and 6600 cal. yBP (84 cm depth) In contrast, the black, organic-rich, laminated silt is characteristic of a lake

with limited glacial input and may represent periods when Rapids Lake no longer received meltwater.

The reddish-gray sand and silt differ from other inorganic layers in Rapids Lake in color and MS values. In addition, the sand grades into the silt, a relationship not seen higher in the core. This gradation could reflect recession of ice in the basin and increasing distance of the glacier from the lake. Moreover, based on color, this silt and sand may have a different source from the inorganic gray bands in the core. One possibility is that the glaciers were more expanded early in the lake history than at any time since and were depositing sediments derived from areas that later remained unglaciated.

The reddish-gray sand and silt also could be deposited in different ways, such as from a mass movement into the lake. However, this explanation is unsatisfactory, because the maximum grain size is very fine sand. If a mass movement occurred, the resulting deposit might be less well sorted and potentially include larger sediments, given the large grain sizes available around the lake shore. Another possibility is that they could represent inwash from runoff during a large storm event. However, the absence of similar inorganic bands in Raven Lake is circumstantial evidence against this hypothesis. A third explanation is that wind or mass movements deposited sediment onto an ice-covered lake during the winter that later melted through during spring break up, but again a poorly sorted deposit would be expected. Yet another possibility is that channels, heading on the adjacent plateaus, collect aeolian sand and silt when not draining water. Once the channels become reactivated by meltwater, the sediments may be washed out into the lake during the initial flushing, creating sand layers that grade into glacial silt. Although

many of these explanations are possible, the simplest is that the reddish-gray sand and silt bands resulted from glacial meltwater and material entering the lake, particularly as their stratigraphic position suggests that they formed soon after the lake itself was deglaciated.

At 84-86 cm depth (6500-6800 cal. yBP), there is an abrupt, large decrease in organic content that corresponds to a thick gray band in the stratigraphy. This likely represents a glacial advance. After this event, the organic material increases to higher levels which are maintained to about 40 cm depth (~1900 cal. yBP). I interpret this organic unit to represent that the lake was receiving minimal or no glacial sediment with the exception of brief periods described below. Today, Rapids Lake receives rock flour and deposition is largely inorganic. This comparison suggests that overall, the mid-Holocene was a period with glaciers and meltwater discharges that were smaller than at present. However, there are several prominent gray clayey-silt bands that interrupt the brown organic silt. Based on the age model, prominent layers formed at ~5900 (77 cm depth), 5100 (70.5cm depth), 4800 (66 cm depth), and ~3400 (52.5 cm depth) cal. yBP. Multiple bands were deposited between ~2300 and 3600 cal. yBP (42-55 cm depth). This presence of inorganic, more clay-rich, gray sediments, likely reflects periods of enhanced glacial meltwater influx to the lake, and therefore glacial expansion.

From ~38 cm depth to the surface, the sediments consist primarily of a thick layer of inorganic, gray clay typical of glacial rock flour interbedded with dark brown clayey-silt laminae at 22-23, 15-18, 14-15, and 5-8 cm depth. The clay unit is much thicker than any of the gray bands seen lower in the core, suggesting it represents the largest glacial advance recorded since the initial deglaciation of Rapids Lake. This clay is constrained with a maximum-limiting radiocarbon date of 1940 cal. yBP (OS-96045), which was

taken from two centimeters below the contact. However, due to the slow sedimentation rate of the organic silt, this age could be significantly older than the onset of glacial sedimentation, which is constrained only to less than ~1900 cal. yBP. Since the clay unit continues to the top of the core, it contains the time period of the LIA, but it also may include earlier glacial fluctuations.

The gray clay contains minor layers of massive dark brown silt, two of which are capped by orange oxidized layers at 22 (322 cal. yBP, AD 1620) and 15 cm depth (135 cal. yBP, AD 1815). These bands represent a change in the oxidation state at the lake bottom. Such changes can come about by lowering of water level. However, it seems odd that lake level would drop during what is generally thought to be a period of expanded glaciers. Water level is controlled by a bedrock outlet, so a drop in lake level would require a significant reduction in water input – likely cessation of outflow from Large Lake.

Overflow from Large Lake could have been stopped if the ice dam was breached (or floated) and water drained northeast catastrophically. Water would return to Rapids and Bunny Lakes when the dam reformed. . An alternative is that the layers may represent oxidized material washed into the lake. However, reworking of material would likely produce a poorly sorted, non-uniform deposit. More study of these layers is necessary before their origin can be understood fully.

Unlike silt deeper in the core, the dark brown silt laminae that interrupt the clay are not of organic origin. One possibility is that during the advance represented by the clay, the largest in the last 8000 cal. yBP in Rapids Lake, plateau glaciers above the lake

may have reformed, allowing contribution of local, and thus more coarse, glacial material to the lake during the coldest intervals.

Sedimentation in Rapids Lake at present does not differ significantly from that during the LIA. The lake is still receiving glacial flour from Large Lake, and organic growth has not returned to values present before the deposition of the clay.

### **4.2.3 Bunny Lake**

Poorly sorted sand and gravel that are typical of proximal glacial deposition comprise the lowest 33 cm of BNL11-1. Larger pebbles (as much as five centimeters in diameter) were probably ice-rafted debris. If so, this would require that ice occupied part of either Rapids or Bunny Lake in order for icebergs to reach the core site.

The timing of deglaciation is constrained by minimum-limiting radiocarbon dates. Sample OS-95640 is from an algae mat directly at the abrupt contact between the poorly-sorted sand and gravel and the overlying laminated organic-rich silt in the southern basin. It yielded a minimum-limiting date of  $7994 \pm 67$  cal. yBP for deglaciation. However, the oldest radiocarbon date in the northern basin, OS-100779, affords a minimum-limiting deglaciation date of  $9494 \pm 51$  cal. yBP. Although this date is not directly at the contact between the poorly-sorted sand and gravel and the overlying laminated organic-rich silt, ice must have been absent from the northern (and probably both) basin by 9500 cal. yBP to allow the deposition of the organic material. The difference in ages between the two basins is likely due to the oldest organic material not being deposited where BNL11-1 was collected, or to the current flowing over BNL11-1 creating an unconformity by eroding material.

Directly above the basal sand and gravel, multiple gray laminae formed within organic silt between ~9.5 and 7.4 ka. Similar to Rapids Lake, these laminations likely represent oscillations in meltwater input. This may be because either the glacier itself was situated near a threshold or water level in Large Lake only periodically overflowed through the western outlet.

Most sediment in BNL11-1 and BNL11-2 is composed predominantly of an organic-rich silt which is black at the base of the unit and gradually lightens in color to a dark grayish-brown. In BNL11-1, the organic silt began at ~8000 cal. yBP (119 cm depth) and persisted to ~1050 cal. yBP (28 cm depth). In BNL11-2, the silt was deposited from ~9500 cal. yBP (152 cm depth) to ~1340 cal. yBP (18 cm depth). In both cores, organic material decreases slightly over time, possibly because of either a greater contribution of glacial material in the second half of the Holocene or a decline in lake productivity due to cooling climate or loss of nutrients.

In both cores, gray bands with increased MS and low organic content typical of glacial sediment punctuate the organic silt. Gray sediments were deposited in BNL11-1 at ~7200-7400 (98-100 cm depth), 6400 (86 cm depth), and ~3000 cal. yBP (52 cm depth). The gray bands are more pronounced and numerous in core BNL11-2 (Table 5). Those at ~8700, ~7400, and ~6000 cal. yBP have fine sand, similar to that seen at the base of Rapids Lake, which grades into gray clay. The lowest gray band, at 152-156 cm depth, ended at  $9494 \pm 51$  cal. yBP and may reflect the onset of organic sedimentation following deglaciation of the lake. These gray bands, represent events of significant size and duration, in which glacial material swamped organic deposition in Bunny Lake.



Table 5: Timing of glacial advances of the Renland Ice Cap. The time between events was calculated by finding the amount of time between mid-points. Glacial advances occurring over a short time span were grouped together with the assumption that these multiple events reflected an oscillation within a general cold period.

		BNL11-2				BNL11-1				RPD11		Timing	
Grey Band	Depth (cm)	Radiocarbon Sample	Age (cal. yBP)	Depth (cm)	Radiocarbon Sample	Age (cal. yBP)	Depth (cm)	Radiocarbon Sample	Age (cal. yBP)	Glacial Advance (ka)	Time Span (ka)		
1	0	present	-60	**	**	**	**	***	***	***	1.3	****	
	18	OS-100376	1337 ± 38	**	**	**	***	***	***				
2	18	OS-100376	1337 ± 38	**	**	**	***	***	***				
	19	OS-100377	1346 ± 39										
3	-	-	-	0	present	-60	0	present	-60	1.0			
	-	-	-	26	OS-96874	1062 ± 85	38	OS-96045	1940 ± 53				
4	51	OS-100378	3642 ± 86	53	OS-96906	3023 ± 61	52.5	Age Model	3400	3.0-3.6			
	61	OS-100379	3511 ± 68	0.5 cm thick			0.2 cm thick						
5	64	OS-100380	3997 ± 91	-	-	-	-	-	-	3.7-4.0			
	65	OS-100381	3762 ± 76	-	-	-	-	-	-				
6	76	Age Model	4900	-	-	-	66, 69.5	Age Model	4770,	4.7-5.0			
	77	OS-100516	4960 ± 94	-	-	-	0.1 cm thick		5100				
7	87	OS-100517	5978 ± 53	86	Age Model	6370	77	Age Model	5880	5.8-6.0			
	89	Age Model	6090	0.2 cm thick			0.3 cm thick						1.4

Table 5: Continued

Grey Band	BNL11-2				BNL11-1				RPD11				Timing	
	Depth (cm)	Radiocarbon Sample	Age (cal. yBP)	Depth (cm)	Radiocarbon Sample	Age (cal. yBP)	Depth (cm)	Radiocarbon Sample	Age (cal. yBP)	Depth (cm)	Radiocarbon Sample	Age (cal. yBP)	Glacial Advance (ka)	Time Span (ka)
8	99	Age Model	7010	-	-	-	84	Age Model	6590					
	0.3 cm thick				-	-	86.00	Age Model	6790					
9	103	Age Model	7330	-	-	-	89.5	Age Model	7140					
	0.1 cm thick				-	-	0.4 cm thick						7.0-7.5	
10	105	OS-100777	7459 ± 46	98	OS-95587	7298 ± 40	91	Age Model	7290					
					OS-95586	7237 ± 80								
	122	OS-100518	7370 ± 58	100	Age Model	7390	92	Age Model	7340					
11	129	OS-100519	7589 ± 33	-	-	-	95	Age Model	7700					
	0.2 cm thick				-	-	96	Age Model	7800				7.6-7.8	
12	134	OS-100520	8101 ± 76	117	Age Model	7990	99	OS-95933	8115 ± 103					1.2
	141	OS-100521	8323 ± 48	0.2 cm thick			106	Age Model	8800				8.1-8.3	
13	145	OS-100778	8841 ± 150	-	-	-	-	-	-					
	148	OS-100522	8678 ± 100	-	-	-	-	-	-				8.6-8.8	
14	152	OS-100779	9494 ± 51	-	-	-	-	-	-					0.9
	*	*	*	-	-	-	-	-	-				9.4	
													Periodicity	1.16

\* End of event not captured in core

\*\* Event 3 continuous to present

\*\*\* Unable to differentiate between first 3 grey bands

\*\*\*\* Likely represents oscillations within a cold climate

The number of glacial advances recorded in the two basins of Bunny Lake differs. BNL11-2, taken from the northern basin, is in a low-energy environment removed from the stream current. The lack of a strong current in the northern basin allows finer particles to settle out and be deposited more readily than in the southern basin. Therefore, the northern basin produced a higher-resolution, more sensitive record. The combined record shows that the gray bands formed in both Bunny Lake basins at ~7200-7500, 6000-6300, and 3000-3500 cal. yBP. Additional layers were deposited in BNL11-2 at 9400, 8600-8800, 8200-8300, 7000, 4900, and 3700-4000 cal. yBP.

Gray clay produced by glacial sedimentation dominates the upper part of both Bunny Lake cores. In BNL11-2, late Holocene clay deposition begins at ~AD 615 and is constrained by two radiocarbon dates directly at the contact. In contrast, in BNL11-1 a date in similar stratigraphic position constrains the start of clay deposition to shortly after ~AD 900. The AD 600 event is not seen, possibly because of erosion from the stream current. Regardless, the upper unit is by far the largest magnitude glacial event in either core. If thickness of sediments is a measure of glacier size and duration, the glacial expansion that caused this upper clay unit was the largest in the Holocene.

The upper clay unit is not uniform. In both basins, it is punctuated by massive fine sand similar to that seen in some of the lower gray bands and not far different from the coarse silt layers that occur within the clay in Rapids Lake. In BNL11-1, sand input began at AD 1470, as dated by a radiocarbon sample taken at the base of the layer. In BNL11-2, a date from the middle of the sand layer indicates that it was still being deposited at AD 1644. Since the younger date was taken from the middle of the layer and the older from the base, it appears that the sand was deposited over time and not in a

single pulse. If true, this rules out flushing of an abandoned channel, mass movement, melting through lake ice, or storm in wash events as possible causes for the sand. One possibility is that meltwater from glaciers on the plateaus above the lake could transport coarse sediment into Bunny Lake. If this were the case, then the length of the time that the sand was deposited reflects the presence of glacial ice on the plateau. Similar to Rapids Lake, the upper gray clay is punctuated further in both cores by multiple 0.1 cm-thick bands of bright orange oxidized material, which may reflect brief intervals of lower lake level.

Bunny Lake is currently still receiving meltwater and rock flour from Large Lake, and the MS, percent organic material and carbonate are similar to that seen during the LIA. We would expect the lake to show glacial conditions until either meltwater into Large Lake decreases or the ice dam is removed, allowing draining to the northeast. Based on comparison with lower sediments in the cores, the configuration of the Renland Ice Cap has not yet returned to what it was prior to ~AD 600, when little to no glacial sediment entered Bunny Lake.

#### **4.3 Glacial History of Raven, Rapids, Bunny Lake**

If the basal age in RAV11-3A-1 is correct, then the Renland Ice Cap retreated from Raven Lake by ~12.6 ka, possibly at the end of the Milne Land Stade (Hall et al., 2008a). Raven Lake lies just inboard of degraded moraines that, based on position and weathering, could date from the Milne Land Stade. Moreover, the lake shows evidence of a higher past level, possible only if ice significantly more extensive than it is now dammed existing outlets. This is consistent with the lake being deglaciated soon after the

Milne Land Stade but while extensive ice was still present in valley occupied now by Large Lake. The end of the Milne Land Stade in central Scoresby Sund may have taken place before ~12.5 ka (Hall et al., 2008b) based on a relative sea-level curve for nearby Kjove Land. Such an early glacial retreat was not observed in Bunny and Rapids Lake, which instead provide minimum-limiting ages for deglaciation of 9.5 ka. I cannot be sure if this difference in basal ages between the sites reflects a time difference in deglaciation or simply the fact that we did not retrieve the lowest sediments from Bunny and Raven Lakes. Moreover, additional work is needed to confirm the early age for deglaciation at Raven Lake.

At Raven Lake, organic deposition persisted for the entire Holocene without any obvious interruption by glacial sediment. Based on evidence given above, I infer that the Renland Ice Cap was not more extensive than it was during the LIA at any time during the Holocene. This limits ice extent to within ~200 m of its present margin. It also suggests rapid retreat after deglaciation in late-glacial time to or within present-day ice-cap limits.

Organic-rich silt also was deposited in Rapids and Bunny Lakes. The basins have the highest organic content in the early- to mid-Holocene, indicating it to be the time of the most productive lakes or the least glacial input. Additional lacustrine records from the Arctic, based on biogenic silica (e.g. Wagner et al., 2000; Cremer et al., 2001; Pordriske and Gajewski, 2007; McKay and Kaufman et al., 2009) show high lake productivity at approximately the same time (7-5 ka). This period of enhanced productivity is traditionally linked to the Holocene Thermal Maximum (9-5 ka) (Larsen et al., 1995).

After the early to mid-Holocene, cores in all three lakes lighten in color, blue color intensity increases, and percent organic material lowers slightly. This gradual

decrease of organic material occurs throughout the cores until the final late Holocene glacial advance when organic content drops to near zero. The gradual decline of organic material over the late-Holocene may indicate an increasing contribution of silt-laden meltwater from the glaciers diluting the organic percent, or a decrease in production of organic material in the lake due to climate or nutrient changes. The fact that the non-glacial Raven Lake also shows a increase in blue color intensity and a small decline in organic content and that there is a corresponding decrease in biogenic silica in lakes across the Arctic (e.g. Wagner et al., 2000; Cremer et al., 2001; Pordriske and Gajewski, 2007; McKay and Kaufman et al., 2009) argues for a change in productivity.

Both glacially fed lakes have short periods of significant glacial input superimposed on the overall record. Based on the presence of inorganic gray clay layers inferred to be rock flour, glaciers were expanded at 9.4, 8.6-8.8, 8.1-8.3, 7.6-7.8, 7.0-7.5, 5.8-6.0, 4.7-5.0, 3.7-4.0, and 3.0-3.6 ka. (Table 5). In addition, glacially fed lakes show a large late Holocene event at or after ~1.4 ka, culminating in the LIA. With the exception of the LIA, most events appear to be of short duration and radiocarbon dates constraining the beginning and end of each event commonly overlap. To test whether these events were periodic, I calculated the time interval between clay layers (Table 5) and then averaged the time spans. I grouped events that occurred close together into a single event and compared the interval between mid-points. There is a rough cyclicity of 1160 years. I assume the 2300-year gap between events in the early Holocene represents a double event. Therefore I calculated the periodicity only with the other values. The variation of times between glacial advances may indicate that the cycle is weak or that the cores do not record every event.

## **4.4 Comparison of Climate Records**

### **4.4.1 Comparisons between the Renland Glacial Record and the Renland Ice Core**

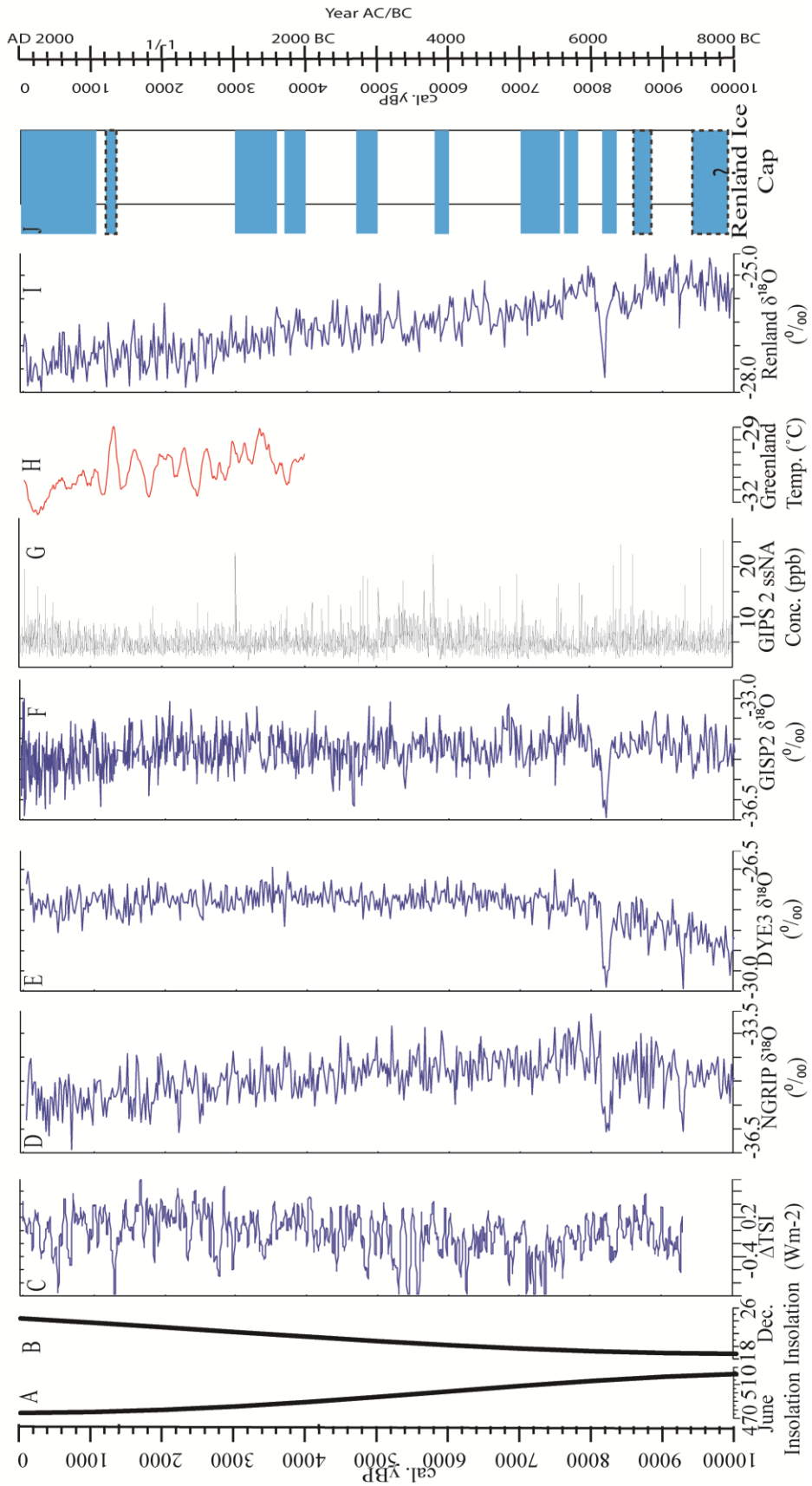
Renland is important, because it is one of only a few sites that allow direct comparison of glacial-margin fluctuations and an ice-core record reconstructed from the same ice mass. Differences between climate proxies can give information on climate and forcing mechanisms. For examples, offsets between temperatures reconstructed from both glacier snowlines and ice-core proxies can indicate changes in seasonality (e.g., Denton et al., 2005), because snowlines record summer conditions and ice cores mean annual.

The Renland Ice Cap was cored to bedrock (Johnsen et al., 1992). Although earlier studies did not find any significant centennial-scale climate events, such as the 8.2 ka event (Johnsen et al., 1992), a new time scale (Fisher et al., 1996), as well as reanalysis at higher resolution (Vinther et al., 2008), resulted in an improved record. The new  $\delta^{18}\text{O}$  record shows a warm early Holocene, peaking around 9 ka. The  $\delta^{18}\text{O}$  values then are interpreted as showing a steady decline in temperatures over the rest of the Holocene. Short-term, abrupt climate cooling occurred at 9.3 and 8.2 ka (Fig. 32).

Broadly, the glacial margin and ice-core records from Renland are in agreement (Fig. 32). The ice core indicates sudden warming during deglaciation from the Milne Land Stade from ~12.5-10 ka. Two abrupt cooling events at 9.3 and 8.2 ka may correlate with glacial advances. All of the cores from glacially fed lakes show multiple fluctuations in meltwater input through this time period. The presence of mostly non-glacial, relatively high-organic content, lacustrine sediments in the early Holocene are consistent

Figure 32: Comparison with Greenland ice cores. (A) and (B) show solar insolation curves for June and Dec. for 60° N throughout the Holocene (Mayewski et al., 2004). (C) Total solar irradiance smoothed with a 40 year average relative to the intensity in 1986 constructed from  $^{10}\text{Be}$  ions in the GISP2 ice core (Steinhilber et al., 2009). (D), (E), and (F) are  $\delta^{18}\text{O}$  profiles for NGRIP (Vinther et al., 2009), DYE 3 (Vinther et al., 2009) and GISP2 ice cores (Grootes and Stuiver, 1997). (F) GISP2 ssNa concentration (ppb) throughout the Holocene. (O'Brien et al., 1995). (H) Paleotemperature reconstruction over the GIS from trapped N and Ar in the GISP2 ice core (Kobashi et al., 2011). (I)  $\delta^{18}\text{O}$  profiles for Renland ice core (Vinther et al., 2008) (J) Periods of glacial expansion of the Renland Ice Cap determined through proglacial lake sediments. The blue blocks indicate periods of glacial expansion, and the dotted borders show advances seen only in BNL11-2. The question mark specifies that the lower boundary of the glacial advance is unknown.





with a warm period of low glacial activity, which agrees well with the HTM from 9-5 ka (Larsen et al., 1995) recorded in the ice core. However, the peak temperature in the ice core occurred at ~9 ka (Vinther et al., 2008), something that is not obvious in the lake records, which show fluctuating glacial activity from 8-9 ka. After the HTM, both the decreasing organic content in the glacially fed lake sediments and the ice core  $\delta^{18}\text{O}$  records suggest a changing climate, possibly cooling conditions through the rest of the Holocene.

The major difference between the records from the glacially fed lakes and the ice core is that none of the small centennial-scale glacial advances shown in the lacustrine sediments after 8.2 ka occur in the Renland ice core  $\delta^{18}\text{O}$  data. This contrast is demonstrated best by the LIA. The ice-core record does not show significant variation during the event (Vinther et al., 2008). However, the local ice caps expanded to their largest extent during the Holocene at this time (e.g., Hall et al., 2008a; Kelly et al., 2008; Lusas, 2011; This study). The lack of high-frequency events in the ice core may be related to the low sampling resolution. However this is unlikely because the 8.2 ka event was observed in the core. The LIA was longer in duration, and since it is younger, less thinning would have occurred to the ice. Therefore the LIA should be easier to detect than the 8.2 ka event. A second possibility is that the  $\delta^{18}\text{O}$  of the Renland ice cap is not recording a pure temperature signal. Instead the record may be influenced by moisture source or precipitation height (Johnsen et al., 1992) Another option is that the mean annual conditions, as recorded by ice cores, did not change significantly on millennial timescales, while summer temperatures, documented by glacier extent, fluctuated.. If this were the case, then winter temperatures would have had to have changed opposite that of

the summer in order to produce the same mean value. This would result from decreased seasonality, with colder summers and warmer winters. In order to test this hypothesis more fully, the Renland ice core needs to be analyzed at high resolution for other proxies, including trapped gases that independently record temperature (i.e., Kobashi et al., 2011).

#### **4.4.2 Holocene Glacier and Climate Fluctuations in Greenland**

The results from my field area fit well with other glacier and climate reconstructions in Greenland. Glaciers retreated to positions similar to or less extensive than at present by the early Holocene and remained behind the LIA limit throughout the HTM, the timing of which is dependent upon location (Kaufmann et al., 2004). In Greenland, the Renland ice core (Larsen et al., 1995), pollen studies (e.g. Fredskild, 1984; Wagner and Melles, 2002; Cremer et al., 2001), and warm-water mollusks in raised marine deposits (e.g. Hall et al., 2008a; Street, 1977) indicate warm temperatures from ~9-5 ka. However, the HTM begins at ~11 ka in Alaska and northwest Canada and is not recorded in the Hudson Bay region until ~7 ka. This spatial variability may be related to the presence of remnants of the LIS, ocean currents, and different positive feedbacks in the widely separated regions (Kaufmann et al., 2004). Our study agrees with Larsen et al. (1995) who identified the HTM in the Renland ice core between 9-5ka.. Sites at lower-elevation, coastal locations north of Scoresby Sund, Ymer Ø (Wagner and Melles, 2002) and Geographical Society Ø (Cremer et al., 2001), reached maximum temperatures and organic productivity at ~8 ka and ~8.5-7 ka, respectively.

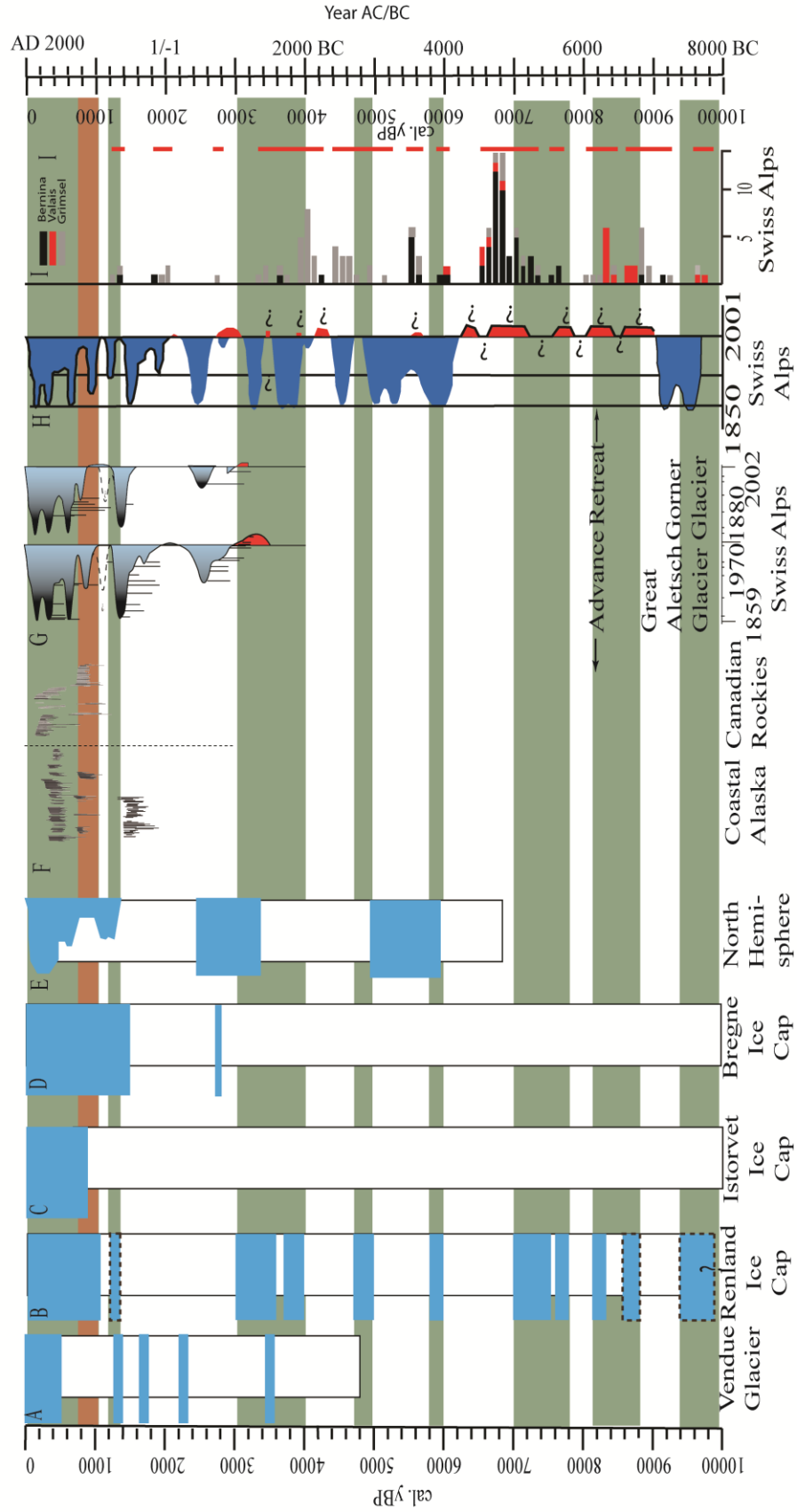
The timing of the HTM maximum may be related to latitude and elevation. The NGRIP and GRIP ice-core temperature records match well, except that the highest

Holocene temperature at NGRIP was reached a few centuries before that at GRIP (Johnsen et al., 2001). Both of these show high temperatures from roughly ~8-4.5 ka, whereas the Dye 3 record, at lower elevation in South Greenland, does not show the HTM until 4.5-4 ka (Dahl-Jensen et al., 1998). This pattern suggests a possible north to south progression of the HTM.

The timing of the HTM in Scoresby Sund may be partially the result of the changing strength of the warm Irminger and the cold East Greenland Currents. The Irminger Current carries saline- and nutrient-rich Atlantic water north. It splits just south of the Denmark Strait, with one branch continuing to flow north and the other flowing south around the southern tip of Greenland. In contrast, the East Greenland Current carries relatively fresh water from the Arctic south along the eastern coast of Greenland. Jennings et al. (2011), based on marine sediment proxies, argued that, particularly at 6.8-4.5 ka, the Irminger Current flowed farther north than at present, bringing warm water up the coast. They further proposed that the change in the current position was related to the strength of the North Atlantic Oscillation (NAO). Warm-water mollusks in raised marine deposits (e.g. Hall et al., 2008a; Street, 1977) confirm warmer-than-present-ocean conditions at this time in the Scoresby Sund region.

Porter and Denton (1967) defined Neoglaciation as the growth and reestablishment of alpine glaciers after the HTM. The timing of this transition in East Greenland is difficult to define precisely because elevation and geography play an important role in glacial growth (Fig. 33). Because of the differences in elevation, the response of glaciers within Scoresby Sund region to changes in forcing is not synchronous. Bone Lake, a threshold lake of the Istorvet Ice Cap in low-elevation (305-

Figure 33: Comparison of Holocene glacial margin records from the Northern Hemisphere. (A), (B), (C), (D), (E) Periods of glacial expansion of the Vendue Glacier (Wilcox, 2012) Renland Ice Cap, Istorvet Ice Cap (Lusas, 2011), Bregne Ice Cap (Levy et al., in review) and a composite of northern hemisphere glaciers (Denton and Karlén, 1973). The blue box represents a period of glacial expansion. The x scale is unitless. The dotted borders show advances seen only in BNL11-2 core. The question mark specifies that the lower boundary of the glacial advance is unknown. (F) Thin bars represent the lifespan of a tree in a proglacial setting in southern Alaska. Multiple tree deaths are inferred to represent glacial expansion (Wiles, 2008). (G) Glacial margin record from the Swiss Alps. Historically dated moraines and in situ stumps of trees killed by glacial advance and dated with dendrochronology afford a known glacier extent for each date (Holzhauser et al., 2005). (H) The record from (G) was extended throughout the Holocene by incorporating the presence of radiocarbon-dated wood. If wood was growing at a location, the glacier was not present (Holzhauser, 2007). (I) Glacial margin reconstructed based on frequency of finding radiocarbon-dated wood in a proglacial setting. Multiple trees dated to the same age are interpreted to represent multiple trees killed in a glacial advance. The graph provides a histogram of number of wood samples dated to a particular time for 3 Swiss glaciers. The red bars indicate periods of glacial expansion. (Joerin et al., 2006). The Green and red bars indicate periods of expansion of the Renland Ice Cap to help in comparison to the other records. The red bar indicates the expansion to near LIA maximum glacial extents in Scoresby Sund.



550 m asl), coastal Liverpool Land, lacks evidence of any Neoglacial advance until the LIA (Lusas, 2011). The first glacial sediment after the HTM to enter Two Move Lake, adjacent to Bregne Ice Cap (720-945 m asl) in Milne Land, occurred in a short pulse at 2.7 ka followed by sustained input at 1.5 ka (Levy et al., in review). Neither of these ice caps is thought to have survived the HTM. In contrast, the Renland Ice Cap (2000 m asl), the highest-elevation of the studied local ice caps, persisted throughout the Holocene (Johnsen et al., 1992) and was sensitive to short cool periods superimposed on the overall warmth.

The Renland Ice Cap meltwater sent glacial material into Bunny Lake at ~9.4, 8.6-8.8, 8.1-8.3, 7.6-7.8, 7.0-7.5, 5.8-6.0, 4.7-5.0, 3.7-4.0, 3.0-3.6, 1.0 (AD 600 and 900) ka (Table 5, Fig. 33). Most of these events are not recorded at the lower-elevation Bregne and Istorvet Ice Caps, although Levy et al. (in review) argued that an increasing clastic content seen in the glacially-fed lakes of the Bregne Ice Cap starting at ~7 ka represents an gradual increase in the amount of snow. The melting of snow mobilized sediment on the landscape and increased the allochthonous sediment into the lake. This event may correspond to the increase in glacial activity seen at about that time in the Renland lakes. However, neither Bregne nor Istorvet Ice Caps show evidence of glacial fluctuations in the mid-Holocene, and it is likely they were absent. The first pulse of glacial activity at Bregne Ice Cap at ~2.7 ka, may correspond to the same climate event that affected Renland lakes a few centuries before. In addition, Vendue Glacier, a nearby outlet of the GIS, also shows advance at 3.3 ka (Wilcox, 2013). Both Renland and Bregne show more vigorous glacial activity during the Dark Ages, as does the Vendue Glacier (Wilcox, 2013). In contrast, lower-elevation Istorvet Ice Cap did not undergo significant growth

until the start of the LIA. The pattern of glaciation at the different ice caps suggests strong elevation control on the timing of Neoglacial expansion. Early Neoglacial expansions were not sufficiently cold to cause glaciation of low-elevation sites, which were only glaciated during the LIA.

The Neoglacial cooling culminated in the largest glacial extent in the Northern Hemisphere during the LIA (Kelly et al., 2008). A date of ~AD 900 affords a maximum-limiting age for the first influx of sediment leading up to the LIA at BNL11-1, although this date may not closely constrain the start of glacial sedimentation. At this time, glaciers from the Renland Ice Cap expanded to the point where they dammed Large Lake. Glacier extent at the very start of this event must have been similar to that at present (or possibly a little less). The earliest date in the Scoresby Sund region that directly constrains when LIA ice neared its maximum comes from the Istorvet Ice Cap, where Lusas (2011) dated the abrupt contact from gyttja to glacial sediments in a threshold lake to AD 1150. Because the lake only received glacial sediment when the ice cap neared the LIA maximum, initial expansion must have been underway prior to this time.

Other records from Greenland agree well with those from Scoresby Sund. In south Greenland, Kaplan et al. (2002) reconstructed the climate from a threshold lake and suggested that the area warmed between 9-6 ka. Neoglaciation began at 3 ka, and the cooling culminated during the LIA. The lake also recorded cooling during Dark Ages at AD 600. The LIA, which appears to have started later than in the Scoresby Sund region (AD 1300), was broken into two major periods separated by warmth at AD 1400-1670.

Briner et al. (2010) reconstructed the glacial and climate history of Jakobshaven Isbræ, a large outlet glacier of the GIS on the west coast of Greenland, from glacially fed



lakes. Deglaciation of the site did not occur until ~7.3 ka. Glaciers were within their modern limits during the mid-Holocene and started to grow at 6-5 ka. Large advances occurred at 2 and 0.5 ka. The latter represents the largest advance after initial deglaciation.

#### **4.4.3 Comparisons between the Glacial Record and the GISP2 Ice Core**

In contrast with the ice-marginal records which show multiple advances, the  $\delta^{18}\text{O}$  record from the GISP2 ice core shows only a single cold event at 8.2 ka (Grootes and Stuiver, 1997) (Fig. 32). Kobashi et al. (2011) analyzed the argon and nitrogen in the trapped air bubbles to reconstruct past temperature fluctuations more accurately than with the  $\delta^{18}\text{O}$ . Overall, their record shows that the climate has been cooling since 4 ka, with the cooling culminating during the LIA. The LIA had the coldest temperature recorded during the last 4 ka.

Superimposed on the general trend are multiple fluctuations of rapid cooling events on the decadal and centennial time scale. Kobashi et al. (2011) found periods of generally cooler conditions during the Bronze Age Cold Period, the Iron Age Cold Period, the Dark Ages, and the Little Ice Age, with numerous short-term cold fluctuations occurring over the last 4 ka. Both the gas record and the lakes in Renland show cooler temperatures and glacier advance at 1700 BC, 1600 BC, AD 600, and AD 900. The temperature over Greenland fluctuated multiple times between 1600 BC and AD 600, with the coldest temperatures reached during that period at 500 BC and AD 250. However, the glacially fed lakes in Renland do not show any variation during this time.

Although the  $\delta^{18}\text{O}$  record does not match that from the Renland Ice Cap margin, the GISP2 chemistry does show some correlation. O'Brien et al. (1995) interpreted positive excursions in chemical ions to indicate atmospheric circulation changes over Greenland at 0-0.6, 2.4-3.1, 5.0-6.1, and 7.8-8.8 ka. All of the positive ion excursions of ions broadly correlate to expansions of the Renland Ice Cap, although there are some differences in exact timing. The glacial record from Renland also shows events at 7.4 and 4.8 ka not seen in the GISP2 core.

#### **4.4.4 European Holocene Glacial and Climate Records**

Overall, the European glacial record is similar to that from east Greenland. Comparisons of European, as well as North American, glacial records with those from Greenland are summarized in figure 33. In general, the warmest climate occurred early in the Holocene at 9-6 ka, with cooling beginning thereafter. Intensification of cooling occurred at ~3.5 ka and culminated in the LIA. One of the best-constrained Holocene glacial records with which to compare the Renland data comes from the Swiss Alps (Holzhauser et al, 2005). Kill dates of glacially-sheared wood, based on dendrochronology, radiocarbon dates, and historical documents, show that glaciers advanced at 1050-900 BC, 800-500 BC (peak at 550 BC), AD 100-200, AD 600-750, AD 900, AD 1100-12000 and AD 1300-1860). By compiling studies that used radiocarbon dates and dendrochronology on glacially transported and overridden wood in glacial forefields, Holzhauser et al. (2007) found that the Holocene was warm in the Alps between 9-6 ka and at 4.5-3.8 ka. Predominantly cold periods occurred at 6-5 ka, and 3.5 ka. Superimposed on the millennial-scale events were shorter-lived cold periods focused

at 9.7-9.4, 8.7-7.8, 7.5-5.9, 5.2-5, 4.7-4.5, and 3.6-3.3 ka. The cold periods produced glacial expansion, even in periods of generally warm climate, such as during the HTM.

Joerin et al. (2006) used radiocarbon dates of wood found in proglacial fluvial deposits to produce dates of when glaciers were smaller than present in the Alps. When the wood grew, the glaciers must have been upvalley of where the wood was found.

According to the authors, glaciers were smaller at 9.85-9.6, 9.3-8.65, 8.55-8.050, 7.7-7.55, 7.450-6.55, 6.15-5.95, 5.7-5.5, 5.2-4.4, 4.3-3.4, 2.8-2.7, 2.15-1.85, and 1.4-1.2 ka.

In Norway, glacially fed lakes record glacial periods at 9.15-9.38, 8.52-8.78, 8.00-8.23, and 1.18-1.29 ka (Hormes et al., 2009). Using a combination of both glacially fed lakes and radiocarbon-dated moraines, Bakke et al. (2005) found that another Norwegian glacier was absent between 9.6-5.2 ka during the HTM. Neoglaciation began at 5.2 with a steady ELA lowering until 2.2 ka. The glacier had two short-lived advances at ~2.2 ka and then continued to grow from 2.0-1.4 ka. After 1.4 ka, the glacier fluctuated and finally reached its maximum Holocene size during the LIA from AD 1350-1930.

#### **4.4.5 North American Holocene Glacial and Climate Record**

The North American glacial record also seems to match that of both Europe and Greenland. Briner et al. (2009) reviewed the literature on the Holocene glacial history for Baffin Island. The Barnes Ice Cap retreated throughout the Holocene, reaching its modern margin by 2 ka, based on radiocarbon- and surface-exposure-dated moraines. Readvances and stillstands represented by ice-margin deposits occurred at 9.5-8.5, 7, and 6 ka. An outlet glacier from the ice cap expanded between AD 1500-1900. Local alpine glaciers showed advance at 10-8, 6, 3.5, and 2.5 ka, and AD 500 and AD 900, with the

LIA reaching peak conditions at AD 1350, 1600, and 1900. Based on an inference that varved sediments record glacial conditions, Thomas et al. (2010) proposed that advances occurred between 9.2-9.0, 8.6-7.5, 7.5-7.2, 6.8-6.3, and 6.2-4.7 ka. A Late Holocene event began at 1.1 ka and was maintained until the end of the LIA.

Wood in proglacial settings provides evidence for glacial expansion between AD 550-650, 1200-1300, 1650-1750, and 1820-1910 in Southern Alaska (Wiles et al., 2008). The authors identified additional periods of glacial expansion, such as between AD 770-810, but the evidence is based on limited data. In western Canada, Clague et al. (2009) identified glacial expansion at 8.2, 6.9-5.6, 4.9-3.8, 3.5-1.9 (peaks at 3.7-3.2, 2.6), 1.7-1.4, and 0.8 ka. Likewise, studies of multiple proxies from glacially fed lake cores revealed periods of expanded ice at 7.4, 3.6-3.8, 2.3, 1.5-1.6, 0.65-0.1 ka in Glacier National Park (Munroe et al., 2012). Luckman (1995) dated the start of the LIA using dendrochronology on sheared tree stumps to before 1142 AD in the Canadian Rockies.

#### **4.5 Holocene Climate Forcing**

Holocene climate change occurs on multiple time scales. Each scale potentially has a different driving mechanism. Long-term Holocene cooling may be driven by decreasing Northern Hemisphere summer insolation (Koç and Jansen, 2004). Using diatom transfer functions, Anderson et al. (2004) showed that the SSTs in the Nordic Seas follow decreasing insolation at 65°N. However, more records are needed to confirm this mechanism. For 65°N in the summer, the insolation reached a maximum ~11 ka, several thousand years before the HTM occurred in Renland.

Superimposed on the long-term Holocene record are millennial-scale events. One of these events at 8.2 ka, has been attributed to glacial outburst through Hudson Strait. Barber et al. (1999) proposed a catastrophic drainage of proglacial Lake Agassiz into the North Atlantic. A large, sudden input of fresh water such as this, would have reduced North Atlantic Deep Water production, which then transported less heat from the equator, cooling the North Atlantic (Broecker, 1989).

Not every short-lived cooling in the Holocene, however, can be attributed to an outburst flood. There are multiple other hypotheses for millennial-scale change, including changing solar intensity (Denton and Karlén, 1973) (Fig. 32), variations in ocean circulation (Denton and Broecker, 2008), and increased volcanic output (Miller et al., 2012).

Miller et al. (2012) argued that the LIA climate shift was the result of four large volcanic eruptions from AD 1275-1300. The volcanic sulfates cooled the Arctic, and multiple positive feedbacks, including increased sea-ice extent and a weakening of the NADW, created a more dramatic and sustained cooling. However, for this theory to be accepted, the LIA must have begun after the proposed volcanic forcing. My results and those of other studies in Scoresby Sund region (e.g. Lusas, 2011; Levy et al., in press; Lowell et al., 2013), the Alps (Holzhauser et al., 2005), and western North America (Wiles et al., 2008), indicate the start of the LIA by ~1150 AD, which rules out volcanic forcing as the primary cause of the LIA. In addition, the LIA is only one of multiple millennial-scale events during the Holocene, and there is no evidence that volcanic activity caused any of the others.

Another potential forcing mechanism is a ‘wobbly ocean conveyor belt’. Based on strong correlation between the Atlantic Multidecadal Oscillation (AMO) and glacial fluctuations in the Alps, Denton and Broecker (2008) proposed that small variations in NADW strength could lead to Holocene climate change in the North Atlantic region. The AMO represents a fluctuation between warm and cold SST modes across the entire North Atlantic (Sutton and Hodson, 2005) and is likely caused by internal variation in the atmospheric-ocean circulation (Schlesinger and Ramankutty, 1994). By using foraminifera to determine past salinity from multiple sediment cores from the Florida Straits, Lund et al. (2006) calculated the variations in volume transported by using the geostrophic flow equation and past changes in relative density between the upper fresh warm water from the South Atlantic and the lower salty water from the North Atlantic subtropical gyre. The current carried less water during the Little Ice Age. The Florida Current comprises a part of the northward meridional overturning circulation, so a weakening would limit the amount of heat transported to the North Atlantic. Denton and Broecker (2008) argued that the continued growth of glaciers in the Northern Hemisphere during the late Holocene indicates a progressive weakening of the NADW throughout the Holocene.

Yet another proposed mechanism for millennial-scale change is solar variability (Denton and Karlén, 1973). Denton and Karlén (1973) observed that solar radiation minima, as inferred from atmospheric radiocarbon variations, coincided with glacial expansion across the Northern Hemisphere. The authors proposed a causal relationship between the two. Nussbaumer et al. (2011) updated the research done by Denton and Karlén (1973), and compared the glacial record of Holzhauser et al. (2007) with solar

fluctuations recorded by the GISP2  $^{10}\text{Be}$  concentration (Steinhilber et al., 2009). Nussbaumer et al. (2011) identified correlation between some of the glacial expansions and a decrease in solar radiation, however not all of the variability was explained by changes in solar output. One problem with this theory is that the changes in radiation throughout the Holocene only differ by a maximum of two watts per meter squared (Steinhilber et al., 2009). Internal amplification within the climate system would be needed to produce the observed climate shifts from such small forcing.

The geographical expression of the Holocene millennial-scale changes affords information on the potential forcing mechanisms. For example, the ‘wobbly ocean conveyor’ hypothesis would favor an out-of-phase relationship between the hemispheres during the Holocene, whereas changes in solar radiation reaching Earth likely would have a global effect. Mayewski et al. (2004) reviewed the literature on Holocene climate variability and proposed that nine rapid climate change events in the Holocene occurred on a global scale, which would favor the solar variability hypothesis. Likewise, Orsi et al. (2012) proposed that the LIA is a globally synchronous event.

Our data cannot rule out either of these two mechanisms at present. The timing of glacial advances from the Southern Alps of New Zealand (e.g., Putnam et al., 2012; Schaefer et al., 2009) differ from those in east Greenland and may indicate an out-of-phase relationship between the hemispheres. However, the lack of abundant, well-constrained Holocene glacial records from both Africa and South America limit any conclusions, particularly as initial data from southern South America seem to differ at least slightly from those in New Zealand (Hall, pers. comm.). There need to be additional

records from the Southern Hemisphere before any inferences on the phase relationship between the hemispheres are certain.



## CHAPTER 5

### CONCLUSIONS

- Sediment cores from both glacially fed and non-glacially fed lakes allow construction of a continuous glacial and climate record for outlet glaciers from Renland Ice Cap. Layers of glacial rock flour in the lake sediments indicate expansion of the Renland Ice Cap at ~9.4, 8.6-8.8, 8.1-8.3, 7.6-7.8, 7.0-7.5, 5.8-6.0, 4.7-5.0, 3.7-4.0, 3.0-3.6, 1.0 (AD 600 and 900) ka.
- The largest advance of the Holocene occurred during the last 1000 years and coincides with the LIA. Moreover, the LIA appears to have been the latest of several, at least semi-periodic millennial-scale events in the Holocene.
- Overall, the record from Renland agrees well with other data from both Scoresby Sund and the high latitudes of the Northern Hemisphere, indicating broad glacier response. The glaciers in Scoresby Sund retreated from the Milne Land Stade at ~12.5-10 ka. The Holocene was the warmest during the HTM (9-5 ka) and the local ice caps retreated behind the LIA limit or disappeared. Neoglaciation began before ~2.7 ka as temperatures cooled and local ice caps reformed. The glaciers reached the maximum extent during the LIA.
- Elevation exerts a strong influence on glacial response. Glaciers at higher elevations will respond first to a snowline lowering and record more events because small variations in ELA will intersect a high-level glacier but may not be sufficient to cause an ice mass to reform at low elevation. The control of elevation points to the need for caution when comparing glaciers across large geographic

regions. Glaciers, although responding to the same forcing, may show differences in duration and magnitude of events due to changes in elevation.

- The data do not support the volcanic forcing mechanism for the LIA proposed by Miller et al. (2012), because the eruptions occurred after the start of the LIA in the glacial records. At this time, I am unable to eliminate either the ‘wobbly ocean conveyor’ model or changes in solar radiation as potential forcing mechanisms for Holocene climate variation. We need more glacial records from the Southern Hemisphere in order to discriminate between the two proposed mechanisms.

## REFERENCES

- Anderson, C., Koç, N., Jennings, A., and Andrews, J.T., 2004. Nonuniform response of the major surface currents in the Nordic Seas to insolation forcing: Implications for the Holocene climate Variability. *Paleoceanography* 19, PA2003, doi:10.1029/2002PA000873.
- Arctic Climate Impact Assessment (ACIA). 2005. Arctic Climate Impact Assessment. Cambridge University Press, Cambridge, U.K., 1024 pp.
- Bakke, J., Lie, O., Nesje, A., Dahl, S.O., and Paasche, O., 2005. Utilizing physical sediment variability in glacier-fed Lakes for continuous glacier reconstructions during the Holocene, Northern Følgefonna, Western Norway. *The Holocene* 15 (2), 161-176.
- Barber, D.C., Dyke, A., Hillaire-Marcel, C., Jennings, A.E., Andrews, J.T., Kerwin, M.W., Bilodeau, G., McNeely, R., Southon, J., Morehead, M.D., and Gagnon, J.-M., 1999. Forcing of the cold event 8,200 years ago by catastrophic drainage of Laurentide lakes. *Nature* 400 (22 July), 344-348.
- Bengtsson, L., Enell, M., 1986. Chemical Analysis. In: Berglund, B.E. (ed.) *Handbook of Holocene Palaeoecology and Palaeohydrology*. John Wiley, Chichester, 423-454.
- Bond, G., Showers, W., Chesby, M., Lotti, R., Almasi, P., deMenocal, P., Priore, P., Cullen, H., Hajdas, I., and Bonani, G., 1997. A pervasive millennial-scale cycle in North Atlantic Holocene and glacial climates. *Science* 278 (14 Nov.), 1257-1266.
- Bond, G., Kromer, B., Beer, J., Muscheler, R., Evans, M.N., Showers, W., Hoffmann, S., Lotti-Bond, R., Hajdas, I., and Bonani, G., 2001. Persistent solar influences on North American climate during the Holocene. *Science* 294 (7 Dec.), 2130-2136.
- Briner, J.P., Davis, T., and Miller, G.H., 2009. Latest Pleistocene and Holocene Glaciation of Baffin Island, Arctic Canada: Key Patterns and Chronologies. *Quaternary Science Reviews* 28, 2075-2087.
- Briner, J.P., Steart, H.A.M., Young, N.E., Philips, W., and Losee, S., 2010. Using proglacial-threshold lakes to constrain fluctuations of the Jakobshavn Isbrea ice margin, Western Greenland, during the Holocene. *Quaternary Science Review*, 29, 3861-3874.
- Broecker, W.S., 1998. Paleocean circulation during the last deglaciation: A bipolar seesaw? *Paleoceanography* 13, 2, 119-121.

- Clague, J.J., Menounos, B., Osborn, G., Luckman, B.H., and Koch, J., 2009. Nomenclature and resolution in Holocene glacial chronologies. *Quaternary Science reviews* 28, 2231-2238.
- Chapman, W.L., and Walsh, J.E. 1993. Recent variations of sea ice and air temperatures in high latitudes. *Bulletin American Meteorological Society* 74 (1), 33-47.
- Cremer, H., Bennike, O., Hakansson, L., Hultsch, N., Klug, M., Kobabe, S., and Wagner, B., 2005. Hydrology and diatom phytoplankton of high arctic lakes and ponds on Store Koldewey, Northeast Greenland. *Internat. Rev. Hydrobiol* 90, 84-99.
- Cremer, H., Melles, M., and Wagner, B., 2001. Holocene climate changes reflected in a diatom succession from Basaltsø, East Greenland. *Can. J. Bot* 79, 649-656.
- Dahl, S.O., Bakke, J., Lie, O., and Nesje, A., 2003. Reconstruction of former glacier equilibrium-line altitudes based on proglacial sites: An evaluation of approaches and selection of sites. *Quaternary Science Reviews* 22, 275-287.
- Dahl-Jensen, D., Mosegaard, K., Gundestrup, N., Clow, G.D., Johnsen, S.J., Hansen, A.W., and Balling, N., 1998. Past temperatures directly from the Greenland Ice Sheet. *Science* 282 (9 Oct.), 268-271.
- Denton, G.H., Alley, R.B., Comer, G.C., and Broecker, W.S., 2005. The role of seasonality in abrupt climate change. *Quaternary Science Reviews* 24, 1159-1182.
- Denton, G.H., and Broecker, W.S., 2008. Wobbly ocean conveyor circulation during the Holocene. *Quaternary Science Reviews* 27, 1939-1950.
- Denton, G.H., and Karlén, W., 1973. Holocene climatic variations-Their pattern and possible cause. *Quaternary Research* 3, 155-205.
- Fisher, D.A., Koerner, R.M., Kuivinen, K., Clausen, H.B., Johnsen, S.J., Steffensen, J.-P., Gundestrup, N., and Hammer, C.U., 1996. Inter-comparison of ice core  $\delta(^{18}\text{O})$  and precipitation records from sites in Canada and Greenland over the last 3500 years and over the last few centuries in detail using EOF techniques. *NATO ASI Series I* 141, 297-328.
- Fredskild, B., 1984. Holocene paleo-winds and climate changes in West Greenland as indicated by long-distance transported and local pollen in lake sediments. In Mörner, N.A., and Karlén W., (eds.) *Climatic Changes on a yearly to Millennial Basis*. D Reidel Publishing Co., Dordrecht, Netherlands, 163-171.

- Fronval, T., and Jansen, E., 1997. Eemian and early Weichselian (140-60 ka) paleoceanography and paleoclimate in the Nordic seas with comparisons to Holocene conditions. *Paleoceanography* 12 (3), 443-462.
- Grootes, P.M., and Stuiver, M., 1997. Oxygen 18/16 variability in Greenland snow and ice with  $10^{-3}$ - to  $10^5$ -year time resolution. *Journal of Geophysical Research* 102 (C12), 26445-26470.
- Hall, B.L., Baroni, C., and Denton, G.H., 2008a. The most extensive Holocene advance in the Stauning Alper, East Greenland, occurred in the Little Ice Age. *Polar Research* 27, 128-134.
- Hall, B.L., Baroni, C., Denton, G.H., Kelly, M.A., and Lowell, T.L., 2008b. Relative sea-level change, Kjove Land, Scoresby Sund, East Greenland: Implications for seasonality in Younger Dryas time. *Quaternary Science Reviews* 27, 2283-2291.
- Hansen, J., Ruedy, R., Sato, M., and Lo, K., 2010. Global surface temperature change. *Review of Geophysics* 48 (RG4004), doi:10.1029/2010RG000345.
- Holzhauser, H., 2007. Holocene glacier fluctuations in the Swiss Alps. In: Ricard, H., Magny, M., and Mordant, C., (eds.) *Environnements et Cultures À l'Âge du Bronze en Europe Occidentale*. Editions du Comité des Travaux, Paris, 29-43.
- Holzhauser, H., Magny, M., and Zumbühl, H.J., 2005. Glacier and lake-level variations in West-Central Europe over the last 3500 years. *The Holocene* 15 (6), 789-801.
- Hormes, A., Blaauw, M., Dahl, S.O., Nesje, A., and Possnert, G., 2009. Radiocarbon wiggle-match dating of proglacial lake sediments-Implications for the 8.2 ka event. *Quaternary Geochronology* 4, 267-277.
- Howat, I.M., Joughin, I., and Scambos, T.A., 2007. Rapid changes in ice discharge from Greenland outlet glaciers. *Science* 315 (16 Mar.), 1559-1561.
- Jennings, A., Andrews, J., and Wilson, L., 2011. Holocene environmental evolution of the SE Greenland Shelf north and south of the Denmark Strait: Irminger and East Greenland Current interactions. *Quaternary Science Reviews* 30, 980-998.
- Joerin, U.E., Stocker, T.F., and Schlüchter, C., 2006. Multicentury glacier fluctuations in the Swiss Alps during the Holocene. *The Holocene* 16 (5), 697-704.

- Johnsen, S.J., Clausen, H.B., Dansgaard, W., Gundestrup, N.S., Hansson, M., Jonsson, P., Steffensen, J.P., and Sveinbjörnsdóttir, A.E., 1992. A “deep” ice core from East Greenland. *Meddr Gronland, Geoscie* 29, 3-22.
- Johnsen, S.J., Dahl-Jensen, D., Gundestrup, N., Steffensen, J.P., Clausen, H.B., Miller, H., Masson-Delmotte, V., Sveinbjörnsdóttir, A.E., and White, J., 2001. Oxygen isotope and paleotemperature records from six Greenland ice-core Stations: Camp Century, Dye-3, GRIP, GISP2, Renland and NorthGRIP. *Journal of Quaternary Science* 16 (4), 299-307.
- Kaplan, M.R., Wolfe, A.P., and Miller, G.H., 2002. Holocene environmental variability in Southern Greenland inferred from lake sediments. *Quaternary Research* 58, 149-159.
- Kaufman, D.S., Ager, T.A., Anderson, N.J., Anderson, P.M., Andrews, J.T., Bartlein, P.J., Brubaker, L.B., Coats, L.L., Cwynar, L.C., Duvall, M.L., Dyke, A.S., Edwards, M.E., Eisner, W.R., Gajewski, K., Geirsdóttir, A., Hu, F.S., Jennings, A.E., Kaplan, M.R., Kerwin, M.W., Lozhkin, A.V., MacDonald, G.M., Miller, G.H., Mock, C.J., Oswald, W.W., Otto-Bliesner, B.L., Porinchu, D.F., Rühland, Smol, J.P., Steig, E.J., and Wolfe, B.B., 2004. Holocene thermal maximum in the Western Arctic (0-180°W). *Quaternary Science Reviews* 23, 529-560.
- Kelly, M.A., Lowell, T.V., Hall, B.L., Schaefer, J.M., Finkel, R.C., Goehring, B.M., Alley, R.B., and Denton, G.H., 2008. A  $^{10}\text{Be}$  chronology of late glacial and Holocene mountain glaciation in the Scoresby Sund region, East Greenland: Implications for seasonality during late glacial time. *Quaternary Science Reviews* 27, 2273-2282.
- Kobashi, T., Kawamura, K., Severinghaus, J.P., Barnola, J.-M., Nakaegawa, T., Vinther, B.M., Johnsen, S.J., and Box, J.E., 2011. High variability of Greenland surface temperature over the past 4000 years estimated from trapped air in an ice core. *Geophysical Research Letters* 38 (L21501), doi:10.1029-2011GL04944.
- Koç, N., and Jansen, E., 1994. Response of high-latitude Northern Hemisphere to orbital climate forcing: Evidence from the Nordic Seas. *Geology* 22 (6), 523-526.
- Koerner, R.M. 2005. Mass balance of glaciers in the Queen Elizabeth Islands, Nunavut, Canada. *Annals of Glaciology* 42, 417-423.
- Krabill, W., Hanna, E., Huybrechts, P., Abdalati, W., Cappelen, J., Csatho, B., Frederick, E., Manizade, S., Martin, C., Sonntag, J., Swift, R., Thomas, R., and Yungel, J.,

2004. Greenland Ice Sheet: Increased coastal thinning. *Geophysical Research Letters* 34 (L24402), doi:10.1029/2004GL021533.
- Kwok, R., Cunningham, G.F., Wensnahan, M., Rigor, I., Zwally, H.J., and Yi, D., 2009. Thinning and volume loss of the Arctic Ocean sea ice cover: 2003-2008. *Journal of Geophysical Research* 114 (C07005), doi:10.1029/2009JC005312.
- Larsen, N.K., Kjaer, K.H., Olsen, J., Funder, S., Kjeldsen, K.K., and Norgaard-Pedersen, N., 2011. Restricted impact of Holocene climate variations on the Southern Greenland Ice Sheet. *Quaternary Science Reviews* 30, 3171-3180.
- Larsen, E., Sejrup, H.P., Johnsen, S.J., and Knudsen, K.L., 1995. Do Greenland ice cores reflect NW European interglacial climate variations? *Quaternary Research* 43, 125-132.
- Leslie, A.G., and Nutman, A.P., 2000. Episodic tectono-thermal Activity in the southern part of the East Greenland Caledonides. *Geology of Greenland Survey Bulletin* 186, 42-49.
- Levy, L.B., Kelly, M.A., Lowell, T.V., Hall, B.L., Hempel, L.A., Honsaker, W.M., Lusas, A.R., Howley, J.A., Axford, Y.L., Holocene fluctuations of Bregne Ice Cap, Scoresby Sund, East Greenland: A proxy for climate along the Greenland Ice Sheet margin. *Quaternary Science Reviews*. in review.
- Lowell, T.V., Hall, B.L., Kelly, M.A., Bennike, O., Lusas, A.R., Honsaker, W., Smith, C.A., Levy, L.B., Travis, S., and Denton, G.H., 2013. Late Holocene expansion of the Istorvet Ice Cap, Liverpool Land, East Greenland. *Quaternary Science Reviews* 63, 128-140.
- Luckman, B.H., 1995. Calendar-dated, early 'Little Ice Age' glacier advance at Robson Glacier, British Columbia, Canada. *The Holocene* 5 (2), 149-159.
- Lund, D.C., Lynch-Stieglitz, J., and Curry, W.B., 2006. Gulf Stream density structure and transport during the past millennium. *Nature* 444 (30 Nov.), 601-604.
- Lusas, A.R. 2011. Holocene fluctuation of the Istorvet Ice Cap, Liverpool Land, East Greenland (Unpublished Master's Thesis). University of Maine, Orono, ME. 149 pp.

- Martin, H.E., and Whalley, W.B., 1987. Rock glaciers part 1: rock glacier morphology: classification and distribution. *Progress in Physical Geograpy* 11, 260-282.
- Mayewski, P.A., Rohling, E.E., Stager, J.C., Karlen, W., Maasch, K.A., Meeker, L.D., Meyerson, E.A., Gasse, F., van Kreveld, S., Holmgren, K., Lee-Thorp, J., Rosqvist, G., Rack, F., Staubwasser, M., Schneider, R.R., and Steig, E.J., 2004. Holocene climate variability. *Quaternary Research* 62, 243-255.
- McKay, N.P., and Kaufman, D.S., 2009. Holocene climate and glacier variability at Hallet and Greyling Lakes, Chugach Mountains, South-Central Alaska. *Journal of Paleolimnology* 41, 143-159.
- Meyers, P.A., and Lallier-Vergès, E., 1999. Lacustrine sedimentary organic matter records of late Quaternary paleoclimates. *Journal of Paleolimnology* 21, 345-372.
- Miller, G.H., Geirsdottir, A., Zhong, Y., Larsen, D.J., Otto-Bliesner, B.L., Holland, M.M., Bailey, D.A., Refsnider, K.A., Lehman, S.J., Southon, J.R., Anderson, C., Bjornsson, H., and Thordarson, T., 2012. Abrupt onset of the Little Ice Age triggered by volcanism and sustained by sea-ice/ocean feedbacks. *Geophysical Research Letters* 39 (L02708), doi:10.1029/2011GL050168.
- Miller, G.H., Alley, R.B., Brigham-Grette, J., Fitzpatrick, J.J., Polyak, L., Serreze, M.C., and White, J.W.C., 2010. Arctic amplification: Can the past constrain the future? *Quaternary Science Reviews* 29, 1779-1790.
- Munore, J.S., Crocker, T.A., Giesche, A.M., Rahlson, L.E., Duran, L.T., Bigl, M.F., and Laabs, B.J.C., 2012. A lacustrine-based Neoglacial record for Glacier National Park, Montana, USA. *Quaternary Science Reviews* 53, 39-54.
- Mybro, A., and Wright, H.E., 2008. Livingstone-Bolivia. *Limnological Research Center Core Facility SOP series*. Last access on 6/14/2013 at <http://lrc.geo.umn.edu/laccore/assets/pdf/sops/livingstone-bolivia.pdf>.
- Nesje, A., Matthew, J.A., Dahl, S.O., Berrisford, M.S., and Andersson, C., 2001. Holocene glacier fluctuations of Flatebreen and winter-precipitation changes in the Jostedalbreen Region, Western Norway, based on glaciolacustrine sediment records. *The Holocene* 11 (3), 267-280.



- Nussbaumer, S.U., Steinhilber, F., Trachesel, M., Breitenmoser, P., Beer, J., Blass, A., Grosjean, M., Hafner, A., Holzhauser, H., Wanner, H., and Zumbühl, H.J., 2011. Alpine climate during the Holocene: A comparison between records of glaciers, lake sediments, and solar activity. *Journal of Quaternary Science* 26 (7), 703-713.
- O'Brien, S.R., Mayewski, P.A., Meeker, L.D., Meese, D.A., Twickler, M.S., and Whitlow, S.I., 1995. Complexity of Holocene as reconstructed from a Greenland ice core. *Science* 270 (22 Dec.), 1962-1964.
- Orsi, A.J., Cornuelle, B.D., and Severinghaus, J.P., 2012. Little Ice Age cold interval in Western Antarctica: Evidence from borehole temperature at the West Antarctic Ice Sheet (WAIS) Divide. *Geophysical Research Letters* 39 (L09710), doi:10.1029/2012GL051260.
- Parizek, B.R., and Alley, R.B., 2004. Implications of increased Greenland surface melt under global-warming scenarios: Ice-sheet simulations. *Quaternary Science Reviews* 23, 1013-1027.
- Podrifske, B., and Gajewski, K., 2007. Diatom community response to multiple scales of Holocene climate variability in a small lake on Victoria Island, NWT, Canada. *Quaternary Science Reviews* 26, 3179-3196.
- Porter, S.C., and Denton, G.H., 1967. Chronology of Neoglaciation in the North American Cordillera. *American Journal of Science* 265, 177-210.
- Putnam, A.E., Schaefer, J.M., Denton, G.H., Barrell, D.J.A., Finkel, R.C., Andersen, B.G., Schwartz, R., Chinn, T.J., and Doughty, A.M., 2012. Regional climate control of glaciers in New Zealand and Europe during the pre-industrial Holocene. *Nature Geoscience* 5 (12 Aug.), 627-630.
- Reimer, P.J., Baillie, M.G.L., Bard, E., Bayliss, A., Beck, J.W., Blackwell, P.G., Ramsey, C.B., Buck, C.E., Burr, G.S., Edwards, R.L., Friedrich, M., Grootes, P.M., Guilderson, T.P., Hajdas, I., Heaton, T.J., Hogg, A.G., Hughen, K.A., Kaiser, K.F., Kromer, B., McCormac, F.G., Manning, S.W., Reimer, R.W., Richards, D.A., Southon, J.R., Talamo, S., Turney, C.S.M., van der Plicht, J., and Weyhenmeyer, C.E., 2009. IntCal09 and Marine09 radiocarbon age calibration curves, 0-50,000 years cal BP. *Radiocarbon* 51 (4), 1111-1150.
- Rignot, E., and Kanagaratnam, P., 2006. Changes in the velocity structure of the Greenland Ice Sheet. *Science* 311(17 Feb.), 986-990.
- Rothrock, D.A., Yu, Y., and Maykut, G.A., 1999. Thinning of the arctic sea-ice cover. *Geophysical Research Letters* 26 (23), 3469-3472.

- Schaefer, J.M., Denton, G.H., Kaplan, M., Putnam, A., Finkel, R.C., Barrell, D.J.A., Andersen, B.G., Schwartz, R., Mackintosh, A., Chinn, T., and Schlüchter, C., 2009. High-frequency Holocene glacier fluctuations in New Zealand differ from the northern signature. *Science* 324 (1 May), 622-625.
- Schlesinger, M.E., and Ramankutty, N., 1994. An oscillation in the global climate system of period 65-70 Years. *Nature* 367 (24 Feb.), 723-726.
- Serreze, M.C., and Barry, R.G., 2011. Processes and impacts of arctic amplification: A research synthesis. *Global and Planetary Change* 77, 85-96.
- Stabel, H.-H., 1986. Calcite precipitation in Lake Constance: Chemical equilibrium, sedimentation, and nucleation by algae. *Limnology and Oceanography* 31 (5), 1081-1093.
- Stearns, L.A., and Hamilton, G.S., 2007. Rapid volume loss from two East Greenland outlet glaciers quantified using repeat stereo satellite imagery. *Geophysical Research Letters* 34 (L05503), doi:10.1029/2006GL028982.
- Steinhilber, F., Beer, J., and Fröhlich, C., 2009. Total solar irradiance during the Holocene. *Geophysical Research Letters* 36 (L19704), doi:10.1029/2009GL040142.
- Street, F.A., 1977. Deglaciation and marine paleoclimates, Schuchert Dal, Scoresby Sund, East Greenland. *Arctic and Alpine Research* 9 (4), 421-426.
- Stroeve, J., Holland, M.M., Meier, W., Scambos, T., and Serreze, M., 2007. Arctic sea ice decline: Faster than forecast. *Geophysical Research Letters* 34 (L09501), doi:10.1029/2007GL029703.
- Stuiver, M., and Reimer, P. J., 1993. Extended 14C database and revised CALIB radiocarbon calibration program. *Radiocarbon* 35, 215-230.
- Sutton, R.T., and Hodson, D.L.R., 2005. Atlantic Ocean forcing of North American and European summer climate. *Science* 309 (1 July), 115-118.
- Thomas, E.K., Szymanski, J., and Briner, J.P., 2010. Holocene alpine glaciation inferred from lacustrine sediments on northeastern Baffin Island, Arctic Canada. *Journal of Quaternary Science* 25 (2), 146-161.

- Vinther, B.M., Buchardt, S.L., Clausen, H.B., Dahl-Jensen, D., Johnsen, S.J., Fisher, D.A., Koerne, R.A., Raynaud, D., Lipenkov, V., Andersen, K.K., Blunier, T., Rasmussen, S.O., Steffensen, J.P., and Svensson, A.M., 2009. Holocene thinning of the Greenland ice sheet. *Nature* 461, 385-388.
- Vinther, B.M., Clausen, H.B., Fisher, D.A., Koerner, R.M., Johnsen, S.J., Anderson, K.K., Dahl-Jensen, D., Rasmussen, S.O., Steffensen, J.P., and Svensson, A.M., 2008. Synchronizing ice cores from the Renland and Agassiz Ice Caps to the Greenland Ice Core Chronology. *Journal of Geophysical Research* 113, doi:10.1029/2007JD009143.
- Wagner, B., and Melles, M. 2002. Holocene environmental history of Western Ymer Ø, East Greenland, inferred from lake sediments. *Quaternary International* 89, 165-176.
- Wagner, B., Melles, M., Hahne, J., Niessen, F., and Hubberten, H.-W., 2000. Holocene climate history of Geographical Society Ø, East Greenland- Evidence from lake sediments. *Paleogeography, Paleoclimatology, Paleoecology* 160, 45-68.
- Wilcox, P., 2013. Late-Holocene expansion of the Greenland Ice Sheet as recorded by the Vendue Glacier, Graben Land, East Greenland (Unpublished Master's Thesis). University of Cincinnati, Cincinnati, OH, 60 pp.
- Wiles, G.C., Barclay, D.J., Calkin, P.E., and Lowell, T.V., 2008. Century to millennial-scale temperatures variations for the last two thousand years indicated from glacial geologic records of southern Alaska. *Global and Planetary Change* 60, 115-125.
- Zachos, J., Pagani, M., Sloan, L., Thomas, E., and Billups, K., 2005. Trends, rhythms, and aberrations in global climate 65 Ma to present. *Science* 292 (27 April), 686-693.

## **APPENDIX A: DETAILED GRAIN SIZE MEASUREMENT METHOD**

In order to measure the grain-size of the cores, I used the following method modified from Northern Arizona University's Sedimentary Records of Environmental Change Lab for preparing samples for a Coulter counter. Using clean spatulas, I placed 0.6-0.9 g of sediment in a 50 mL centrifuge tube. Approximately 5 mL of 30% H<sub>2</sub>O<sub>2</sub> was added before I agitated the samples with a vortex mixer breaking up the sample and knocking it off the walls of the tube. The cap was unscrewed and the samples were placed in a ~50 °C water bath that was heated by hot plate. The samples sat in the bath for six hours, and I agitated the samples with the vortex mixer after the second, fourth, and sixth hour. After six hours the hotplate was turned off and the samples remained in the water bath overnight. The following day I added ~15 mL of DI water and then centrifuged the samples at 3400 rpm for 10 min. I decanted the liquid and filled the test tube with an additional ~15 mL of DI water and then hand shook the tubes. I then centrifuged the sample at the same settings, decanting the excess liquid. Next I added ~30 mL of Na<sub>2</sub>CO<sub>3</sub> to the test tubes, and I mixed the samples using the vortex mixer. The samples were placed in an oven at ~80 °C for five hours, being shaken by hand after the second and fourth hour. After five hours the samples were centrifuged at 3400 rpm for 10 mins, and the liquid decanted. The tube was filled again with ~30 mL of DI water, shaken, and then centrifuged at the same settings. The liquid was then decanted. The procedure removed any organic material or biogenic silica in the sample. Five milliliters of DI was added to prevent the sample from drying out during cold storage.

I brought the samples to Dartmouth College, where I centrifuged the samples at 3400 rpm for 10 min. and decanted the DI water. I added a dispersant, ~5 mL of Na-Hexametaphosphate. I analyzed the samples with Beckman LS230 Coulter Counter with

Fluid Module. I followed standard operating procedures to analyze the sediment (see instruction manual for procedures and brief discussion on the principles of how the particles are measured). Before the sample was added, I mixed the sediment with dispersant on a vortex mixer for a minimum of 30 sec. I then hand shook the test tube and as the sediment was suspended, sucked up the sample with a disposable pipette. Using the pipette, I added the sediment solution to the Coulter counter until the desired obscuration was reached. Between runs, I flushed the Coulter counter a minimum of four times with DI water to ensure no cross contamination.

## APPENDIX B: Core LOGS

# BNL11-1A-1

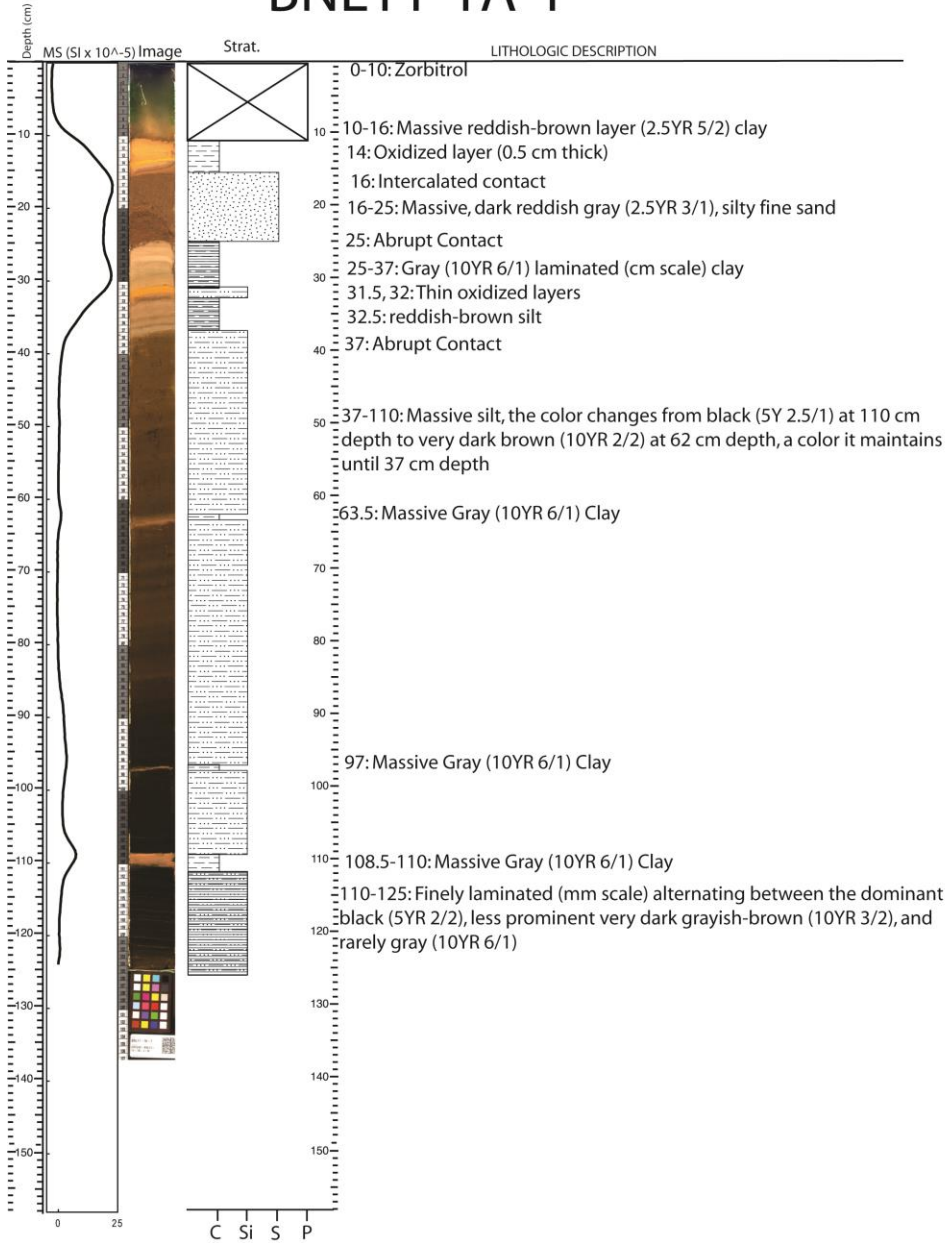


Figure 34: Initial description of core BNL11-1A-1

# BNL11-1B-1

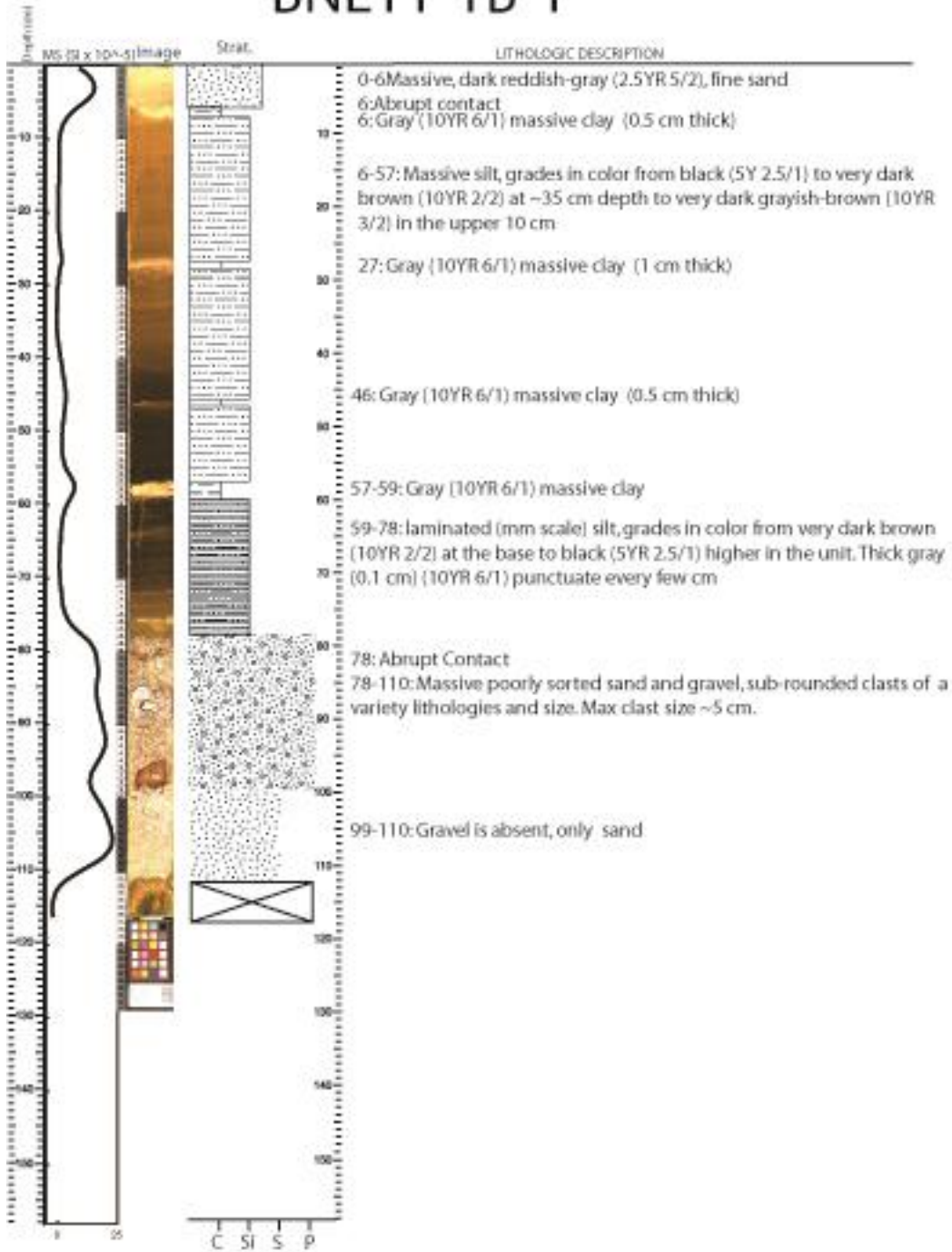


Figure 35: Initial description of core BNL11-1B-1

# BNL11-2A-1

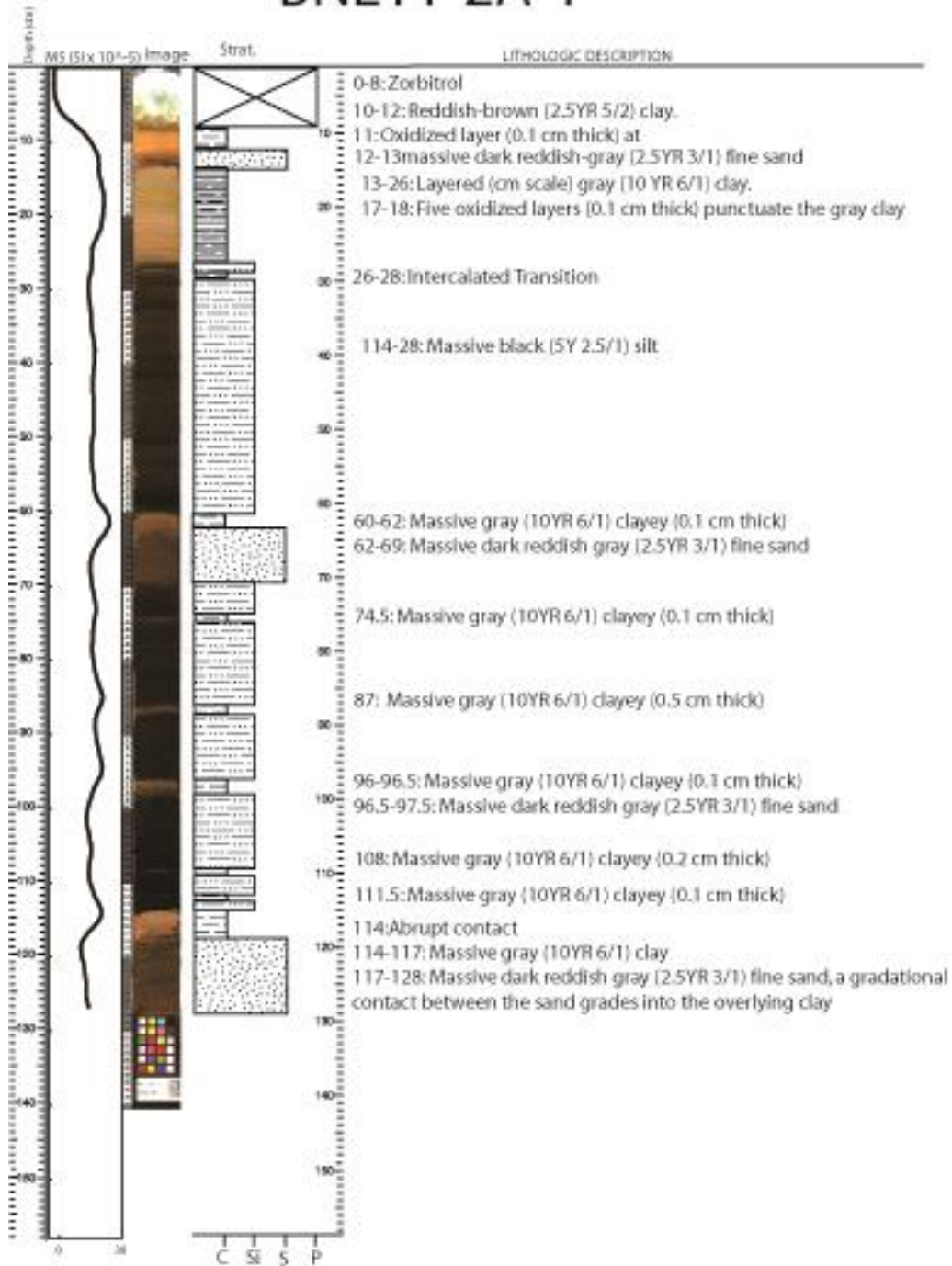


Figure 36: Initial description of core BNL11-2A-1



# BNL11-2A-2

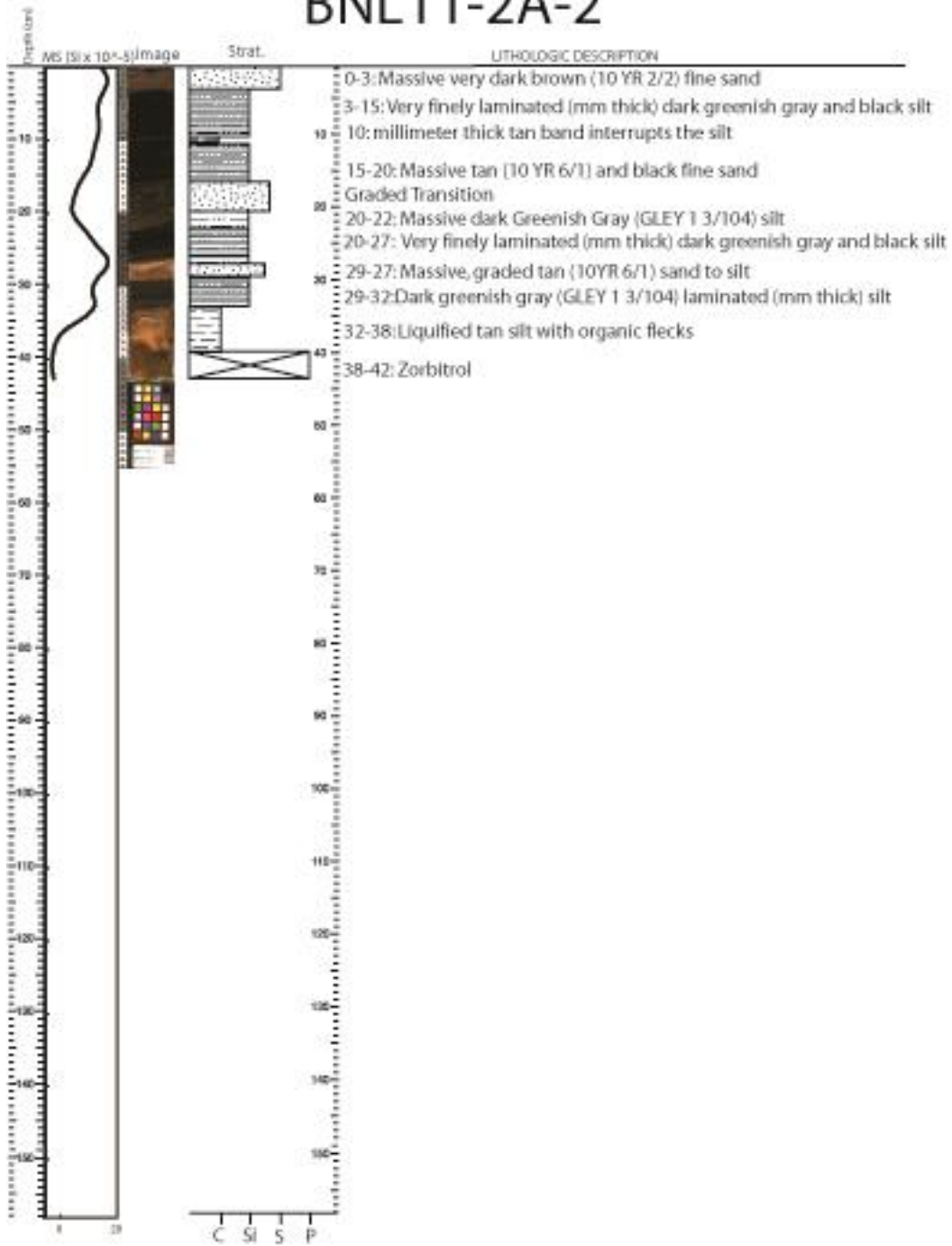


Figure 37: Initial description of core BNL11-2A-2

# BNL11-3A-1

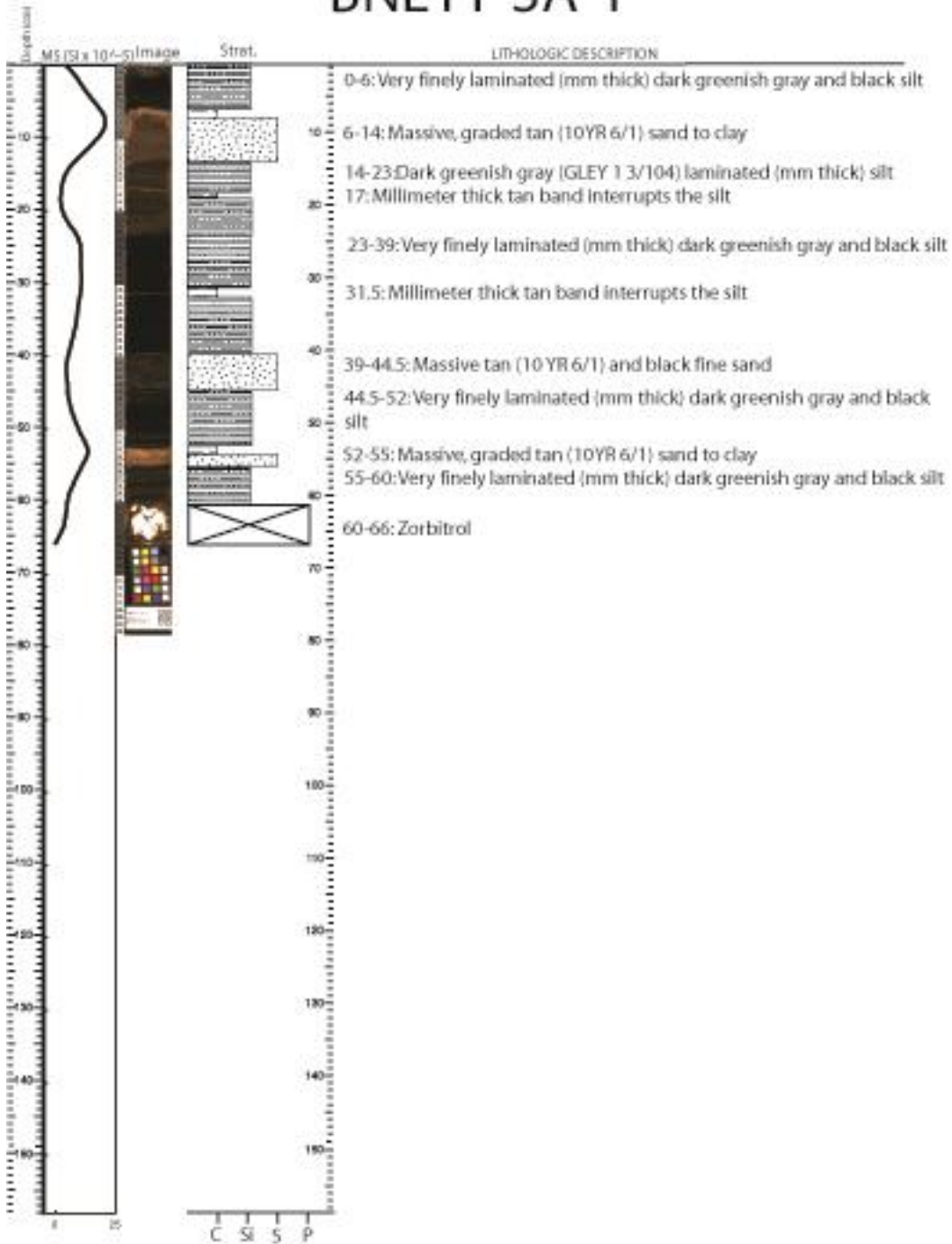


Figure 38: Initial description of core BNL11-3A-1

# RAV11-1A-1

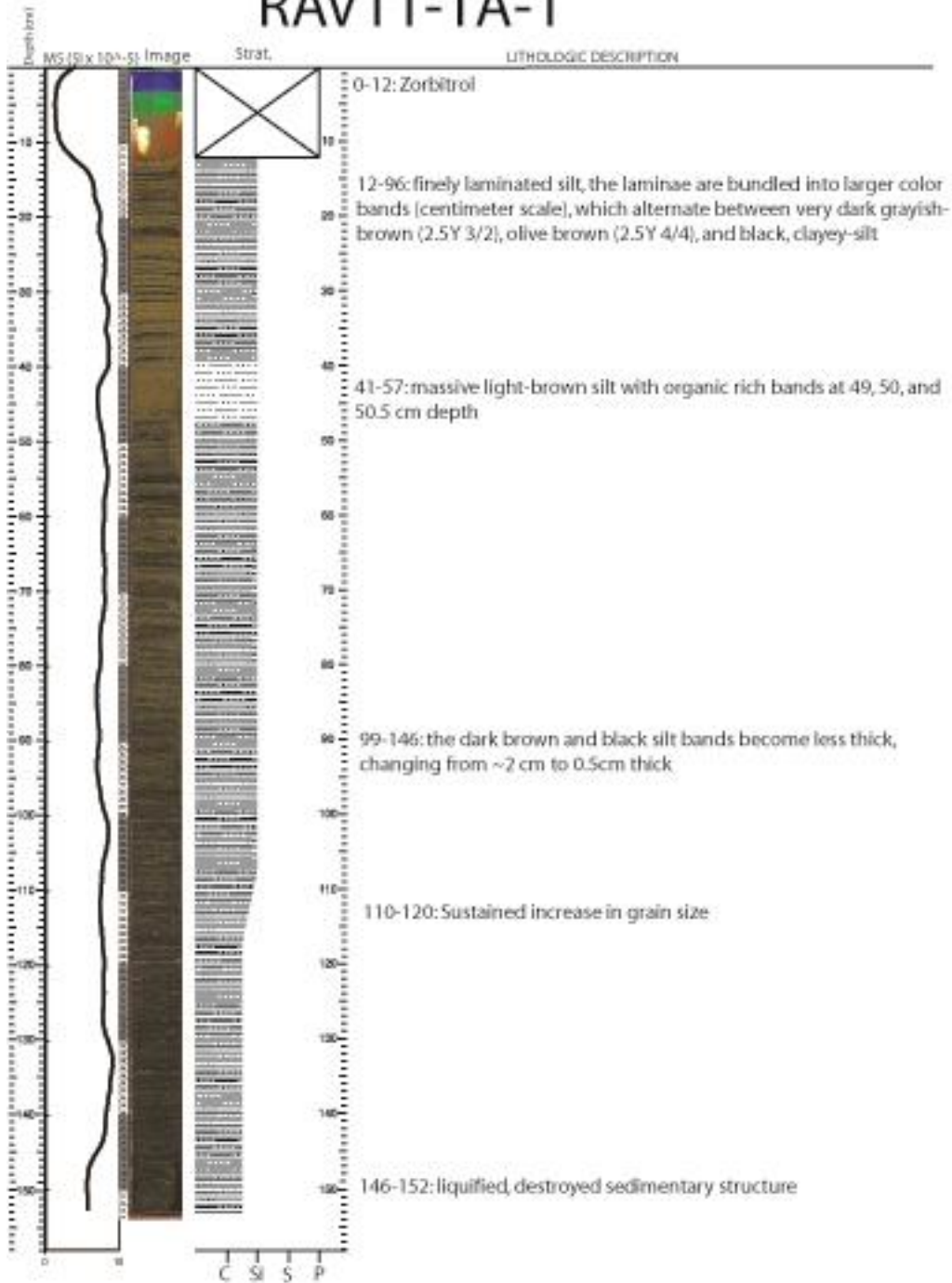


Figure 39: Initial description of core RAV11-1A-1

# RAV11-1A-2

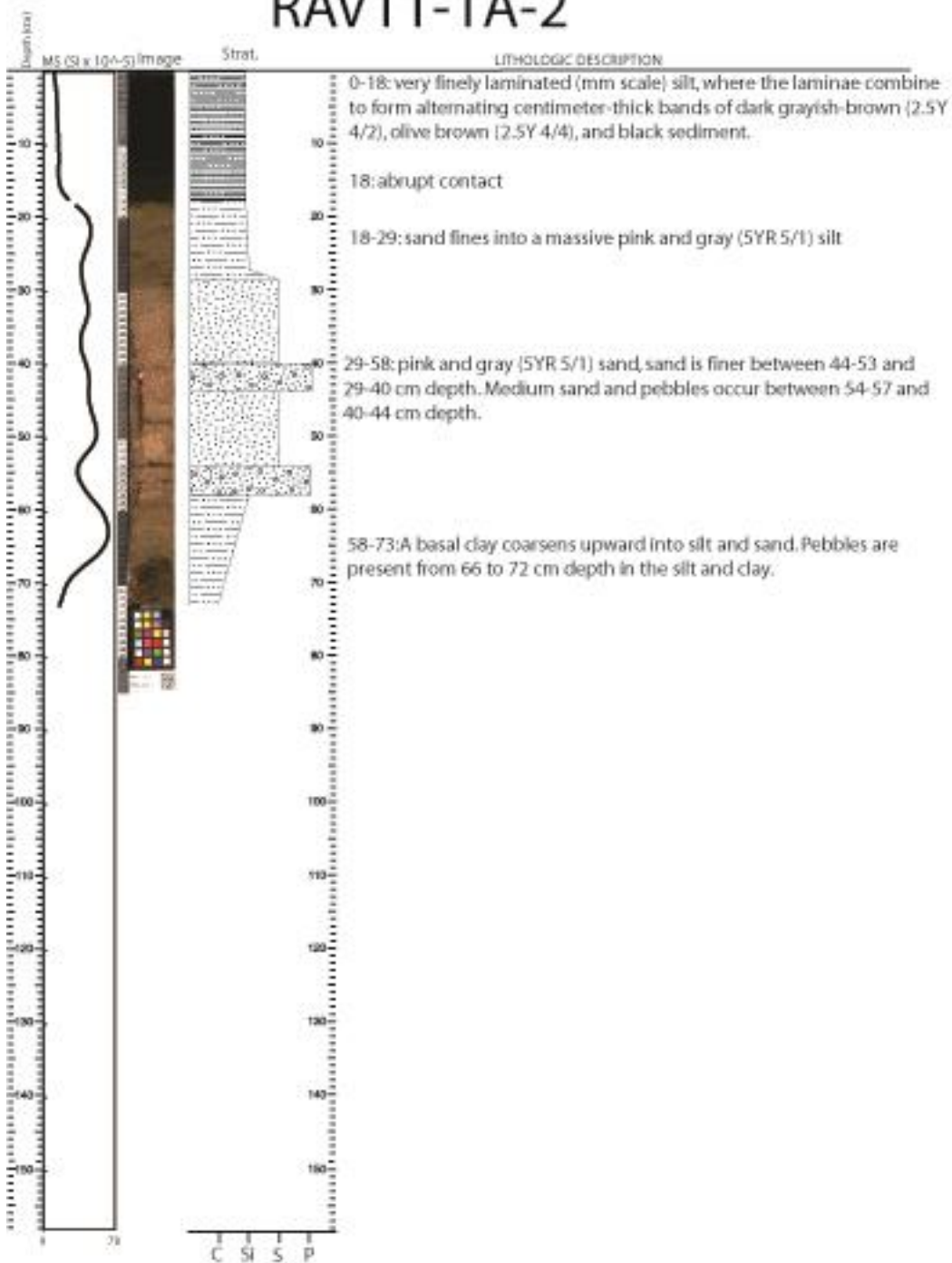


Figure 40: Initial description of core RAV11-1A-2

# RAV11-2A-1

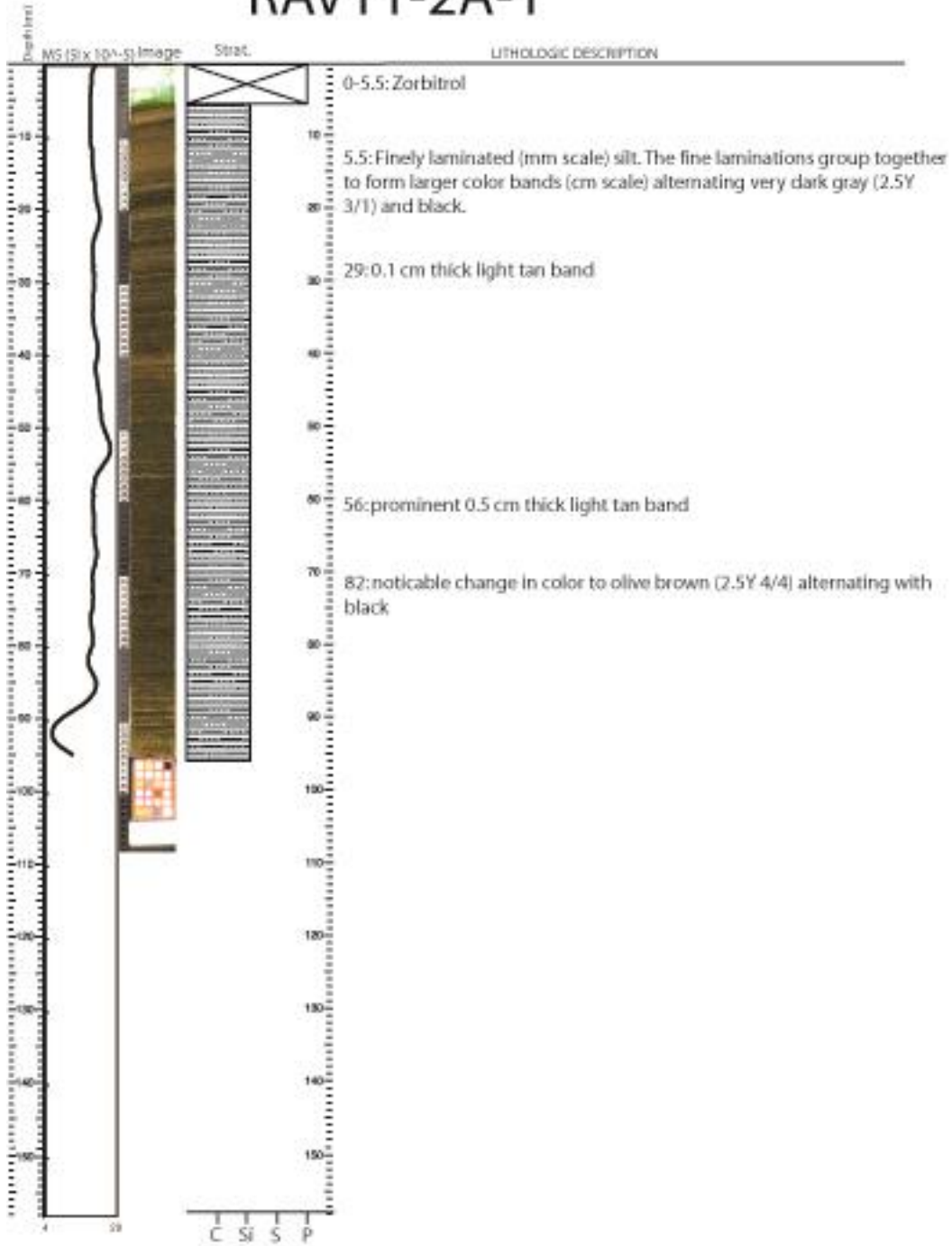


Figure 41: Initial description of core RAV11-2A-1

# RAV11-3A-1

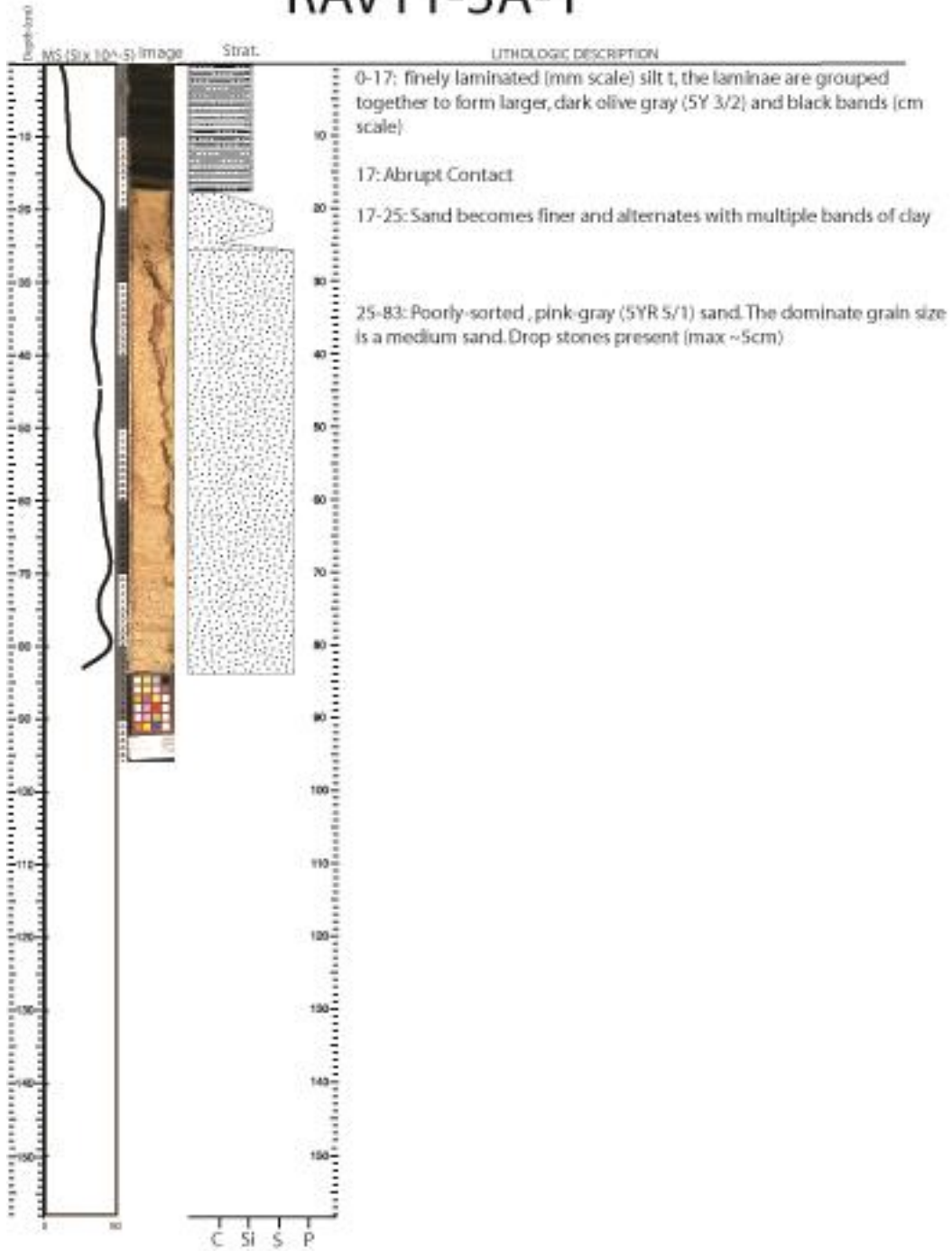


Figure 42: Initial description of core RAV11-3A-1

# RAV11-4A-1

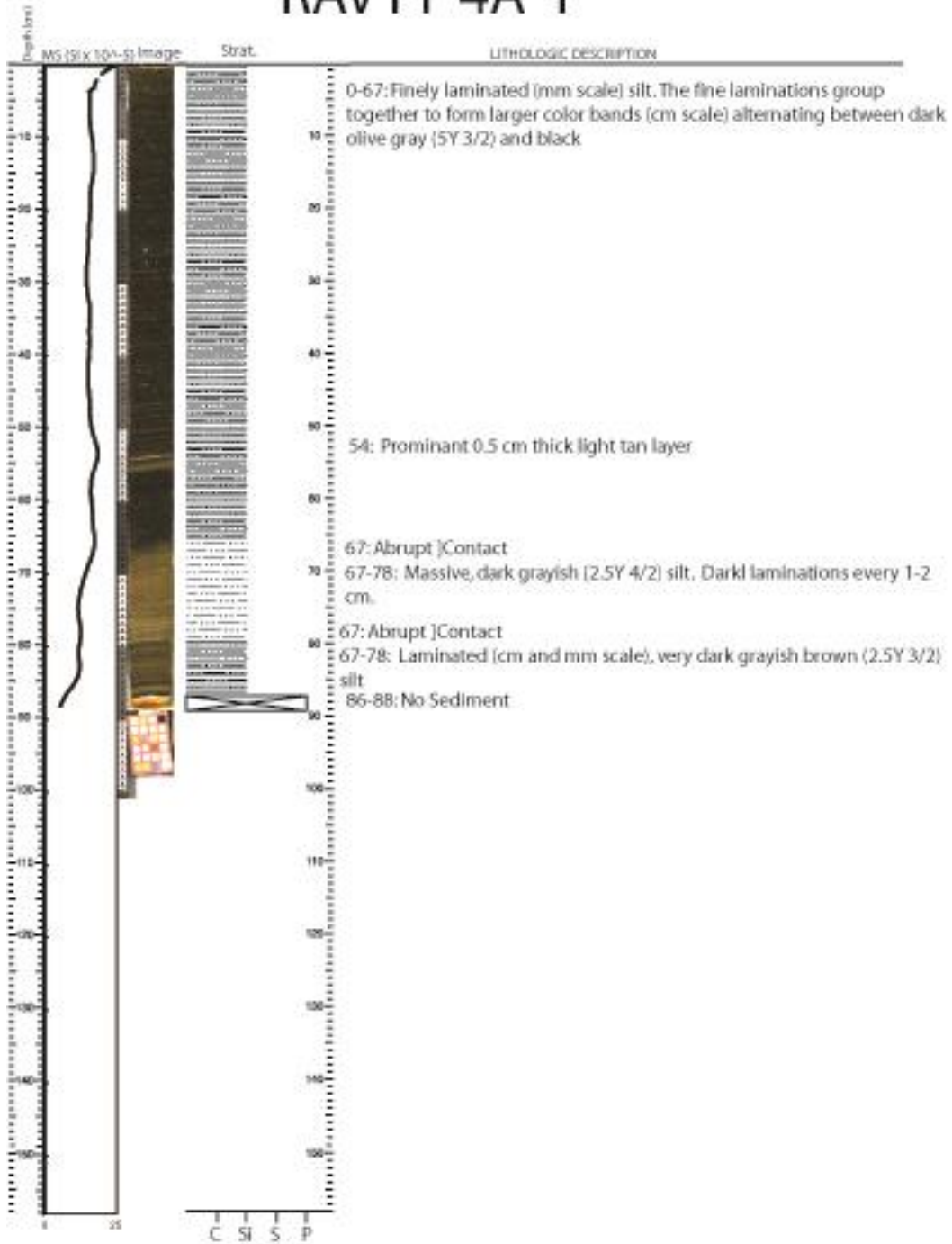


Figure 43: Initial description of core RAV11-4A-1

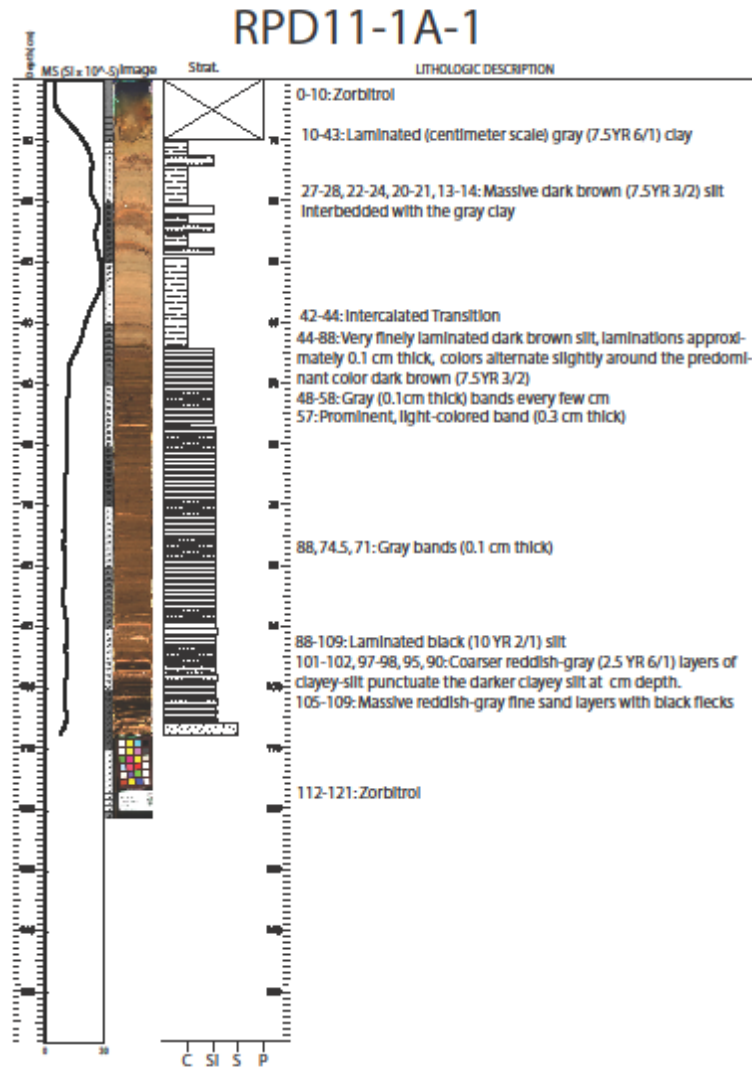


Figure 44: Initial description of core RPD11-1A-1



# RPD11-1B-1

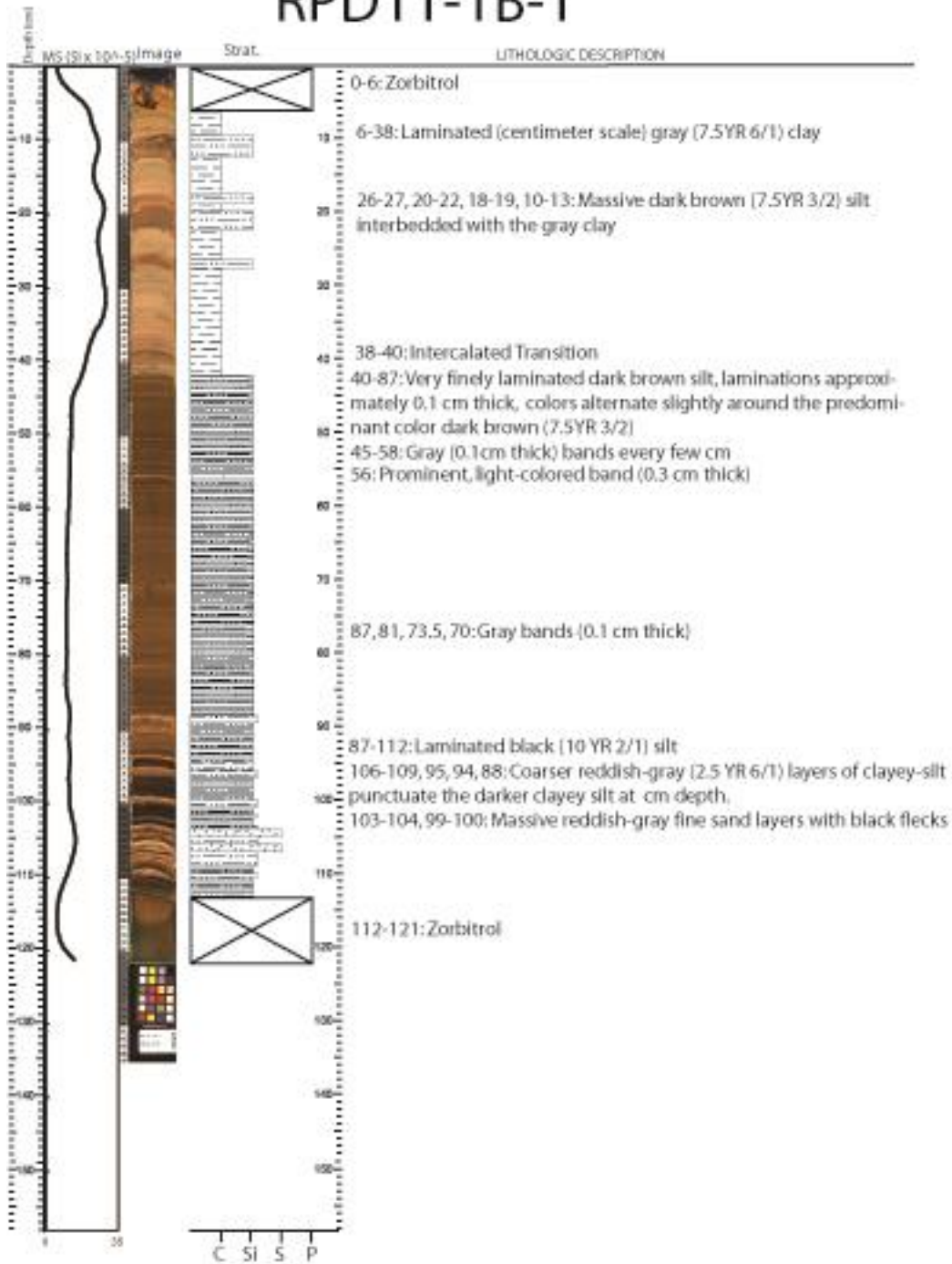


Figure 45: Initial description of core RPD11-1B-1

# RPD11-1C-1

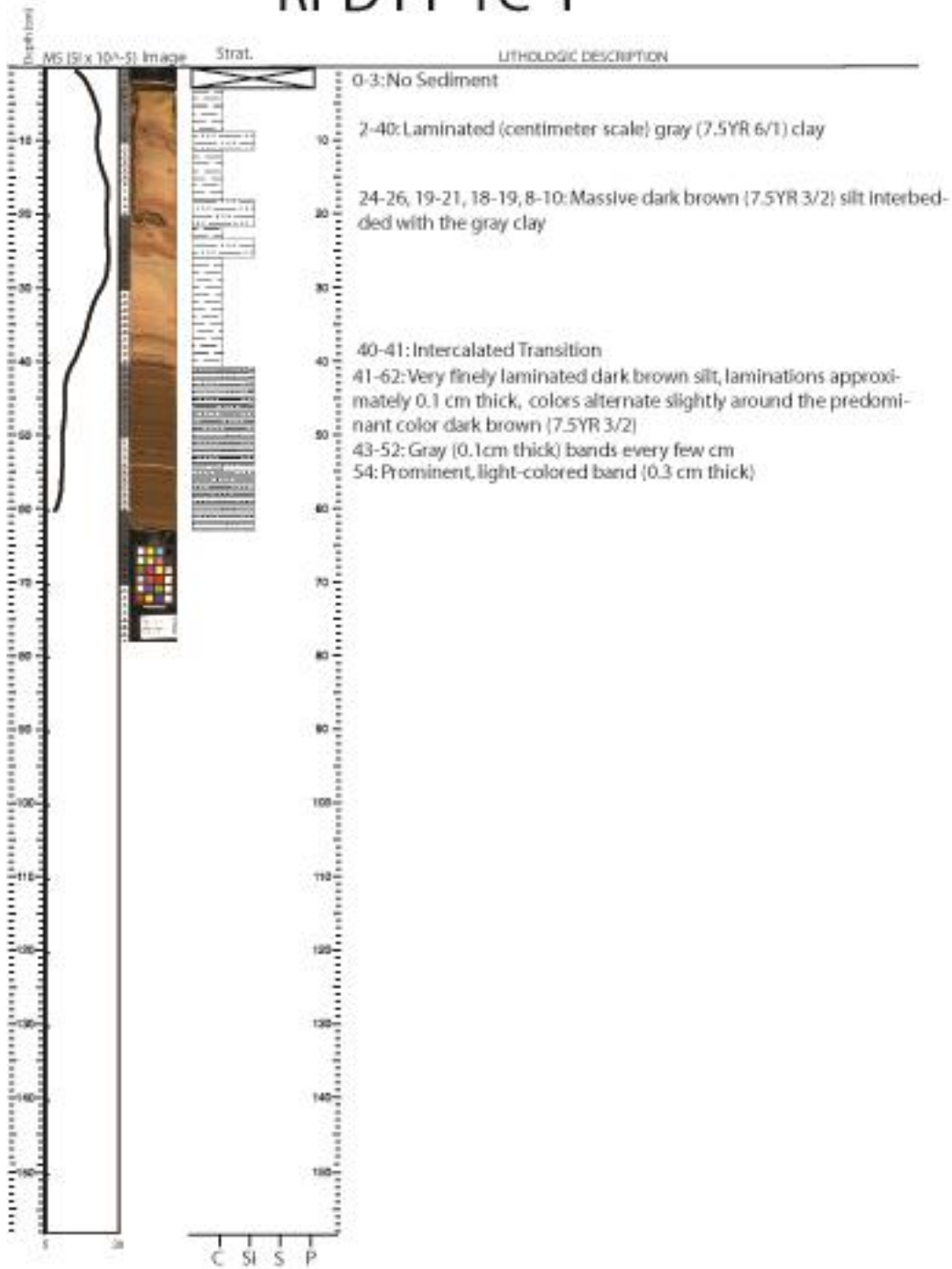


Figure 46: Initial description of core RPD11-1C-1

# RPD11-2A-1

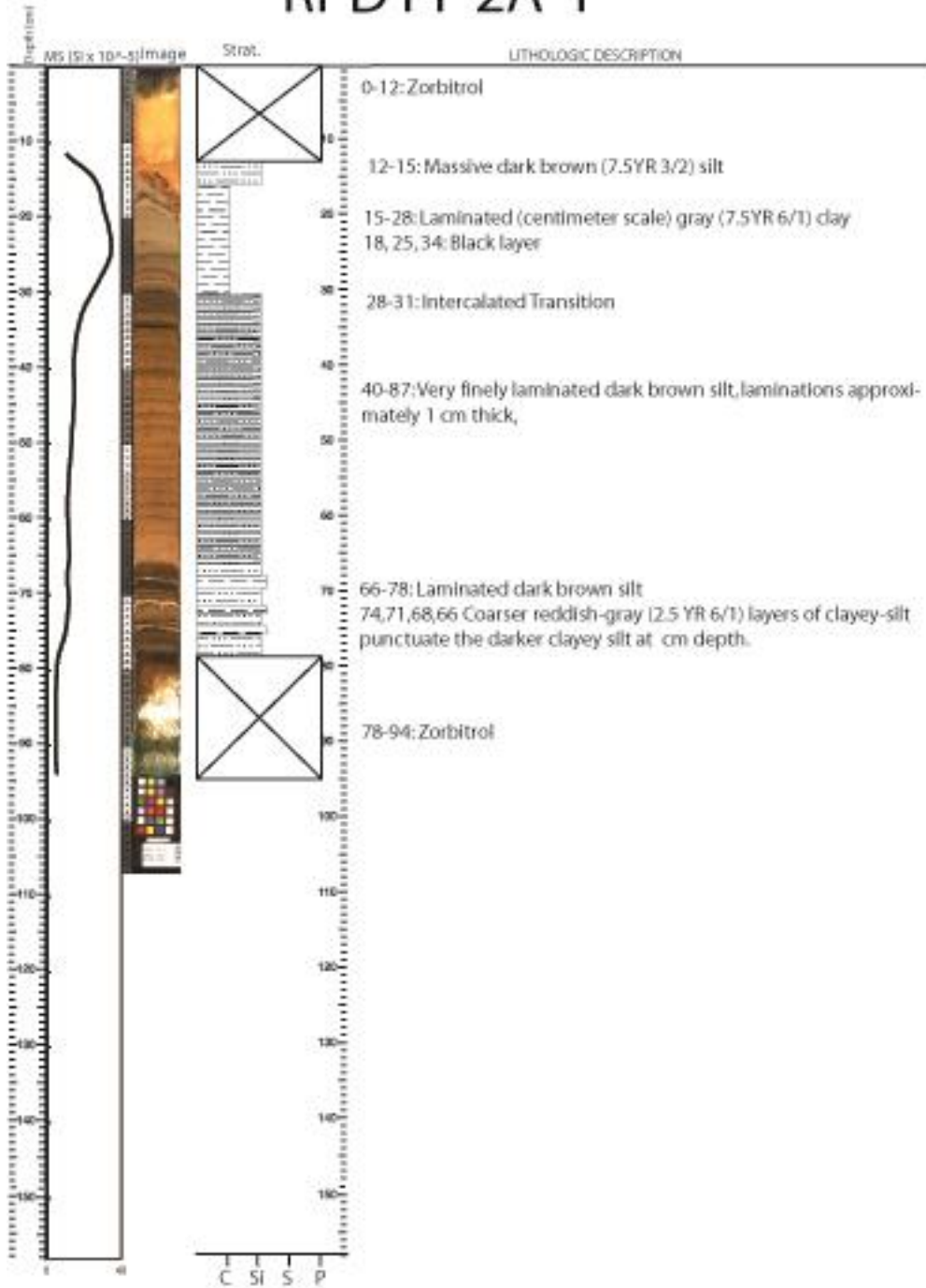


Figure 47: Initial description of core RPD11-2A-1

## **BIOGRAPHY OF AUTHOR**

Aaron Medford was born in Hudson, NY on May 11, 1989. He moved to Cortland, NY in 1999, where Aaron graduated Cortland Jr.-Sr. High School in 2007. Aaron then attended Lafayette College for a liberal arts undergraduate education. He spent a semester abroad in Leeds, England in 2009, and received a Bachelor of Science in geology in 2011. Aaron immediately began graduate education at The University of Maine, focusing in glacial geology. Aaron Medford is a candidate for the Master of Science degree in Earth and Climate Sciences from The University of Maine in August 2013.